

# **Design and Development of a Multi-Mission UAS through Modular Component Integration and Additive Manufacturing**

A project present to  
The Faculty of the Department of Aerospace Engineering  
San Jose State University

in partial fulfillment of the requirements for the degree  
*Master of Science in Aerospace Engineering*

By

**Kim Lau**

August, 2018

approved by



Dr. Nikos Mourtos  
Faculty Advisor



## Table of Contents

1. Introduction.....	5
1.1. Motivation.....	5
1.2. Literature Review .....	5
1.2.1. UAV Design and Development Trends .....	5
1.2.2. Push for Modularity .....	7
1.2.3. Additive Manufacturing.....	8
1.3. Project Proposal .....	11
1.4. Methodology .....	11
2. Design Process.....	12
2.1. Mission Specification and Comparative Study.....	12
2.1.1. Mission Specification .....	12
2.1.1.1. Mission Specification .....	12
2.1.1.1.1. Surveillance .....	12
2.1.1.1.2. Attack.....	13
2.1.1.1.3. Resupply .....	13
2.1.1.2. Mission Profile.....	13
2.1.1.2.1. Surveillance .....	13
2.1.1.2.2. Attack.....	14
2.1.1.2.3. Resupply .....	14
2.1.1.3. Critical Mission Requirements .....	15
2.1.2. Comparative Study of Similar Airplanes.....	15
2.1.2.1. Mission Capabilities and Configuration Selection .....	15
2.1.2.2. Comparison of Important Design Parameters.....	15
2.2. Configuration Design.....	16
2.2.1. Comparative Study of Airplanes with Similar Mission Performance .....	16
2.2.1.1. Comparison of Weights/Performance/Geometry of Similar Airplanes..	16
2.2.1.2. Configuration Comparison of Similar Airplanes.....	17
2.2.1.2.1. AliExpress SkyEye .....	17
2.2.1.2.2. Applied Aeronautics Albatross.....	18
2.2.1.2.3. Optimum Solutions Condor 300.....	18
2.2.1.2.4. Optimum Solutions Leonardo.....	19
2.2.1.2.5. Penguin BE Electric.....	19
2.2.1.2.6. RQ-11 Raven .....	20
2.2.1.2.7. RQ-14 Dragon Eye .....	20
2.2.1.2.8. RQ-20 Puma .....	21
2.2.1.2.9. Bye Aerospace Silent Falcon.....	21
2.2.1.2.10. SkyPro V200.....	21
2.2.1.2.11. Discussion.....	22
2.2.2. Configuration Selection .....	22
2.2.2.1. Overall Configuration .....	22
2.2.2.2. Wing Configuration .....	22
2.2.2.3. Empennage Configuration .....	22
2.2.2.4. Integration of the Propulsion System.....	22
2.2.2.5. Landing Gear Disposition.....	22
2.3. Weight Sizing & Weight Sensitivities .....	22

2.3.1. Mission Weight Estimates .....	23
2.3.1.1. Database for Takeoff/Empty Weights of Similar Airplanes.....	23
2.3.1.2. Determination of Regression Coefficients A and B .....	23
2.3.1.3. Determination of Mission Weights.....	24
2.3.1.4. Takeoff Weight Sensitivities .....	26
2.3.1.4.1. Calculation of Takeoff Weight Sensitivities.....	26
2.3.1.4.2. Trade Studies .....	26
2.4. Performance Constraint Analysis .....	27
2.4.1. Calculation of Performance Constraints .....	27
2.4.1.1. Stall Speed .....	27
2.4.1.2. Takeoff Distance.....	28
2.4.1.3. Landing Distance .....	28
2.4.1.4. Drag Polar Estimation.....	30
2.4.1.5. Climb Constraints .....	30
2.4.1.6. Speed Constraints .....	31
2.4.1.7. Summary of Performance Constraints.....	32
2.4.2. Selection of Propulsion System .....	33
2.4.2.1. Selection of the Propulsion System Type.....	33
2.4.2.2. Selection of the Number of Engines .....	33
2.4.3. Discussion.....	35
2.5. Fuselage Design.....	35
2.5.1. Layout Design of the Fuselage .....	35
2.6. Wing, High-Lift System & Lateral Control Design .....	37
2.6.1. Wing Planform Design .....	37
2.6.2. Airfoil Selection.....	39
2.6.3. Wing Design Evaluation.....	43
2.6.4. Design of the High-Lift Devices and Lateral Control Surfaces.....	43
2.6.4.1. High-Lift Devices .....	43
2.6.4.2. Lateral Control Surfaces .....	46
2.6.4.3. Layout of High Lift Devices and Lateral Control Surfaces.....	48
2.7. Design of the Empennage & the Longitudinal and Directional Controls.....	48
2.7.1. Overall Empennage Design .....	48
2.7.2. Design of the Horizontal Stabilizer .....	50
2.7.3. Design of the Vertical Stabilizer.....	51
2.7.4. Design Of The Longitudinal And Directional Controls .....	53
2.7.4.1. Longitudinal Control .....	53
2.7.4.2. Directional Control .....	55
2.8. Landing Gear Design and Weight & Balance Analysis .....	57
2.8.1. Estimation of the Center of Gravity Location for the Airplane.....	57
2.8.2. Landing Gear Design .....	58
2.8.3. Weight and Balance .....	59
2.9. Stability and Control Analysis.....	61
2.9.1. Static Longitudinal Stability .....	61
2.9.2. Static Directional Stability.....	62
2.10. Drag Polar Estimation.....	62
2.10.1. Airplane Zero Lift Drag.....	63

2.10.2. Low Speed Drag Increments.....	65
2.10.3. Airplane Drag Polars .....	66
3. Manufacturing and Build Process.....	68
3.1. Methodology.....	68
3.2. Manufacturing.....	70
4. Flight Testing.....	75
4.1. Objectives .....	75
4.2. Methodology.....	75
4.3. Uncertainties in Testing Data .....	76
4.4. Testing Phases.....	77
4.4.1. Static/Ground Testing .....	77
4.4.1.1. Weight and Center of Gravity.....	77
4.4.1.2. Thrust.....	77
4.4.2. Performance .....	78
4.4.2.1. Stall Speed .....	78
4.4.2.2. Thrust Available .....	81
4.4.2.3. Drag Polar .....	82
4.4.2.4. Range and Endurance .....	85
4.4.2.5. Climb .....	86
4.4.2.6. Takeoff and Landing.....	87
4.4.3. Stability and Control.....	90
4.4.3.1. Static Longitudinal Stability .....	92
4.4.3.2. Dynamic Longitudinal Stability.....	93
4.4.3.3. Longitudinal Maneuvering, Control, and Trim .....	94
4.4.3.4. Static Lateral-Directional Stability .....	94
4.4.3.5. Dynamic Lateral-Directional Stability.....	96
4.4.3.6. Lateral-Directional Control.....	98
4.4.4. Aircraft Limitations .....	99
4.4.4.1. Stall Characteristics .....	99
4.4.4.2. Flutter, Vibration, Buffeting .....	100

# 1. Introduction

## 1.1. Motivation

The methodology of aircraft design has remained relatively unchanged for decades. Almost all aircraft today are designed to fit a specific mission. In some cases, existing designs are able to be modified and adapted to fulfill a similar mission, i.e. passenger aircraft converted to cargo plane, or to increase its current capability, such as increasing passenger capacity. In others, the aircraft is designed with multiple missions in mind. This usually leads to an aircraft that can do many things but none of them well. A prime example of this is the Air Force's F-35 Lightning II. Its design and development process has been littered with cost overruns and questions about compromised capabilities due to the need to satisfy the requirements of the different branches of the military that are acquiring the aircraft. There needs to be a middle ground between highly specialized and multirole/multi-mission capable designs.

## 1.2. Literature Review

### 1.2.1. UAV Design and Development Trends

The advent of UAVs (Unmanned Aerial Vehicles) bore out of necessity due to the nature of the certain military missions which were either too dangerous or exceeded the physical limitations of human operators. Initially, these missions were mainly reconnaissance and surveillance in type. They eventually evolved into a first/quick strike capability during the War on Terror as the need for fast action on high value targets arose. This saw the adaptation of non-lethal sensor platforms modified to carry combat payloads into areas of conflict. Although there is an established military

use for UAVs, there has been little development and implementation in civil and commercial applications, mostly due to government regulations that prohibit their use. There is a growing segment for private/recreational use of UAVs but those are generally limited to lightweight vehicles, usually less than 20 kgs, whereas military developments are usually vehicles in the higher weight classes. The higher weight of military UAVs are necessary as they have a wider operational envelope as well as missions that necessitate complex systems and payloads.

UAS Category	Max Gross Takeoff Weight	Normal Operating Altitude (Ft)	Airspeed	Current Army UAS in Operation
Group 1	< 20 pounds	< 1200 above ground level (AGL)	<100 Knots	RQ-11B Raven
Group 2	21-55 pounds	< 3500 AGL	<250 Knots	No current system
Group 3	< 1320 pounds	<18,000 mean sea level (MSL)		RQ-7B Shadow
Group 4	> 1320 pounds	> 18,000 MSL	Any Airspeed	MQ-5B, MQ-1C
Group 5			No current system	

Table 1. US military UAV classifications. [17]

There are several different classifications of UAVs depending on the governing body. The US military has five categorical groups for UAVs, based on weight and range capability, in accordance with the DoD 2009-2034 Unmanned Systems Integrated Roadmap. [17] Lately, most development work has centered around MALE/HALE (Medium/High Altitude Long Endurance Air Vehicle) and UCAVs (Unmanned Combat Air Vehicle). Examples of these include the MQ-1A/B Predator (MALE), MQ-9 Reaper (MALE), RQ-4 Global Hawk (HALE), and upcoming Northrop Grumman X-47B (UCAV). There is an even greater push for more UAVs as each branch of the military finds uses for them. As noted in [14], the Navy is assessing fixed-wing and rotary-wing RPAs (Remotely Piloted Aircraft) and UAVs for fleet defense, reconnaissance, and broad-area maritime surveillance. A family of RPAs and UAVs is a major component of the Army Future Combat System, and USSOCOM and the Marine Corps are increasing their development, procurement, and employment of various small UAVs as lightweight, man-portable systems allow for a unique instant access, bird's eye view capability to the warfighter on the ground.

UAVs are an increasingly popular option with the different branches of the US military as there are several factors which make them now more attractive and feasible than traditional aircraft. Recent technological advances have allowed for sensor and weapon payloads to become smaller, lighter, and more capable, providing great capability per unit of weight. In addition, improvements in propulsion system efficiency and the use of composite materials result in lighter, smaller, and more stealthy airframes, with the resulting fuel efficiency leading to levels of endurance that exceed human tolerance. This is due to the fact that engines and airframes can be designed without regard to human factors limitations; the space and weight normally allocated to the pilot/crew and the supporting systems can now be made available for more payload and/or fuel, or they can be eliminated in order to design a smaller vehicle. [14] Unmanned systems can operate in environments contaminated by chemical, biological, or radioactive agents. Additionally, they can also operate in other environments denied to manned systems, such as areas without air superiority and at altitudes both lower and higher than those typically traversed by manned aircraft. The long endurance of some RPAs and UAVs provides sustained support for more efficient time-critical targeting. Long endurance systems translates into reduced sortie rates. Reduced sortie rates also lowers the number of flight hours "lost" due to transit time to station.

UAVs were originally envisioned to only be sensor platforms, performing a wide range of missions including intelligence, surveillance and reconnaissance (ISR) missions, target acquisition, battle damage assessment, SIGINT, COMINT (Communications Intelligence) and ELINT (Electronic Intelligence). Only the advent of light, precision weapons allowed legacy systems to be modified into strike platforms. This is in conjunction to enhanced autonomous target acquisition and recognition technologies. The continued development of strategic and tactical UAVs follows the line of employing UAVs as multi-role multi-mission platforms. UAVs will see progressive developments towards both ends of the size spectrum. Strategic UAVs will see continuous growth in size for better endurance, reliability and payload capacity, while the mini- and micro- UAVs will grow smaller, lighter and more expendable. The tactical, close range platforms will become more versatile, with multi-mission, multi-role capability. [3]

As the strengths of UAV platforms are its long endurance and loiter times, a logical next-step would be its adaptation as an AWACS (Airborne Warning and Control System) platform. Currently this capability is fulfilled by the E-2C Hawkeye and E-3 Sentry. These systems, introduced in the '60s and '70s, respectively, are approaching a point in their service life in which maintenance and continual operation are growing increasingly expensive. They are also handicapped by the penalties associated with human physiology, resulting in limited endurance and lowered payload capacity. The E-3 replacement, the E-10 MC2A, was canceled by the DOD due to budgetary constraints. The Air Force has now begun performing incremental improvements, mainly to the mission crew and air battle management sections, as well as significantly upgraded electronic equipment, to bring the E-3 up to current standards of performance. They are also considering other modernization programs such as retrofitting newer, more efficient engines to the E-3, which based on the Boeing 707. At that point, it would seem to make more sense to design a system best suited for today's battle requirements. An AWACS UAV would provide that capability comparable to or even exceeding that of a manned system at a price lower point.

In the future, the U.S. Army hopes envisions UAS capabilities to expand beyond surveillance and attack. They foresee the possibility of combat support and sustainment as a growing field in UAS development. Unmanned aircraft systems may provide routine sustainment functions in the delivery of supplies and materials to forward deployed units. A sustainment/cargo UAS asset could provide responsive and precise transport of small, high value payloads. [17] Through the mid-term, the Army foresees itself fielding a sustainment/cargo UAS. Research, experimentation, and development on advanced payload capabilities, and autonomy continues to expand capabilities for sustainment/cargo UAS. Also in this timeframe, medical resupply operations are expected to mature with final operational testing and deployment of platforms. [17]

Legacy UAVs have served as a weapons platform for over a decade in the United States. They have mostly been adapted from aircraft designed with non-lethal original mission specifications. Systems currently in development are designed towards strike focused set of capabilities as they are better optimized for the roles required for today's battlefields. It is difficult to regulate these emerging systems based on current weapons platform classifications due to the nature of UAVs as a disruptive technology. These regulations have become less relevant as UAVs have been developed across all weight classes and increasingly smaller systems are capable of employing weapons, or being modified for this purpose. This is further complicated by the fact that certain remotely piloted vehicles have been designed to function as loitering munitions, hence blurring the line between UAVs and cruise missiles. [15] The UN fears that advances in technology will change the nature of contemporary warfare and could have ramifications for future strategic

stability. Such advances could lead to systems that could pose similar challenges as armed drones to humanitarian concerns, human rights and international security. [15]

### 1.2.2. Push for Modularity

As UAVs are integrated across the various branches of the military, there becomes a push for an ever expanding set of capabilities. One solution in meeting the various requirements is to design for multi-mission capability, ideally through modularity. The main driver for this design philosophy is cost. [13] Cost reduction can come in a multitude of ways, either during design and development or after the system is operational, where it will incur repair, maintenance costs. This is due to commonality of parts and subsystems across various systems which allows for their procurement in large numbers to reduce unit costs. It also allows for the development cost to be spread over a larger number of operators. [13]

Often times, technologies employed in UAVs and their developments are new and emerging. It is difficult to follow a traditional aircraft design and certification process as it makes the program prohibitively expensive, nearing that of manned systems. It is proposed in [9] and [11], that the employment of spiral development/certification cycles will limit costs and provide for a faster time to operational service. This is possible due to designing the aircraft to achieve the minimum to be successful. In other words, the goal of the design phase is to create a base vehicle to test design soundness and functionality. Additional capabilities will be determined, developed and integrated through incremental improvements and upgrades at later points in the development and operation process. [9] This offers an intermediate step that allows the user to qualify the aircraft for limited operational usage with much less testing that is performed for full operational usage, but more testing than is used for the prototype vehicle. The intermediate step is focused on assuring that the vehicle will operate safely in limited operational environment for a reduced lifetime consistent with that operation.

A common theme in the requirements for many future systems is that they should be able to respond to changing needs. Reconfigurable systems, i.e., those that can change their configurations, can potentially satisfy changing system requirements. The need for reconfigurability is generally driven by three main factors:

- Multiability: the system performs multiple distinctly different functions at different times.
- Evolvability: the system changes easily over time by removing, substituting, and adding new elements and functions.
- Survivability: the system remains functional, possibly in a degraded state, despite a few failures. [12]

By starting with a base design that focuses on modularity, multi-mission capability is readily achievable. Modularity will allow for the platform to adapt to the changing conditions and operational requirements of the future, effectively eliminating obsolescence in components that experience relatively rapid technological advancements such as electronics and sensors. This is not limited to electronics, modular payloads allow for mission flexibility as well as the implementation of new weapons designs. Modularity may also be a means to change airframe performance characteristics. This can be as simple as a re-engine to improve fuel efficiency or a new wing design for higher payload capacity. One important aspect in designing for modularity is that for every configuration of a reconfigurable system, there exists a corresponding dedicated

system that is at least equal in performance. A good reconfigurable design is one in which the performance of each configuration approaches that of the corresponding dedicated system. [13]

This development philosophy can be seen on the infamous M/RQ-1 Predator. Originally developed as a light reconnaissance plane, it has been subsequently upgraded and improved through new engines, avionics, wings, and de-icing systems to improve reliability. Later versions were able to be retrofitted to carry weapons, turning it into a multi-role/mission system. Ideally, when attempting to reconfigure and/or repurpose existing systems, it is necessary to identify the limitations of the system as well as critical structures or systems in order to address them and make improvements. [7] Separating and compartmentalizing systems into modules allows for ease of configurability later down the line. Obviously, systems with similar modules have the highest degree of reconfigurability. Common modules should be maximized across configurations to save on costs. [12]

Although the Air Force was able to fulfill multiple requirements with one airframe, the success has not been able to be translated across the branches of the military. Several unmanned aircraft programs have achieved airframe commonality, service-driven acquisition processes and ineffective collaboration are key factors that have inhibited commonality among subsystems, payloads, and ground control stations. Often, services established requirements that were often so specific that they demanded service unique solutions—thereby precluding opportunities for commonality. Yet none of those programs were able to provide justification into pursuing their unique solutions or to show why common solutions would not work. [13] For example, The Navy BAMS and Air Force Global Hawk programs have achieved some commonality between their unmanned aircraft systems—specifically, the airframes for the two systems are common. However, the payload and subsystem requirements differ; and while some BAMS ground station requirements are common with those of the Global Hawk. The Navy and Air Force have worked together to identify commonalities to gain additional efficiencies where possible. According to a Navy official, one of the goals of this partnership is for the BAMS program to benefit from lessons learned by the Global Hawk program and thereby avoid the types of problems Global Hawk experienced during development. [13]

### 1.2.3. Additive Manufacturing

Additive manufacturing is an umbrella term for a manufacturing technique used to construct physical models, prototypes, tooling and components from a three dimensional digital model. Additive manufacturing forms the object layer by layer by the joining of liquid, powder, or sheet material. It is referred to additive manufacturing as it builds the object from the ground up, compared to traditional manufacturing methods such as machining which is a subtractive process of removing material to achieve the final form. There are several types of additive manufacturing:

- FDM – fused deposition modelling
- SLA – stereolithography
- SLS – selective laser sintering
- Polyjet

The most common in commercial and private use are FDM, SLA, and SLS. For fused deposition modelling, objects are created layer-by-layer by extruding a heated plastic filament through a nozzle. A wide range of thermoplastics can be processed via this method such as polylactic acid (PLA), Nylon and aerospace grade Ultem. Stereolithography uses ultraviolet (UV) light to

polymerize photosensitive liquid resin in a layer-by-layer manner. Selective laser sintering process employs selective melting and solidifying of each successive powder layers to build complex 3D parts made of thermoplastics, metal or ceramics. [1] The advantages and disadvantages of each technique are listed in the Table 2.

Table 2. Advantages and disadvantages of additive manufacturing techniques. [1]

Advantages and disadvantages of different AM techniques employed to fabricate UAV.

Types of AM techniques	Advantages	Disadvantages	Name of UAVs/ printed parts
FDM	<ul style="list-style-type: none"> <li>High strength material such as Ultem is available</li> <li>ABS plastic has higher survival rate compared to balsa during impacts</li> </ul>	<ul style="list-style-type: none"> <li>Obvious stair stepping effect in z-direction</li> <li>Poor surface finish compared to polyjet and SLA</li> </ul>	Fully printed UAV structure AMRC UAV VAST UAV Entomopter frame, gear, tail
Polyjet	<ul style="list-style-type: none"> <li>Ability to create functionally graded parts with multi-material printing</li> <li>Ability to print fine features</li> <li>Good surface finish</li> <li>Insignificant stair stepping effect</li> </ul>	<ul style="list-style-type: none"> <li>Slow recovery rate from high loading condition</li> <li>Strength of AM material is still inferior to that of the biological bone</li> </ul>	Lattice structure wing strut Bar-like ornithopter Replica of insect wing
SLA	<ul style="list-style-type: none"> <li>Ability to print fine feature size</li> <li>Good surface finish</li> <li>Insignificant stair stepping effect</li> </ul>	<ul style="list-style-type: none"> <li>Degradation of photosensitive materials leading to poor performance under load.</li> <li>Low tensile strength of material</li> </ul>	Entomopter Stingray UAV Flap Wind tunnel UAV model
SLS	<ul style="list-style-type: none"> <li>Ability to print parts with good mechanical strength</li> <li>Large build area</li> <li>Relatively low cost</li> </ul>	<ul style="list-style-type: none"> <li>Rough surface finish</li> </ul>	SULSA UAV Scaled-down UAV model for wind tunnel test Spotter UAV

From an economic standpoint, additive manufacturing is most advantageous in environments characterized by a great demand for customization, flexibility, design complexity, and high transportation costs for the delivery of end products. It facilitates product innovation because design iterations are relatively inexpensive and parts can be rapidly produced. [1] Various other economic characteristics of additive manufacturing is listed in Table 2.

Table 3. Economic characteristics of additive manufacturing. [1]

Economic characteristics of AM	
Opportunities	Limitations
<ul style="list-style-type: none"> <li>Acceleration and simplification of product innovation: iterations are not costly and end products are rapidly available</li> <li>Price premiums can be achieved through customization or functional improvement (e.g. lightweight) of products</li> <li>Customer co-design of products without incurring cost penalty in manufacturing</li> <li>Resolving "scale-scope dilemma": no cost penalties in manufacturing for higher product variety</li> <li>Inventories can become obsolete when supported by make-to-order processes</li> <li>Reduction of assembly work with one-step production of functional products</li> <li>Lowering barriers to market entry</li> <li>Local production enabled</li> <li>Cost advantages of low-wage countries might diminish in the long run</li> </ul>	<ul style="list-style-type: none"> <li>High marginal cost of production (raw material costs and energy intensity)</li> <li>No economies of scale</li> <li>Missing quality standards</li> <li>Product offering limited to technological feasibility (solution space, reproducibility, quality, speed)</li> <li>Intellectual property rights and warranty related limitations</li> <li>Training efforts required</li> <li>Skilled labor and strong experience needed</li> </ul>

Structural efficiency of an UAV can be improved via two methods, through the use of lightweight structures and the use of high-strength-to-weight materials. Both aviation and UAV industries are now moving towards composite materials, which combine numerous advantages like high strength, low weight, high corrosion, fatigue resistance and easy processing. Composites can also be tuned to provide 'stealth' capabilities and low thermal expansion, making them attractive for defense and high altitude applications. FDM remains the popular choice as it allows the flexibility

of printing through simple modification in printer head or nozzle. The introduction of carbon fiber reinforcement to thermoplastics allows for the creation of lightweight and high strength parts. Obviously, have poor mechanical properties compared when compared to those fabricated using conventional methods. Test has shown that the short carbon fibers increased the tensile modulus E1 (respective to the printing direction) of the reinforced PLA+CF by about 2.2 times, in comparison to regular PLA. The tensile modulus E2 (transverse to the printing direction) and the shear modulus G12 (respective to the plane of printing) were also increased by the short fibers, respectively 1.25 and 1.16 times. [2]

To counteract this reduction in strength compared to traditional materials and construction methods, the structural design can be optimized to take advantage of additive manufacturing's ability to create complex geometries such as functionally-graded structures and conformal mesoscopic cellular structures. [1] This is achieved through topology optimization which intends to find an optimal structural configuration within a given design domain for specified objectives, constraints, loads and boundary conditions. [20] In the future, most aerospace structures will be designed and fabricated as integral structural systems to save the structural weight and simplify the assembling procedure. With this new concept, the combination of topology optimization and additive manufacturing will for sure play significant roles in developing high performance and lightweight structure systems. [20] Earlier methods of lightening and strengthening a structure were focused around the use of cellular material structures, such as honeycombs and lattice structures, which enable unprecedented stiffness and strength characteristics, for a given weight. [10] In addition, cellular structure also provide good energy absorption characteristics and good thermal and acoustic insulation properties. The combination of cellular materials/structure, topology optimization, and composite materials has the potential to stretch the limits of design.

### 1.3. Project Proposal

The main objective of this project is to design and build an aircraft that can fulfill three distinct mission profiles and specifications. The goal is to incorporate a modular architecture in order to reconfigure the aircraft in order to excel in each given mission. The secondary objective is to test the feasibility of 3D printed parts and structures to allow for faster prototyping and construction as well as increased capabilities and performance.

### 1.4. Methodology

The first step is to identify the specific roles and mission the military is looking to fill with future aircraft. From these, we can create a list of mission specifications and identify the critical specifications that govern the design of each type of aircraft. This will allow for a final mission specification list that will serve as the basis for the UAS.

The second step is to design the UAS. Special consideration will be taken with certain parts of the design process in order to optimize the design for each role. This may include the wing, empennage, and fuselage design sections. The designs from these sections must also take into consideration how each one will integrate with the modular architecture.

The third step is to build and assemble the various subsystems and structures in order to test and evaluate the design of the aircraft. The ultimate goal is to flight test the aircraft and to benchmark the performance with the mission specifications.

The last step is to perform a CFD analysis of the various components in order to find areas of improvement. Iterative improvements should be fairly straightforward and simple to implement due to the modular nature of the aircraft.

## 2. Design Process

The design process of the aircraft will closely mirror the methodology prescribed in Roskam. This will allow for a through design process that will ensure a viable and realistic aircraft. Special modifications to the methodology will be employed due to the electric propulsion consideration, specifically in the mission weight sizing.

### 2.1. Mission Specification and Comparative Study

The purpose of this section is to outline the desired capabilities and mission requirements that are expected of the aircraft. These capabilities and mission requirements will serve to guide the sizing and design of the aircraft in following sections.

#### 2.1.1. Mission Specification

##### 2.1.1.1. Mission Specification ??? SAME SUBTITLE? YOU CAN HAVE THE INTRO TO THIS SECTION W/O A SUBSECTION NUMBER

As previously stated, the objective of this project is to design an aircraft that will be able to fulfill three distinct missions by adapting the aircraft to each mission's needs. From the literature review section, it can be seen that the current and future use of UAVs will be in the attack, surveillance, and resupply missions. Each mission has defining criteria that influence each type of aircraft's characteristics. Surveillance missions are characterized by high endurance and range, enabling the aircraft to gather maximum information with as little time lost to transit as possible. Attack missions are characterized by speed and payload capacity, allowing for a quick reaction to

changing and emerging situations. Resupply missions are characterized by high payload capacity with special structural considerations due to the airborne delivery requirement.

Below are the chosen mission specifications for each type of aircraft. There are some similarities, mainly cruise speed and cruise altitude, which are the result of FAA regulations for UAVs.

#### 2.1.1.1.1. Surveillance

- Payload capacity (~~number of passengers, cargo weight~~ and volume) **DO NOT INCLUDE ITEMS WHICH ARE NOT RELEVANT TO YOUR MISSION**
  - Cameras and sensors **GIVE ESTIMATE OF THE WEIGHT, IF YOU CAN.**
- Range
  - 10 km
  - Loiter **LOITER IS DIFFERENT THAN RANGE...WHY UNDER THE SAME HEADING?**
- Endurance
  - 2 hours
- cruise speed
  - 100 kmh
  - 160 kmh sprint to station (FAA limited)
- cruise altitude
  - Class G airspace 350 meters, 150 meters (FAA limited)
- take-off field length
  - 150 meters (SCCMAS Facility)
- landing field length
  - 150 meters (SCCMAS Facility)

#### 2.1.1.1.2. Attack

- Payload capacity (number of passengers, cargo weight and volume)
  - 178 mm diameter, 510 mm length, 9kg (Hellfire warhead)
- Range
  - 10 km
- cruise speed
  - 240 kmh (unrestricted), 160 kmh (FAA limited)
- cruise altitude
  - Class G airspace 350 meters, 150 meters (FAA limited)
- take-off field length
  - 150 meters (SCCMAS Facility)

#### 2.1.1.1.3. Resupply

- Payload capacity (number of passengers, cargo weight and volume)
  - 10 kg (MTOW <25 kg, FAA limited), deliverable
- Range
  - 5 km
- Endurance
  - 1 hour
- cruise speed
  - 160 kmh (FAA limited)
- cruise altitude

- Class G airspace 350 meters, 150 meters (FAA limited)
- take-off field length
  - 150 meters (SCCMAS Facility)
- landing field length
  - 150 meters (SCCMAS Facility)

2.1.1.2. Mission Profile

2.1.1.2.1. Surveillance

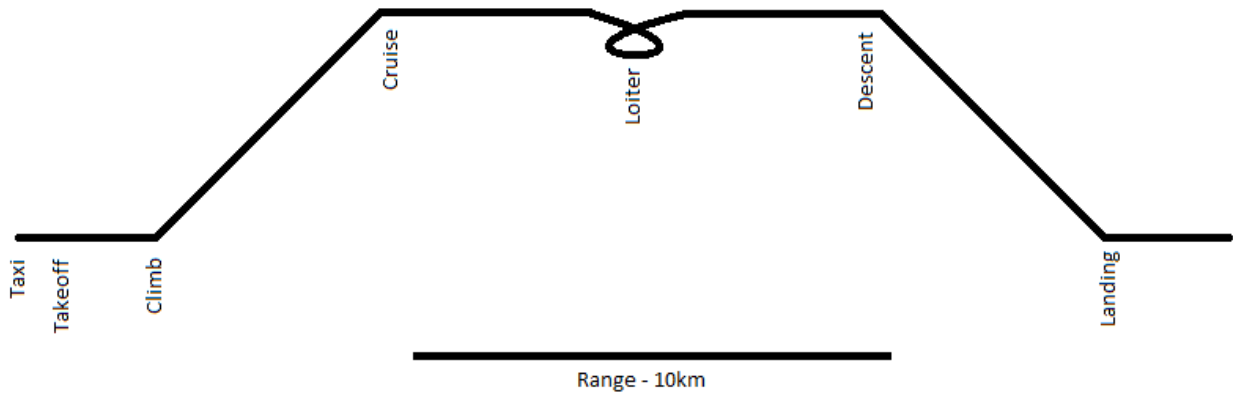


Figure 1. Surveillance mission profile

2.1.1.2.2. Attack

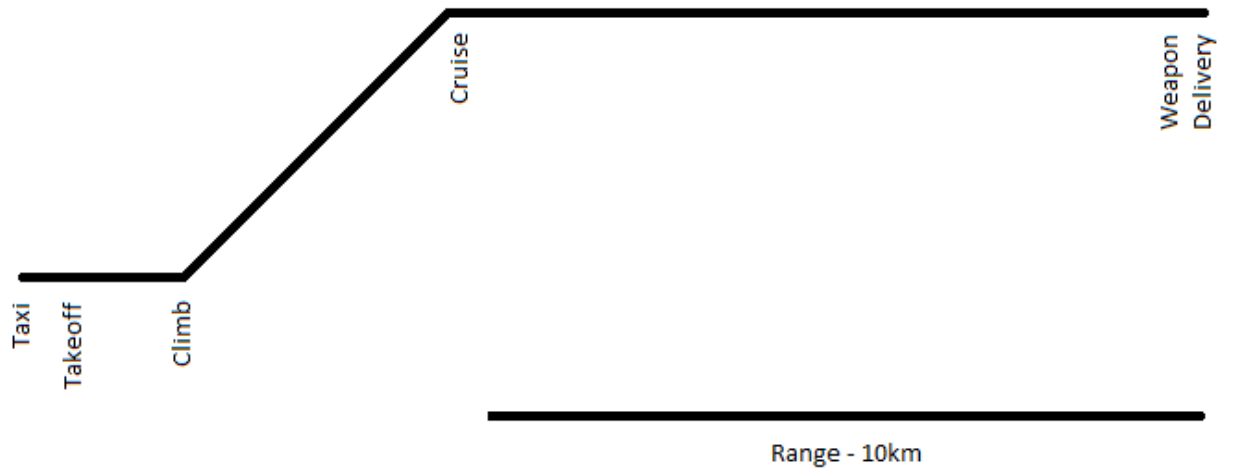


Figure 2. Attack mission profile

2.1.1.2.3. Resupply

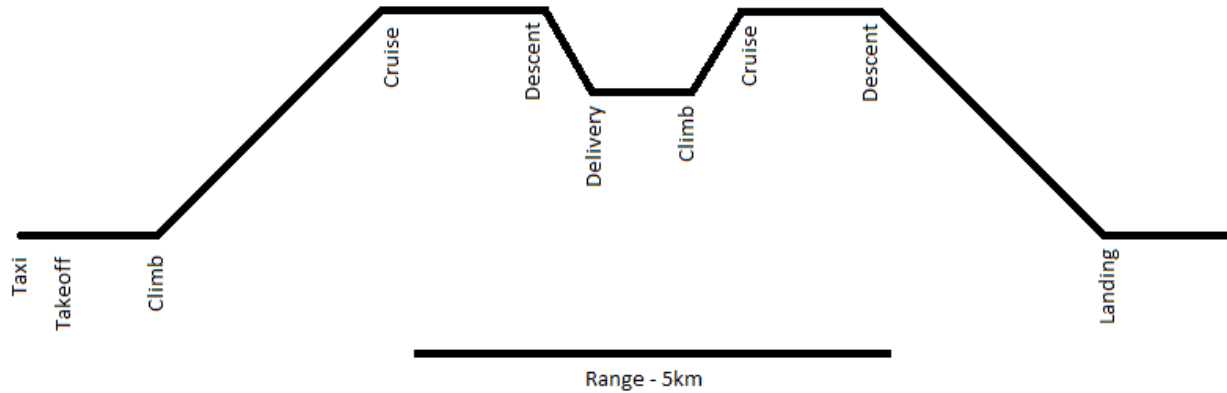


Figure 3. Resupply mission profile

### 2.1.1.3. Critical Mission Requirements

The critical mission requirements of each mission configuration are centered around their purpose. The surveillance configuration places importance on range and endurance. The attack configuration focuses on speed, payload capacity, and range. The resupply configuration focuses on payload capacity. It should be noted that the operating radius for the surveillance and resupply missions are half of the range. The attack configuration does not have a combat radius as it is designed as an expendable system in that configuration, thus the lack of landing phase in its mission profile.

### 2.1.2. Comparative Study of Similar Airplanes

#### 2.1.2.1. Mission Capabilities and Configuration Selection

Table 4. Mission capabilities of similar aircraft

Name	Weight	Payload	Cruise Speed	Range	Endurance	Cruise Altitude
AliExpress SkyEye	28 kg	14 kg	100 km/h	N/A	2 hours	N/A
Applied Aeronautics Albatross	10 kg	4.4 kg	64 km/h	100 km	5 hours	N/A
Optimum Solutions Condor 300	18 kg	6 kg	90 km/h		4 hours	3000 m
Optimum Solutions Leonardo	5.5 kg	N/A	45 km/h	30 km	4 hour	500 m
Penguin BE Electric	21.5 kg	6.6 kg	79 km/h	N/A	1.86 hours	6000 m
RQ-11 Raven	1.9 kg	0.2 kg	81 km/h	10 km	1.5 hours	150 m
RQ-14 Dragon Eye	2.7 kg	N/A	65 km/h	5 km	1 hour	150 m

RQ-20 Puma	6.3 kg	N/A	80 km/h	20 km	3 hours	150 m
Bye Aerospace Silent Falcon	14.5 kg	3 kg	90 km/h	15 km	5 hours	6000 m
SkyPro V200	5 kg	.9 kg	65 km/h	20 km	3 hours	3500 m

### 2.1.2.2. Comparison of Important Design Parameters

Table 5. Design parameters of similar aircraft

Name	Power	Battery	S	b	AR	Wing	Tail	Motor
AliExpress SkyEye	2x190kV (2450 W ea.)	12S (40000 mAh)	N/A	4500 mm		High wing, cantilever	Single-boom V	2xWing mounted puller
Applied Aeronautics Albatross	540 kV (1850 W)	2x6S (13600 mAh, 1.3 kg ea.)	0.66 m <sup>2</sup>	3000 mm	13.6	High wing, cantilever	Twin-boom inverted V	Single pusher
Optimum Solutions Condor 300	N/A	N/A	N/A	3200 mm	N/A	Low wing, cantilever	T-Tail	2xWing mounted puller
Optimum Solutions Leonardo	N/A	N/A	N/A	2600 mm	N/A	High wing, cantilever	Single-boom V	Single pusher
Penguin BE Electric	2700 W	4x12S (14414 mAh ea.)	0.79 m <sup>2</sup>	3300 mm	13.78	High wing, cantilever	Twin-boom inverted V	Single pusher
RQ-11 Raven	726 kV (400 W?)	N/A	N/A	1372 mm	N/A	High wing, cantilever	Conventional cruciform	Single pusher
RQ-14 Dragon Eye	2x726 kV (400 W?)?	N/A	N/A	1140 mm	N/A	High wing, cantilever	Rudder only	Wing mounted puller
RQ-20 Puma	N/A	N/A	N/A	2800 mm	N/A	High wing, cantilever	Conventional cruciform	Single puller
Bye Aerospace Silent Falcon	1.3 hp (~1000 W)	N/A	N/A	4400 mm	N/A	High wing, cantilever	Conventional cruciform	Single puller
SkyPro V200	N/A	N/A	N/A	2000 mm	N/A	High wing, cantilever	V tail	Single pusher

## 2.2. Configuration Design

### 2.2.1. Comparative Study of Airplanes with Similar Mission Performance

#### 2.2.1.1. Comparison of Weights, Performance and Geometry of Similar Airplanes.

Table 6. Comparison of mission specifications and configurations of similar aircraft

Name	Weight	Payload	Cruise Speed	Range	Endurance	Wing	Tail	Motor
AliExpress SkyEye	28 kg	14 kg	100 km/h	N/A	2 hours	High wing, cantilever	Single-boom V	2xWing mounted puller
Applied Aeronautics Albatross	10 kg	4.4 kg	64 km/h	100 km	5 hours	High wing, cantilever	Twin-boom inverted V	Single pusher
Optimum Solutions Condor 300	18 kg	6 kg	90 km/h	N/A	4 hours	Low wing, cantilever	T-Tail	2xWing mounted puller
Optimum Solutions Leonardo	5.5 kg	N/A	45 km/h	30 km	4 hour	High wing, cantilever	Single-boom V	Single pusher
Penguin BE Electric	21.5 kg	6.6 kg	79 km/h	N/A	1.86 hours	High wing, cantilever	Twin-boom inverted V	Single pusher
RQ-11 Raven	1.9 kg	0.2 kg	81 km/h	10 km	1.5 hours	High wing, cantilever	Conventional cruciform	Single pusher
RQ-14 Dragon Eye	2.7 kg	N/A	65 km/h	5 km	1 hour	High wing, cantilever	Rudder only	Wing mounted puller
RQ-20 Puma	6.3 kg	N/A	80 km/h	20 km	3 hours	High wing, cantilever	Conventional cruciform	Single puller
Bye Aerospace Silent Falcon	14.5 kg	3 kg	90 km/h	15 km	5 hours	High wing, cantilever	Conventional cruciform	Single puller
SkyPro V200	5 kg	.9 kg	65 km/h	20 km	3 hours	High wing, cantilever	V tail	Single pusher

#### 2.2.1.2. Configuration Comparison of Similar Airplanes

#### 2.2.1.2.1. AliExpress SkyEye



Figure 4. Image of AliExpress SkyEye

#### 2.2.1.2.2. Applied Aeronautics Albatross



Figure 5. Image of Applied Aeronautics Albatross

#### 2.2.1.2.3. Optimum Solutions Condor 300



Figure 6. Image of Optimum Solutions Condor 300

#### 2.2.1.2.4. Optimum Solutions Leonardo



Figure 7. Image of Optimum Solutions Leonardo

#### 2.2.1.2.5. Penguin BE Electric



Figure 8. Image of Penguin BE Electric

#### 2.2.1.2.6. RQ-11 Raven



Courtesy of AeroVironment Inc

Figure 9. Image of RQ-11 Raven

2.2.1.2.7. RQ-14 Dragon Eye



Figure 10. Image of RQ-14 Dragon Eye

2.2.1.2.8. RQ-20 Puma



Figure 11. Image of RQ-20 Puma

#### 2.2.1.2.9. Bye Aerospace Silent Falcon



Figure 12. Image of Bye Aerospace Silent Falcon

#### 2.2.1.2.10. SkyPro V200



Figure 13. Image of SkyPro V200

#### 2.2.1.2.11. Discussion

A common theme in the design of these UAVs is the wing placement. Almost all the aircraft with the exception of the Condor 300 utilize a high wing configuration. This is not surprising as the high wing configuration allows for the simplification of the cargo area design and efficient usage of the area.

The engine selection and placement between the aircraft are also similar. In this case, the Condor 300, Dragon Eye and Skyeye are the exception. These aircraft employ multiple wing mounted motors due to either their size or speed requirement. Most aircraft employ a single motor in either push or pull (tractor) configuration. In general, the pusher configuration aircraft employ some sort of V-tail to ensure smooth, laminar airflow is achieved on the empennage.

## 2.2.2. Configuration Selection

### 2.2.2.1. Overall Configuration

The overall configuration will be a conventional design, meaning a single fuselage with a forward mounted wing and traditional empennage in the rear. This configuration was chosen for its simplicity and ease of design, which will allow for the implantation of a modular design philosophy.

### 2.2.2.2. Wing Configuration

A high wing configuration was chosen in order to maximize the cargo volume and capacity for the attack and resupply missions. The high wing configuration also allows for the implementation of an airborne cargo delivery system and ideal camera and sensor placement for the surveillance mission. Lastly, the high wing configuration will allow for a wide variety of engine/motor sizes, providing for greater flexibility in propulsion selection.

### 2.2.2.3. Empennage Configuration

A conventional cruciform empennage configuration was chosen ~~in order~~ to simplify structural design and control integration. **AS ROSKAM LIKES TO SAY: THE WORDS "IN ORDER" ARE ALMOST ALWAYS OUT OF ORDER...(YOU DON'T NEED THEM HERE)**

### 2.2.2.4. Integration of the Propulsion System

The propulsion system will be wing mounted in engine nacelles. This will provide ample flexibility in engine placement and sizing.

### 2.2.2.5. Landing Gear Disposition

A tricycle landing gear is chosen for its inherent stability and advantages during takeoff and landing, allowing for greater rotation compared to a tail-dragger configuration. The landing gear will be fixed for simplicity. In the event that the speed requirements are not able to be met, a retractable configuration will be considered to reduce drag.

## 2.3. Weight Sizing & Weight Sensitivities

In this section, the weight sizing of the aircraft will be conducted in order to correctly estimate the takeoff weight and empty weight. These weights can further be broken down into various components in order to provide for a rough estimate for the size and magnitude of the aircraft.

### 2.3.1. Mission Weight Estimates

#### 2.3.1.1. Data Base for Takeoff Weights and Empty Weights of Similar Airplanes

Table 7. Takeoff, empty, and payload weight of similar aircraft

Name	Takeoff Weight	Empty Weight	Engine Weight	Structure Weight	Max Payload Weight	Max Fuel Weight	Max Fuel + Payload
C-130	70305	34274	3132	31142	19958	27216	36031
C-5	381000	172371	14520	157851	122470	154880	208629
C-17	265350	128100	12884	115216	77520	107644	137250
737	79002	41413	4781	36632	17955	21000	37589
777	351533	167829	17528	150301	102000	136928	183704
787	227930	119950	12295	107655	41440	100968	107980
MQ-9	4760	2223	151	2072	1701	1814	2537
MQ-1	1020	512	78	434	204	300	508
RQ-4	14628	6781	762	6019	1360	7847	7847
B-52	220000	83250	16872	66378	31500	145288	136750

#### 2.3.1.2. Determination of Regression Coefficients A and B

The regression coefficients are calculated based on the empty and takeoff weights of the similar aircraft database shown above. The regression coefficients will demonstrate the correlation between the takeoff weight and the empty weight, which could then be used to determine a weight for any similar aircraft. The table above lists various aircraft with similar configuration and mission designs. These aircraft were chosen irrelevant of their propulsion design as the goal is to determine the structural weight of the aircraft. The total weight of the aircraft will be calculated after determining the battery requirements. The relationship between the takeoff weight and empty weight for the proposed aircraft is given by Equation (2) and rearranged to Equation (3) to compare to the trend line.

$$\log W_{TO} = A + B \log W_E \quad (1)$$

$$\log W_E = (\log W_{TO} - A) / B \quad (2)$$

Comparing the Equation (1) and (3), the following relationship exists:

$$y = \log W_E \quad (3)$$

$$x = \log W_{TO} \quad (4)$$

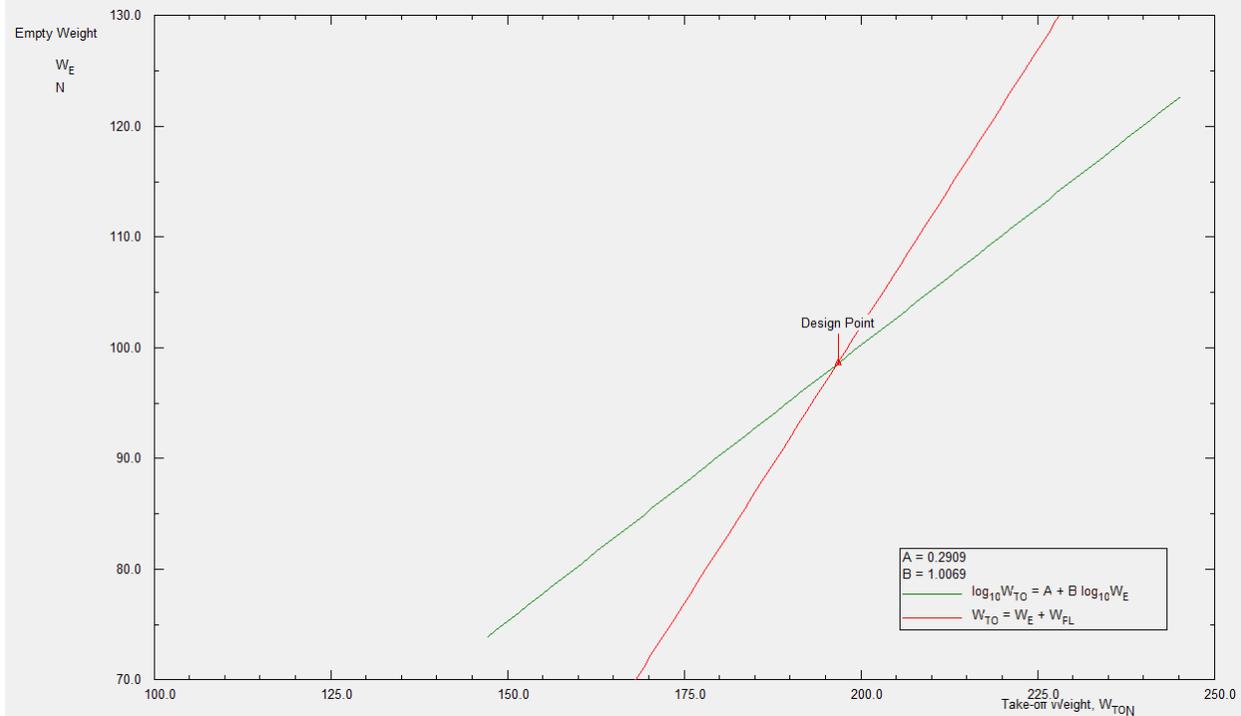


Figure 14. Log-log plot of aircraft weights

Takeoff Weight	196.8 N (20.06 kg)
Empty Weight	98.7 N (10.06 kg)
Payload Weight	98.1 N (10 kg)
A	0.2909
B	1.0069

### 2.3.1.3. Determination of Mission Weights

In order to determine the mission weight, i.e. the battery weight, we must calculate the empty weight of the aircraft based on the proposed payload weight and maximum theoretical takeoff weight of the aircraft as limited by the FAA (22 kg or 55 lbs.). The takeoff weight can be simplified as into the weight components below.

$$W_{TO} = W_{Payload} + W_{Empty} + W_{Battery} \quad (5)$$

The empty weight can be approximated by using Roskam's estimates for class I sizing of aircraft components that make up the gross weight.

	McDonnell-Douglas		Boeing		Ourania
	DC-9-30	MD-80	737-200	727-100	Average
Pwr Plt/GW	0.076	0.079	0.071	0.078	0.076
Fix Eqp/GW	0.175	0.182	0.129	0.133	0.155
Empty Wht/GW	0.538	0.564	0.521	0.552	0.544
Wing Grp/GW	0.106	0.111	0.092	0.111	0.105
Emp. Grp/GW	0.026	0.024	0.024	0.026	0.025
Fus. Grp/GW	0.103	0.115	0.105	0.111	0.109
Nac. Grp/GW	0.013	0.015	0.012	0.024	0.016
Gear Grp/GW	0.039	0.038	0.038	0.045	0.040

Figure 15. Jet transport weight fractions

We are able to utilize the weight fractions from Roskam due to the similarity of our aircraft with the jet transport examples used to calculate the fractions. The maximum allowable gross weight will be used to determine the weight fractions of each component. Changes will be made to the weight fractions for the power plant and empty weight utilizing the weight database from Table 7.

Table 8. Component weight fractions and resultant weight

Component	Weight Fraction	Weight (kg)
Power Plant	0.053	1.166
Fixed Equipment	0.155	3.41
Wing	0.105	2.31
Empennage	0.025	0.55
Fuselage	0.109	2.398
Nacelles	0.016	0.352
Landing Gear	0.040	0.88
	Total	11.066 (108.55 N)

This results in an estimated empty weight,  $W_e$ , of 11.066 kg and a structural weight,  $W_{structure}$ , of 6.49 kg.

The fixed equipment and power plant weight can be further estimated through the selection of components in order to give a rough idea on their impact to the weight of the aircraft. The table below lists various common required equipment for electric aircraft of this scale.

Table 9. Fixed equipment weight estimation

Component	Specification	Weight (g)
Aileron 1	HobbyKing Mi Digital High Torque Servo	60
Aileron 2	HobbyKing Mi Digital High Torque Servo	60
Flap 1	HobbyKing Mi Digital High Torque Servo	60
Flap 2	HobbyKing Mi Digital High Torque Servo	60

Rudder	HobbyKing Mi Digital High Torque Servo	60
Elevator	HobbyKing Mi Digital High Torque Servo	60
Engine 1	Turnigy SK3 Fandrive - 3994-850kv	544
Engine 2	Turnigy SK3 Fandrive - 3994-850kv	544
Fan 1	Jetfan 120mm ECO EDF	333
Fan 2	Jetfan 120mm ECO EDF	333
ESC 1	AeroStar Advance 150A HV Brushless ESC	123
ESC 2	AeroStar Advance 150A HV Brushless ESC	123
Battery	Vant Battery 4x12S 44.4V 4x4500mAh 45C	6472
Receiver	AR6600T 6 Ch Air Integrated Telemetry Receiver	13
	Total	8845
	Total (w/o battery and power plant)	619

Table 10. Revised weight fractions

Component	Weight Fraction	Weight (kg)
Power Plant		1.754
Fixed Equipment		0.619
Wing	0.105	2.31
Empennage	0.025	0.55
Fuselage	0.109	2.398
Nacelles	0.016	0.352
Landing Gear	0.040	0.88
	Total	9.743 (95.58 N)

Utilizing this fixed equipment weight, the revised empty weight,  $W_e$ , of the aircraft is estimated to be 9.743 kg. Utilizing Equation 5, the allowable battery weight,  $W_{\text{Battery}}$ , is calculated to be 3.257 kg. This is less than the specified battery in Table 9. It must be noted that the weight fractions employed by Roskam are based on the assumption of a traditional, metal construction. This difference can be accommodated through the planned use of 3D printing and composite materials. Roskam states a 15% reduction in structural weight is a conservative estimate and readily achievable. This would result in a reduction of 0.9735 kg from the structure, increasing allowable battery weight to 4.23 kg.

#### 2.3.1.4. Takeoff Weight Sensitivities

##### 2.3.1.4.1. Calculation of Takeoff Weight Sensitivities using the AAA Program

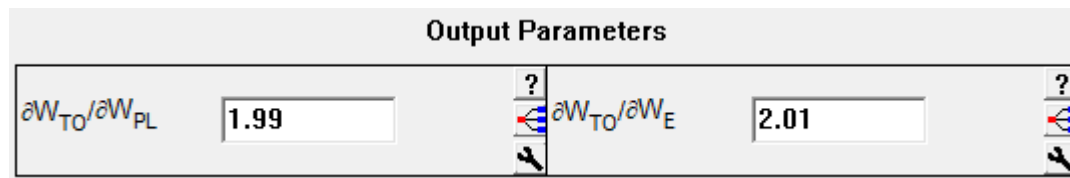


Figure 16. Takeoff weight sensitivities

##### 2.3.1.4.2. Trade Studies

## 2.4. Performance Constraint Analysis

In this section, the performance of the aircraft will be determined in order to size the propulsion system and wing. These key elements will dictate the performance and design of the rest of the aircraft.

### 2.4.1. Calculation of Performance Constraints

The calculation of the performance constraints will mainly be completed through the use of the Advanced Aircraft Analysis (AAA) program.

#### 2.4.1.1. Stall Speed

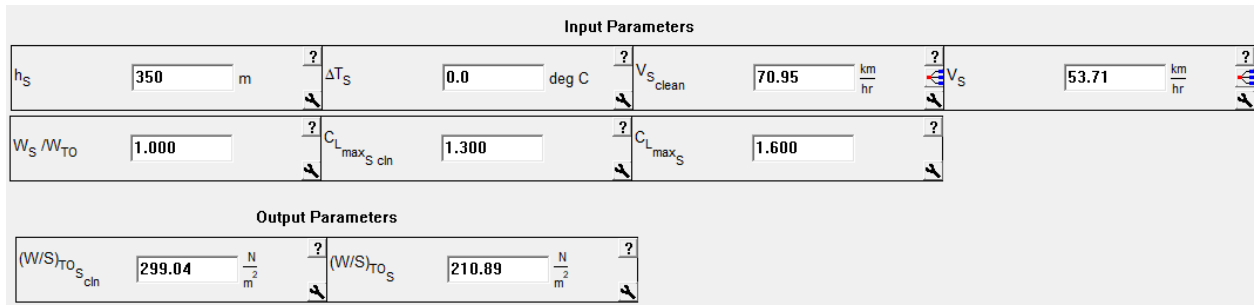


Figure 17. Stall speed constraint (attack configuration)

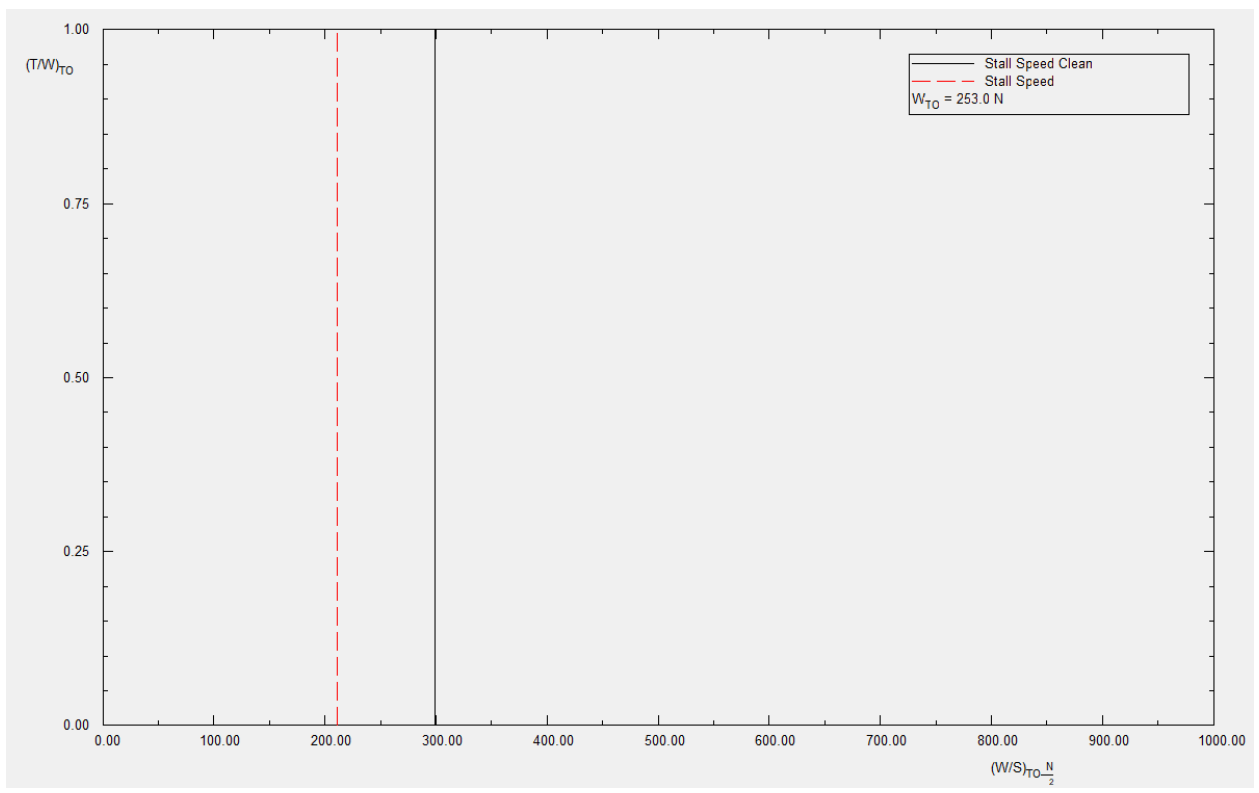


Figure 18. Stall speed constraint plot (attack/surveillance/resupply configuration)

### 2.4.1.2. Takeoff Distance

Input Parameters					
$h_{TO}$	<input type="text" value="0"/> m	$F_{TO}$	<input type="text" value="0.900"/>	$\Delta T_{TO}$	<input type="text" value="0.0"/> deg C
$S_{TO}$	<input type="text" value="300"/> m	$C_{L_{max_{TO}}}$	<input type="text" value="1.500"/>	Plot $\Delta C_{L_{max}}$	<input type="text" value="0.200"/>

Figure 19. Takeoff distance constraint (attack/surveillance/resupply configuration)

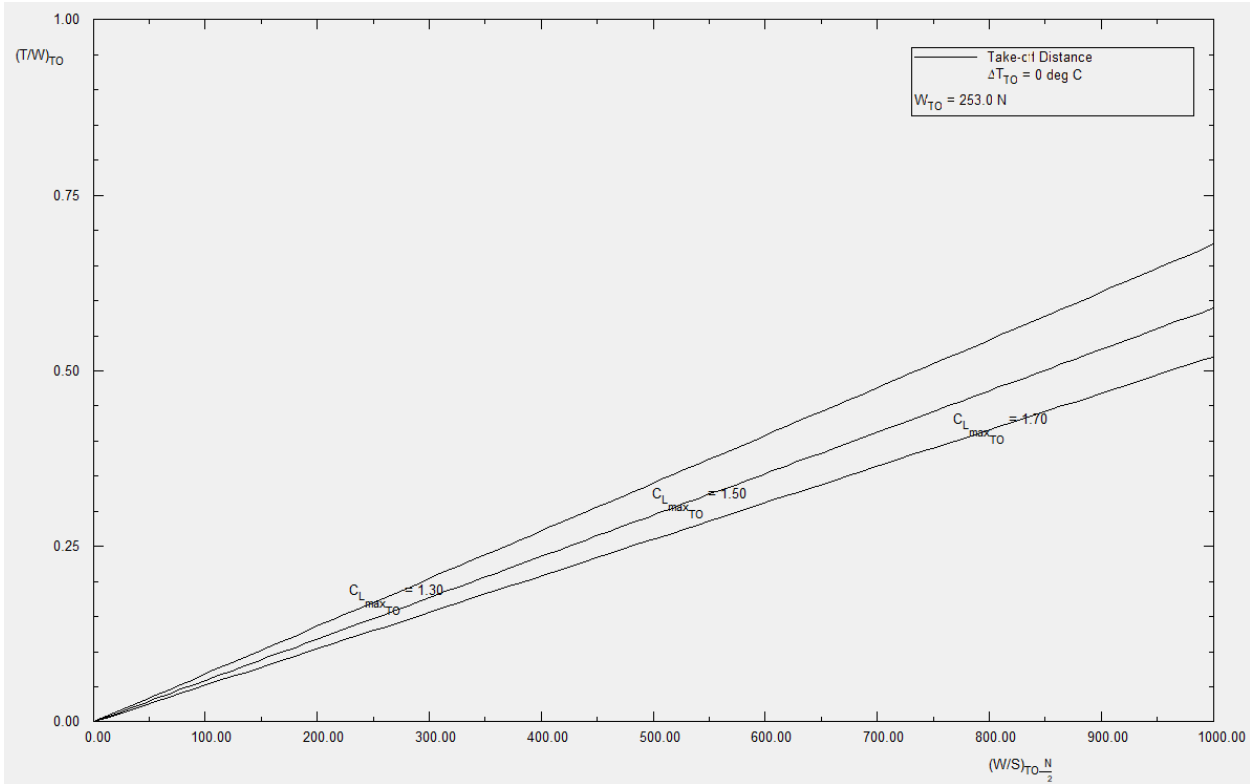


Figure 20. Takeoff distance constraint plot (attack/surveillance/resupply configuration)

### 2.4.1.3. Landing Distance

Input Parameters					
$h_L$	<input type="text" value="0"/> m	$\Delta T_L$	<input type="text" value="0.0"/> deg C	$W_L / W_{TO}$	<input type="text" value="1.000"/>
$C_{L_{max_L}}$	<input type="text" value="1.400"/>	Plot $\Delta C_{L_{max}}$	<input type="text" value="0.200"/>	$S_L$	<input type="text" value="262"/> m
Output Parameters					
$S_{FL}$	<input type="text" value="437"/> m	$(W/S)_L$	<input type="text" value="641.16"/> $\frac{N}{m^2}$		

Figure 21. Landing distance speed constraint (surveillance configuration)

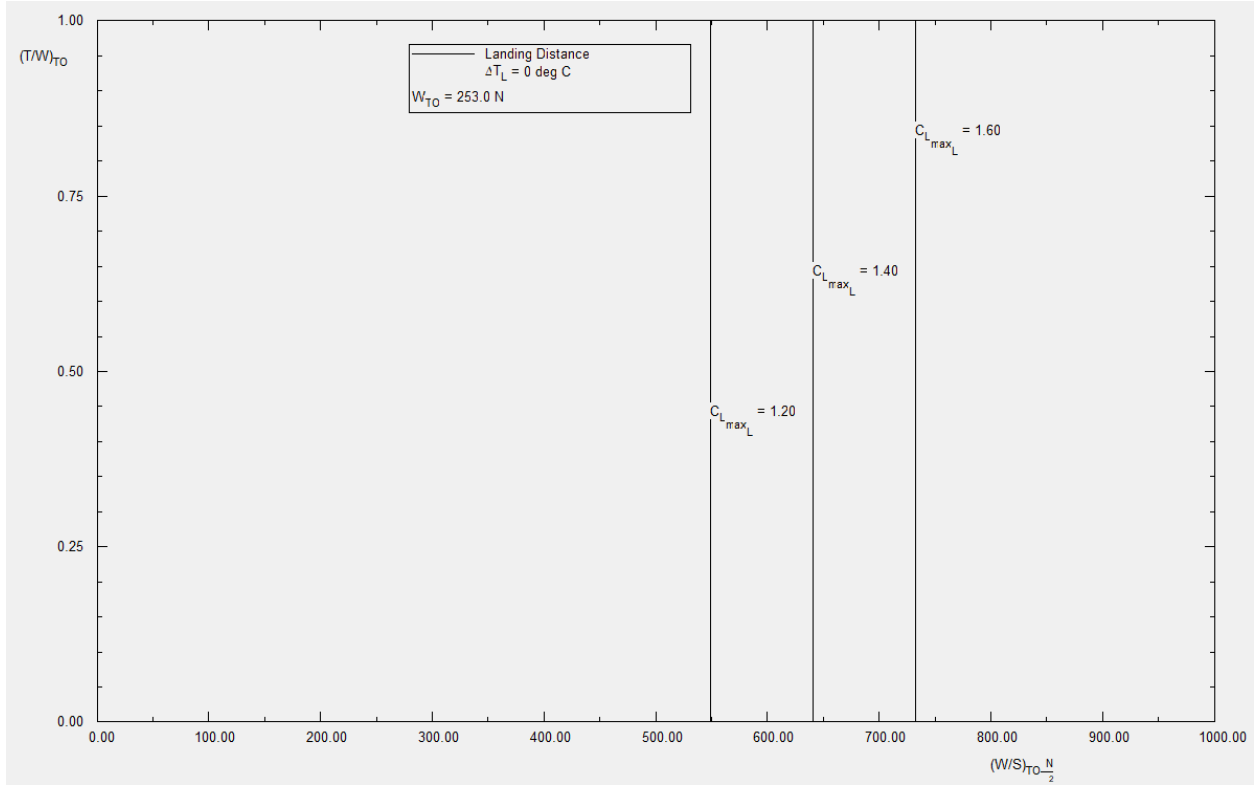


Figure 22. Landing distance speed constraint plot (surveillance configuration)

Input Parameters					
$h_L$	0 m	$\Delta T_L$	0.0 deg C	$W_L / W_{TO}$	0.600
$C_{L_{max_L}}$	1.400	Plot $\Delta C_{L_{max}}$	0.200	$S_L$	262 m
Output Parameters					
$S_{FL}$	437 m	$(W/S)_L$	1068.60 $\frac{N}{m^2}$		

Figure 23. Landing distance speed constraint (resupply configuration)

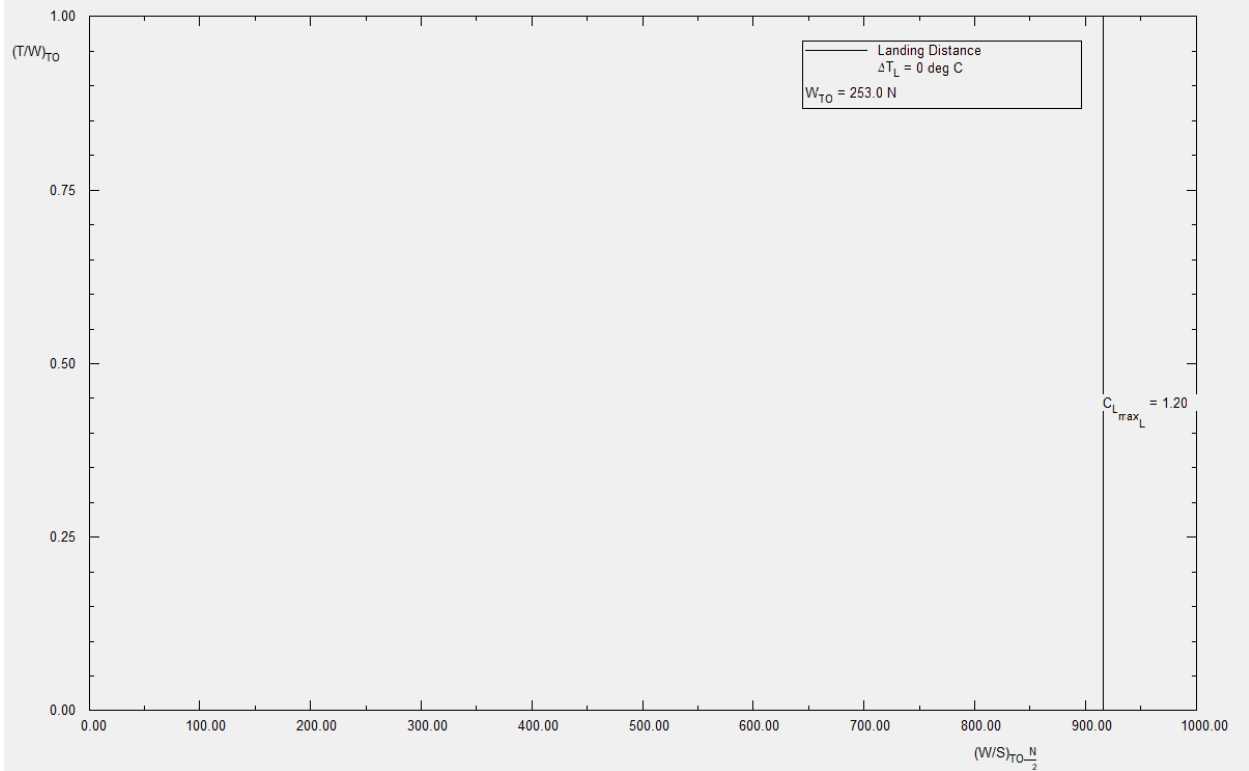


Figure 24. Landing distance speed constraint plot (resupply configuration)

### 2.4.1.4. Drag Polar Estimation

Input Parameters									
$W_{TO}$	253.0 N	$AR_w$	10.00	$b$	1.0000	$d$	0.7531	$\Delta C_{D_{o\_clean}}$	0.0000
$S_w$	0.90 m <sup>2</sup>	$a$	-2.5229	$c$	0.0199	$e_{clean}$	0.8000	$C_{L_{plot\_min}}$	
Output Parameters									
$S_{wet}$	2.04 m <sup>2</sup>	$f$	0.01 m <sup>2</sup>	$C_{D_{o\_clean}}$	0.0068	$C_{D_{o\_clean,M}}$	0.0068	$B_{DP\_clean}$	0.0398

Figure 25. Drag polar estimation (attack configuration)

Input Parameters									
$W_{TO}$	253.0 N	$AR_w$	14.00	$b$	1.0000	$d$	0.7531	$\Delta C_{D_{o\_clean}}$	0.0000
$S_w$	0.90 m <sup>2</sup>	$a$	-2.5229	$c$	0.0199	$e_{clean}$	0.8000	$C_{L_{plot\_min}}$	
Output Parameters									
$S_{wet}$	1.69 m <sup>2</sup>	$f$	0.01 m <sup>2</sup>	$C_{D_{o\_clean}}$	0.0039	$C_{D_{o\_clean,M}}$	0.0039	$B_{DP\_clean}$	0.0284

Figure 26. Drag polar estimation (surveillance/resupply configuration)

### 2.4.1.5. Climb Constraints

Input Parameters							
$F_{MaxCont}$	0.800	$C_{L_{max_A}}$	1.000	$e_{clean}$	0.8000	$e_L$	0.7500
$F_{8sec}$	0.800	$C_{L_{max_L}}$	1.400	$C_{D_{0_{clean,M}}}$	0.0039	$C_{D_{0_L_{down}}}$	0.0542
$C_{L_{max_{clean}}}$	1.100	$W_L/W_{TO}$	1.000	$e_{TO}$	0.7500	$\Delta C_{D_{0_A}}$	
$C_{L_{max_{TO}}}$	1.500	$AR_w$	10.00	$C_{D_{0_{TO_{down}}}}$	0.0342	$C_{D_{wm}}$	
Output Parameters							
$B_{DP_{clean}}$	0.0398	$B_{DP_{TO_{down}}}$	0.0424	$B_{DP_{L_{down}}}$	0.0424		

Figure 27. Climb constraint (attack configuration)

Input Parameters							
$F_{MaxCont}$	0.800	$C_{L_{max_A}}$	1.000	$e_{clean}$	0.8000	$e_L$	0.7500
$F_{8sec}$	0.800	$C_{L_{max_L}}$	1.400	$C_{D_{0_{clean,M}}}$	0.0039	$C_{D_{0_L_{down}}}$	0.0542
$C_{L_{max_{clean}}}$	1.100	$W_L/W_{TO}$	1.000	$e_{TO}$	0.7500	$\Delta C_{D_{0_A}}$	
$C_{L_{max_{TO}}}$	1.500	$AR_w$	14.00	$C_{D_{0_{TO_{down}}}}$	0.0342	$C_{D_{wm}}$	
Output Parameters							
$B_{DP_{clean}}$	0.0284	$B_{DP_{TO_{down}}}$	0.0424	$B_{DP_{L_{down}}}$	0.0424		

Figure 28. Climb constraint (surveillance/resupply configuration)

### 2.4.1.6. Speed Constraints

Input Parameters							
$h_{cr}$	350 m	$V_{Cr_{max}}$	240.00 km/hr	$AR_w$	11.00	$e_{clean}$	0.8000
$F_{Cr}$	0.600	$W_{Cr}/W_{TO}$	1.000	$C_{D_{0_{clean,M}}}$	0.0042	$\eta_{prop}$	0.800
Output Parameters							
$M_{Cr_{max}}$	0.197	$B_{DP_{clean}}$	0.0362				

Figure 29. Cruise speed constraint (attack configuration)

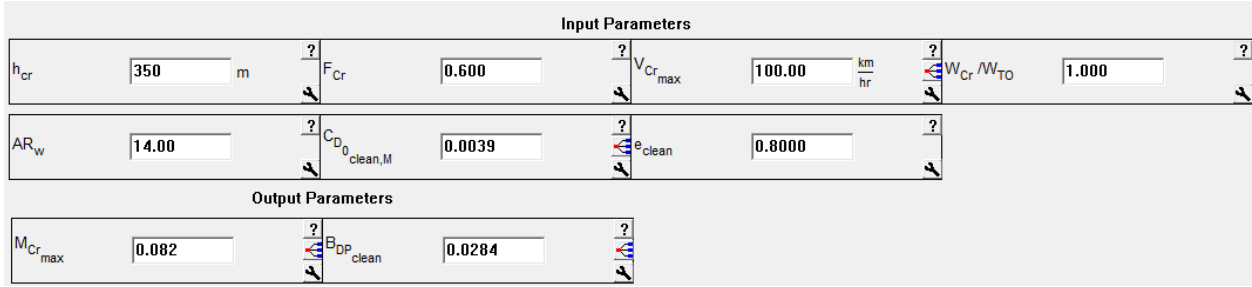


Figure 30. Cruise speed constraint (surveillance configuration)

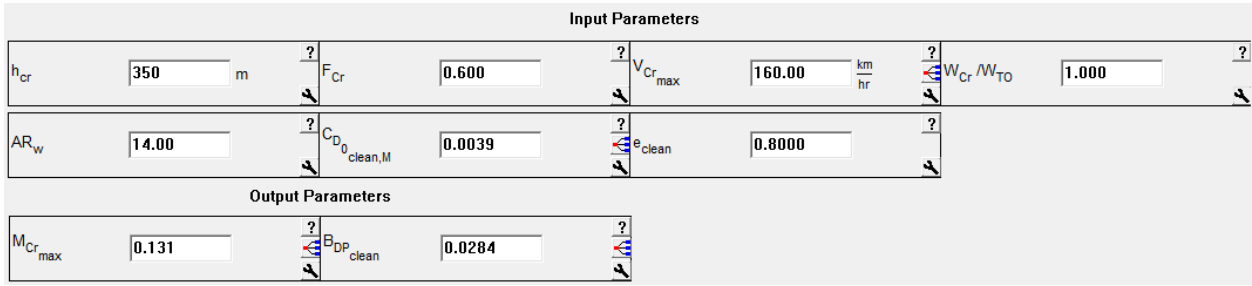


Figure 31. Cruise speed constraint (resupply configuration)

### 2.4.1.7. Summary of Performance Constraints

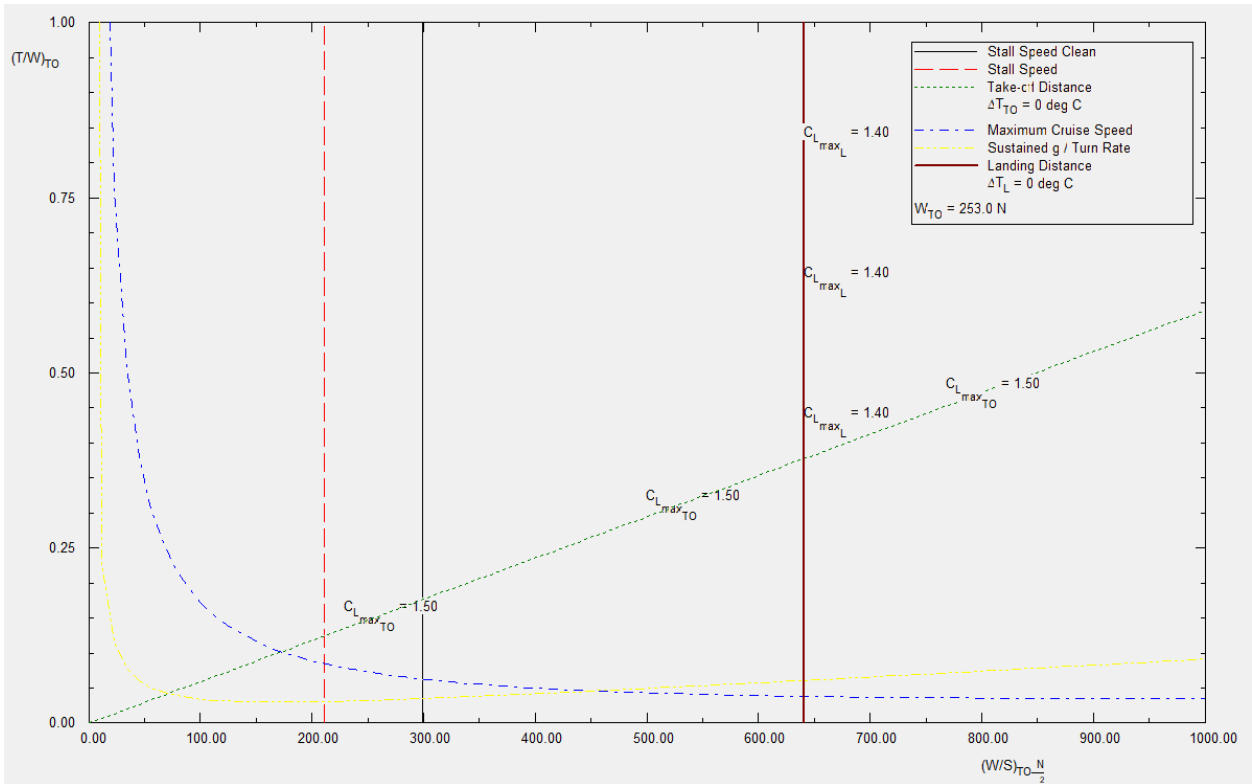


Figure 32. Matching plot (attack configuration)

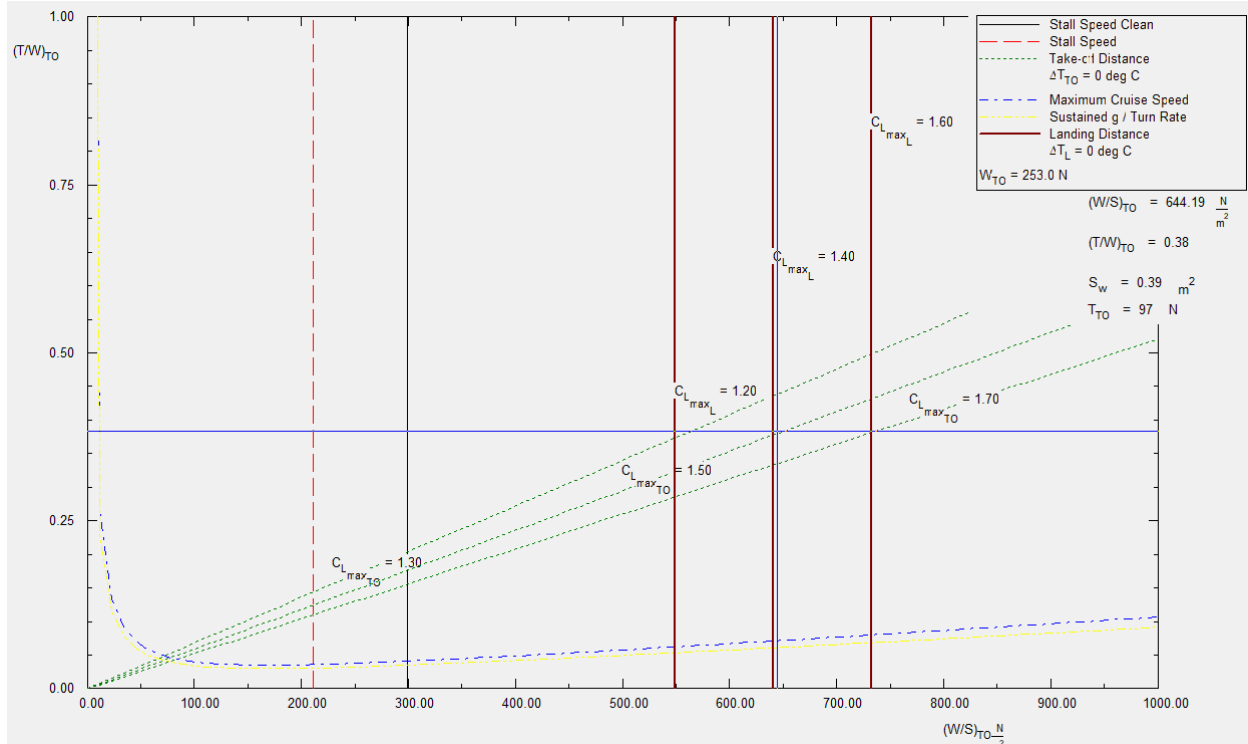


Figure 33. Matching plot (surveillance /resupply configuration)

## 2.4.2. Selection of Propulsion System

### 2.4.2.1. Selection of the Propulsion System Type

A ducted fan propulsion was chosen due to its efficiency over propeller systems and cost effectiveness vs. turbojet/turbofan. In particular, it will be an electric ducted fan (EDF) which is popular in the remote controlled aircraft community, where it enjoys high levels of development and offers vast amounts of experience and support. An EDF operates very similarly to a turbofan engine. This is the reason the power sizing was complete in terms of thrust vs. power, the metric most common in electric propulsion.

### 2.4.2.2. Selection of the Number of Engines

From the readily available EDF systems on the market, it is clear that a minimum of 2 systems will be needed to generate the required thrust to achieve the performance criteria set in the mission specifications. From the research into available systems, a pair of high performance 120mm EDF systems will be needed to generate the nearly 10 kg of thrust. An online calculator with a database of commercially available electric motors and fan systems was utilized to estimate the thrust output of various combinations and power requirements.

<b>General</b>	Model Weight: 22000 g incl. Drive 776 oz	# of Motors: 2 (on same Battery)	Wing Area: 100 dm <sup>2</sup> 1550 in <sup>2</sup>	Drag: simplified 0.05 Cd	Cross Section: 0 dm <sup>2</sup> 0 in <sup>2</sup>	Field Elevation: 0 m ASL 0 ft ASL	Air Temperature: 20 °C 68 °F	Pressure (QNH): 1013 hPa 29.91 inHg
<b>Battery Cell</b>	Type (Cont. / max. C) - charge state: LiPo 4200mAh - 55/80C - normal	Configuration: 10 S 1 P	Cell Capacity: 4200 mAh 4200 mAh total	max. discharge: 85%	Resistance: 0.0029 Ohm	Voltage: 3.7 V	C-Rate: 55 C cont. 80 C max	Weight: 113 g 4 oz
<b>Controller</b>	Type: max 300A	Current: 300 A cont. 300 A max	Resistance: 0.0008 Ohm	Weight: 390 g 13.8 oz	Wire extension battery: AWG10=5.27mm <sup>2</sup>	Length: 0 mm 0 inch	Wire extension motor: AWG10=5.27mm <sup>2</sup>	Length: 0 mm 0 inch
<b>Motor</b>	Manufacturer - Type (Kv) - Cooling: HET (Typhoon) - 700-98-1170 (1170) excellent	KV (w/o torque): 1170 rpm/V Prop-Kv-Wizard	no-load Current: 2.3 A @ 12 V	Limit (up to 15s): 4800 W	Resistance: 0.0071 Ohm	Case Length: 98 mm 3.86 inch	# mag. Poles: 4	Weight: 560 g 19.8 oz
<b>Ducted Fan</b>	Type: Ejets Jetfan120 ECO (120mm)	Thrust Duct for: 100 % FSA	Flight Speed: 160 km/h 99.4 mph	Gear Ratio: 1 : 1	<input type="button" value="calculate"/>			

Figure 34. Inputs for online thrust calculator

<b>Battery</b>	<b>Motor @ Optimum Efficiency</b>	<b>Motor @ Maximum</b>	<b>Ducted Fan</b>	<b>Total Drive</b>	<b>Airplane</b>
Load: 94.82 C Voltage: 25.45 V Rated Voltage: 37.00 V Energy: 155.4 Wh Total Capacity: 4200 mAh Used Capacity: 3570 mAh min. Flight Time: 0.5 min Mixed Flight Time: 0.7 min Weight: 1130 g 39.9 oz	Current: 126.37 A Voltage: 29.57 V Revolutions*: 33547 rpm electric Power: 3736.6 W mech. Power: 3520.7 W Efficiency: 94.2 %	Current: 199.12 A Voltage: 25.29 V Revolutions*: 27937 rpm electric Power: 5036.1 W mech. Power: 4681.2 W Efficiency: 93.0 % est. Temperature: 47 °C 117 °F  Wattmeter readings Current: 398.24 A Voltage: 25.45 V Power: 10135.2 W	Static Thrust: 7713 g 272.1 oz Revolutions*: 27937 rpm Thrust @ Speed: 3723 g 131.3 oz Jet Efflux: 309.2 km/h 85.9 m/s 192.1 mph 281.8 ft/s specific Thrust: 1.53 g/W 0.05 oz/W	Drive Weight: 3333 g 117.6 oz Power-Weight: 670 W/kg 304 W/lb Thrust-Weight: 0.70 : 1 Current @ max: 398.24 A P(in) @ max: 14734.9 W P(out) @ max: 7021.8 W Efficiency @ max: 47.7 % Torque: 1.60 Nm 1.18 lbf.ft	All-up Weight: 22000 g 776 oz Wing Load: 220 g/dm <sup>2</sup> 72.1 oz/ft <sup>2</sup> Cubic Wing Load: 22.0 est. Stall Speed: 68 km/h 42 mph est. Speed (level): 237 km/h 147 mph est. Speed (vertical): - km/h - mph est. rate of climb: 13.4 m/s 2640 f/min

Figure 35. Outputs for online thrust calculator

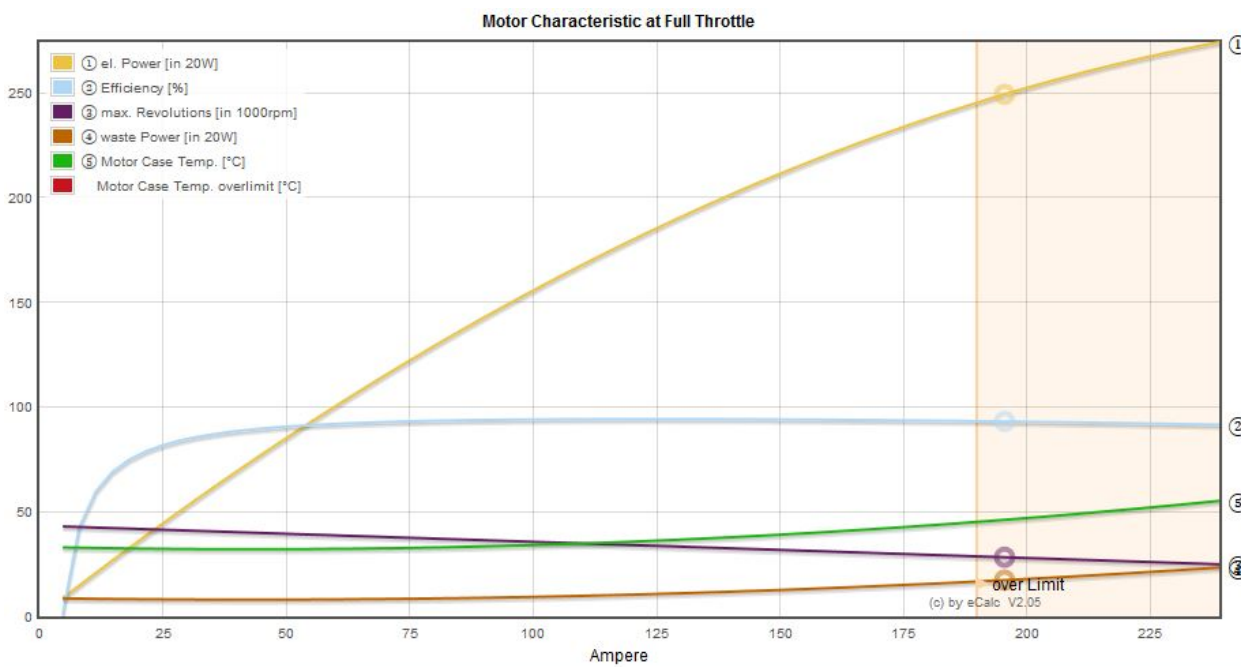


Figure 36. Motor characteristics at max throttle

### 2.4.3. Discussion

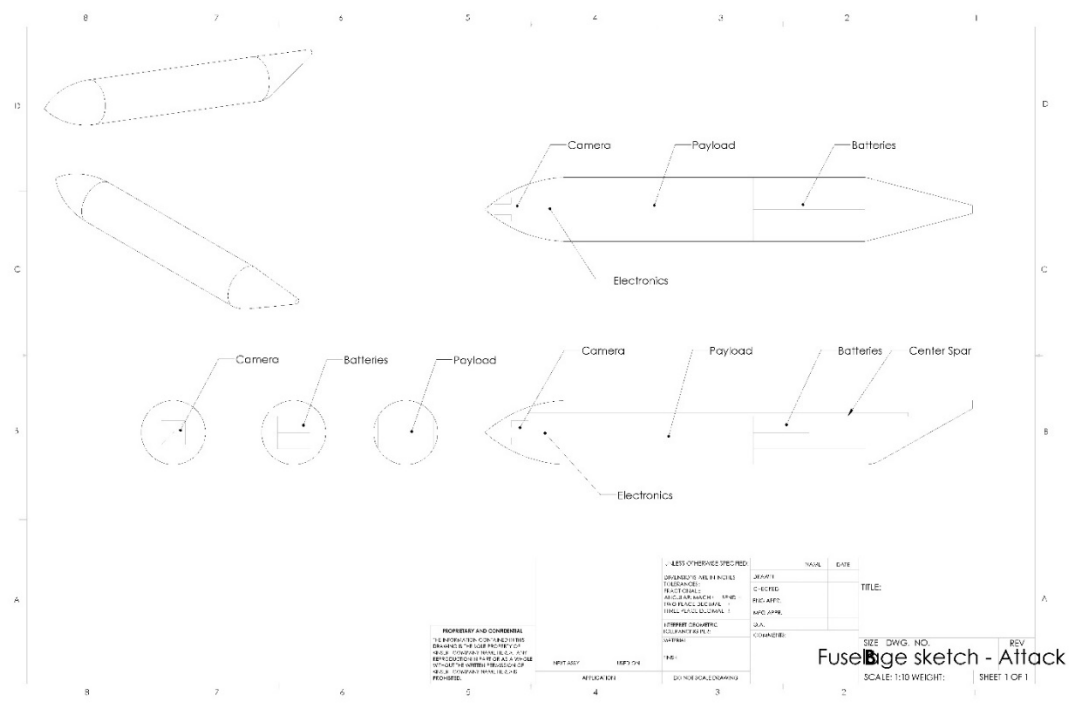
The results for the performance constraint analysis seem to corroborate with what is expected. The takeoff and landing performance is dictating the thrust and wing sizing. Interestingly enough, the cruise speed requirement is a non-factor. This revelation is somewhat expected as the payload requirement has a large impact on the weight sizing, which in turn affects the takeoff and landing performance.

It is interesting to note the outputs from the thrust calculator. Utilizing the proposed EDF and motor, it calculates a maximum speed of 237 kmh, slightly lower than the design cruise speed of the attack configuration. This number is not accurate as the calculator utilizes a fixed Cd of 0.05 when the estimated drag polar puts the drag of the aircraft at cruise at nearly half this amount. This should raise the maximum speed considerably.

## 2.5. Fuselage Design

### 2.5.1. Layout Design of the Fuselage

The fuselage layout will be determined based on the mission configuration in respect to the center of gravity of the aircraft. As the payload is the largest single component to the weight and center of gravity of the aircraft, its purpose during each mission must be considered for its optimum placement to be determined. In the attack mission, the payload does not need to be removed or dropped, thus the payload will be moved in front of the battery for better CG placement. For the resupply mission, the payload is expected to be removed and the aircraft flown without the payload. Setting the payload behind the battery allows for a forward CG location after the payload is removed.





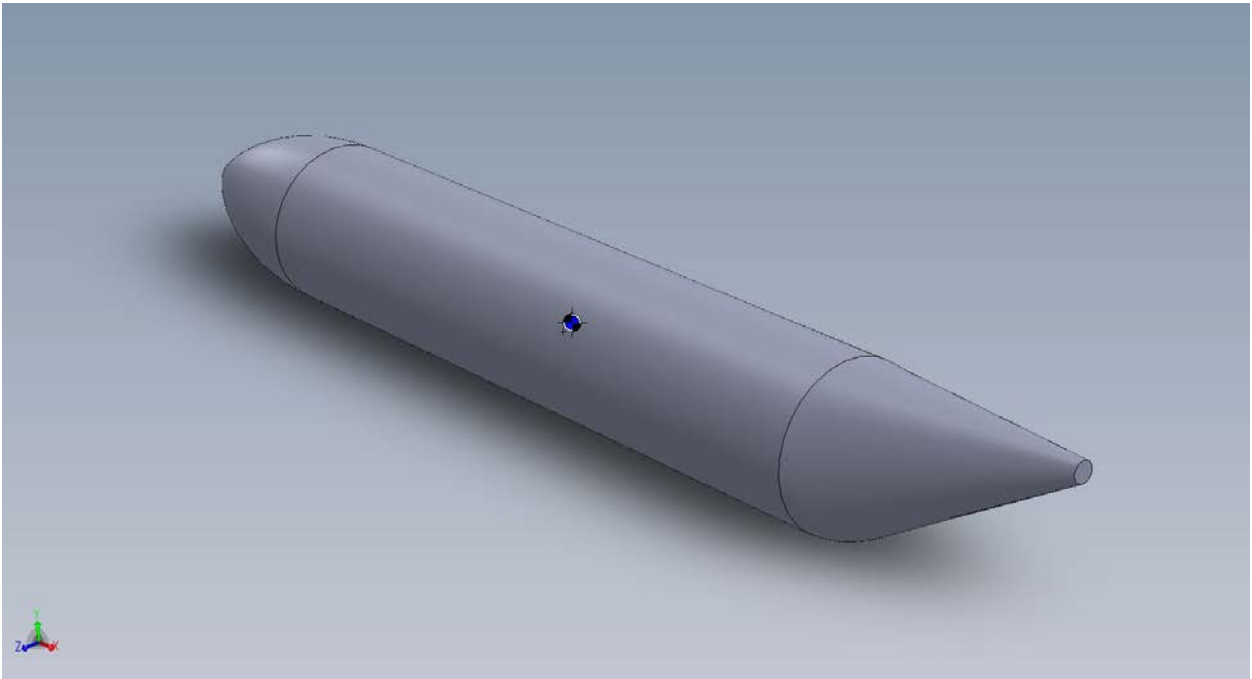


Figure 40. Rear isometric view of fuselage

The payload compartment is designed to be able to house the warhead of a Hellfire missile. Available information places the warhead dimensions at 178 mm in diameter and 510 mm in length. The chosen batteries are approximately 45x45x310mm. The aircraft will utilize four in parallel. The nose cone and tail cone are approximately 200 and 300 mm, respectively.

## 2.6. Wing, High-Lift System & Lateral Control Design

### 2.6.1. Wing Planform Design

From Chapter 2.4, we know the following wing parameters: gross wing area and aspect ratio. This will allow us to determine the basic shape of the wing. From the configuration selection, we know this wing will be a cantilever, high wing configuration for all missions. For all three missions, the wing area will remain the same but the aspect ratio will vary. The selected wing area based on the performance constraint analysis is 0.39 meters squared. The Attack mission will utilize an aspect ratio of 10 while the Reconnaissance/Surveillance and Resupply missions will utilize an aspect ratio of 14.

The wing will not be swept for structural and aerodynamic considerations. It will however be tapered. Tapering the wing will reduce wing bending moment by altering the efficiency and lift distribution of the wing. A taper ratio of 0.5 should be sufficient and is within the range based on aircraft of similar configuration and mission. Naturally, tapering the wing will lead to a leading edge sweep but the change should be insignificant.

Due to the high wing configuration of the aircraft, dihedral angle is not needed as the aircraft will be inherently roll stable. The removal of dihedral angle also allows for simplified construction and structural design. It allows for a continuous spar to span between the wings.

**Input Parameters**

$AR_w$	10.00	$S_w$	0.39 m <sup>2</sup>	$\lambda_w$	0.50
$\Lambda_{c/4_w}$	0.0 deg	$X_{apex_w}$	0.00 m	$Y_{offset_w}$	0.00 m

**Output Parameters**

$c_{r_w}$	0.26 m	$b_w$	1.97 m	$y_{mgc_w}$	0.44 m	$\Lambda_{LE_w}$	1.9 deg
$c_{t_w}$	0.13 m	$\bar{c}_w$	0.20 m	$x_{mgc_w}$	0.01 m	$\Lambda_{TE_w}$	-5.7 deg

**Straight Tapered Wing Geometry: Output Parameters**

Panel	$c_r$ m	$c_t$ m	$X_r$ m	$X_t$ m	$Y_r$ m
1	0.2633	0.1317	0.0000	0.0329	0.0000

Figure 41. Attack configuration wing inputs

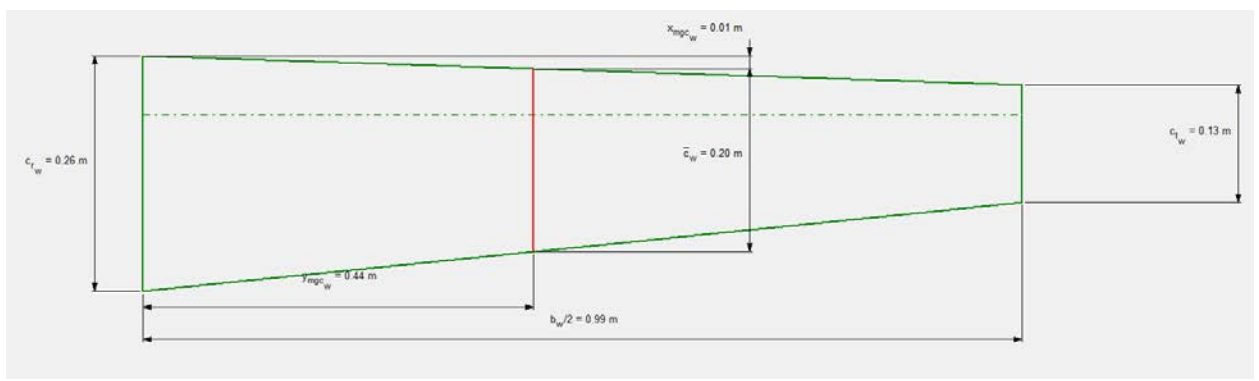


Figure 42. Attack configuration wing drawing

**Input Parameters**

$AR_w$	14.00	$S_w$	0.39 m <sup>2</sup>	$\lambda_w$	0.50
$\Lambda_{c/4_w}$	0.0 deg	$X_{apex_w}$	m	$Y_{offset_w}$	0.00 m

**Output Parameters**

$c_{r_w}$	0.22 m	$b_w$	2.34 m	$y_{mgc_w}$	0.52 m	$\Lambda_{LE_w}$	1.4 deg
$c_{t_w}$	0.11 m	$\bar{c}_w$	0.17 m	$x_{mgc_w}$	0.01 m	$\Lambda_{TE_w}$	-4.1 deg

**Straight Tapered Wing Geometry: Output Parameters**

Panel	$c_r$ m	$c_t$ m	$X_r$ m	$X_t$ m	$Y_r$ m
1	0.2225	0.1113			0.0000

Figure 43. Surveillance/Resupply configuration wing inputs

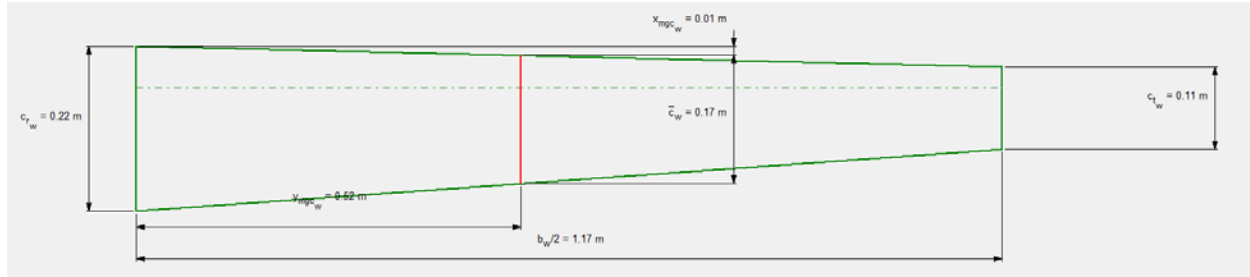


Figure 44. Surveillance/Resupply configuration wing drawing

From the selected wing parameters, the general layout and geometry of the wings can be determined. The difference in aspect ratio is apparent, with the surveillance/resupply wing configuration having a 34% increase in wingspan over the attack configuration.

The wing will not have any significant sweep as it will be flying at a relatively low Mach number. The miniscule amount of sweep present in the current design is a result of the tapering of the wing. As stated previously, the main consideration for having 0 degrees of quarter chord wing sweep is for structural design considerations. No wing sweep will allow for a continuous wing spar to span the length of the wing. This allows for the wing to be designed and constructed in sections without major consideration for structural integrity as the spar will bear most of the forces generated/experienced by the wing.

### 2.6.2. Airfoil Selection

The airfoil selection is critical for this aircraft due to the lift requirements and operating conditions. As this aircraft is a large UAV, it operates in a regime between full size aircraft and hobby level remote control aircraft. This dictates a relatively low Reynolds number operating regime when compared to full sized aircraft. At low Reynolds numbers, viscous forces are the driving factor when determining drag. This dramatically increases zero-lift drag and is one of the reasons the power sizing of this aircraft from Chapter 2.4 is not very accurate. The dramatic increase in zero lift drag greatly reduces the lift-to-drag ratio. Thus it is important to be able to operate the airfoil close to the maximum lift coefficient.

This requires the selection of an airfoil with a high lift coefficient as well as delayed flow separation. A high lift-to-drag ratio is also desired as the mission requirements for range and endurance are very taxing. Due to the proposed weight of the aircraft, the wing will have to be very strong. The main disadvantage of additive manufacturing is the inherent lack of strength in the created component. A composite spar will need to be added to support the wing and increase strength and stiffness. This will require a minimum airfoil thickness of 10% in order to adequately accommodate the spar. If possible, an airfoil with a 12% thickness would be ideal if the performance is sufficient.

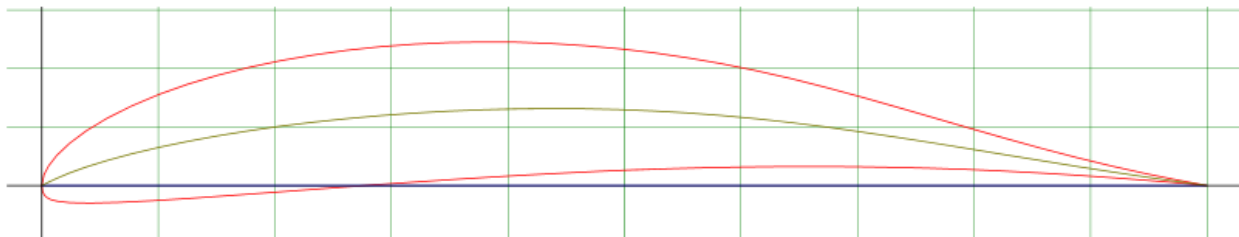


Figure 45. Gottingen GOE 322 airfoil

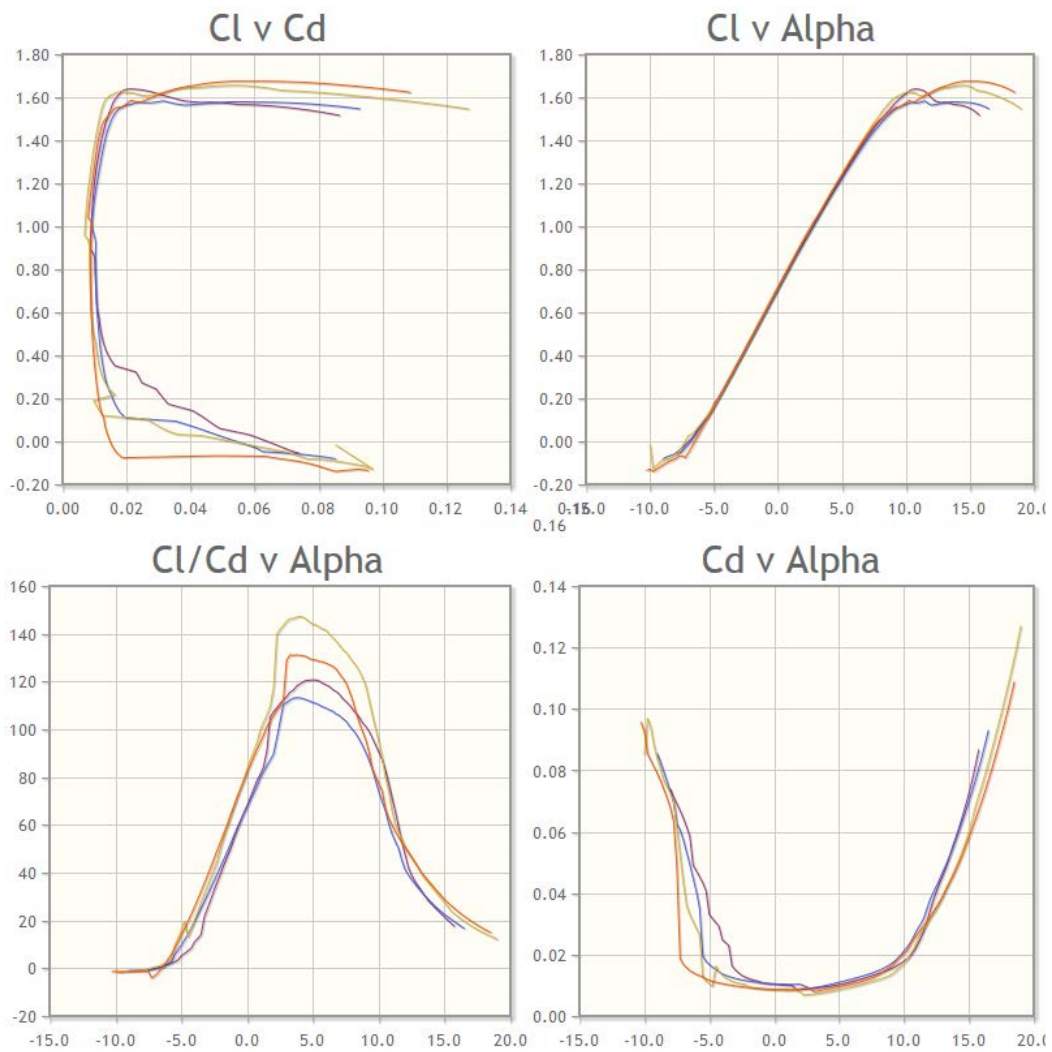


Figure 46. Gottingen GOE 322 airfoil polars



Figure 47. Gottingen GOE 528 airfoil

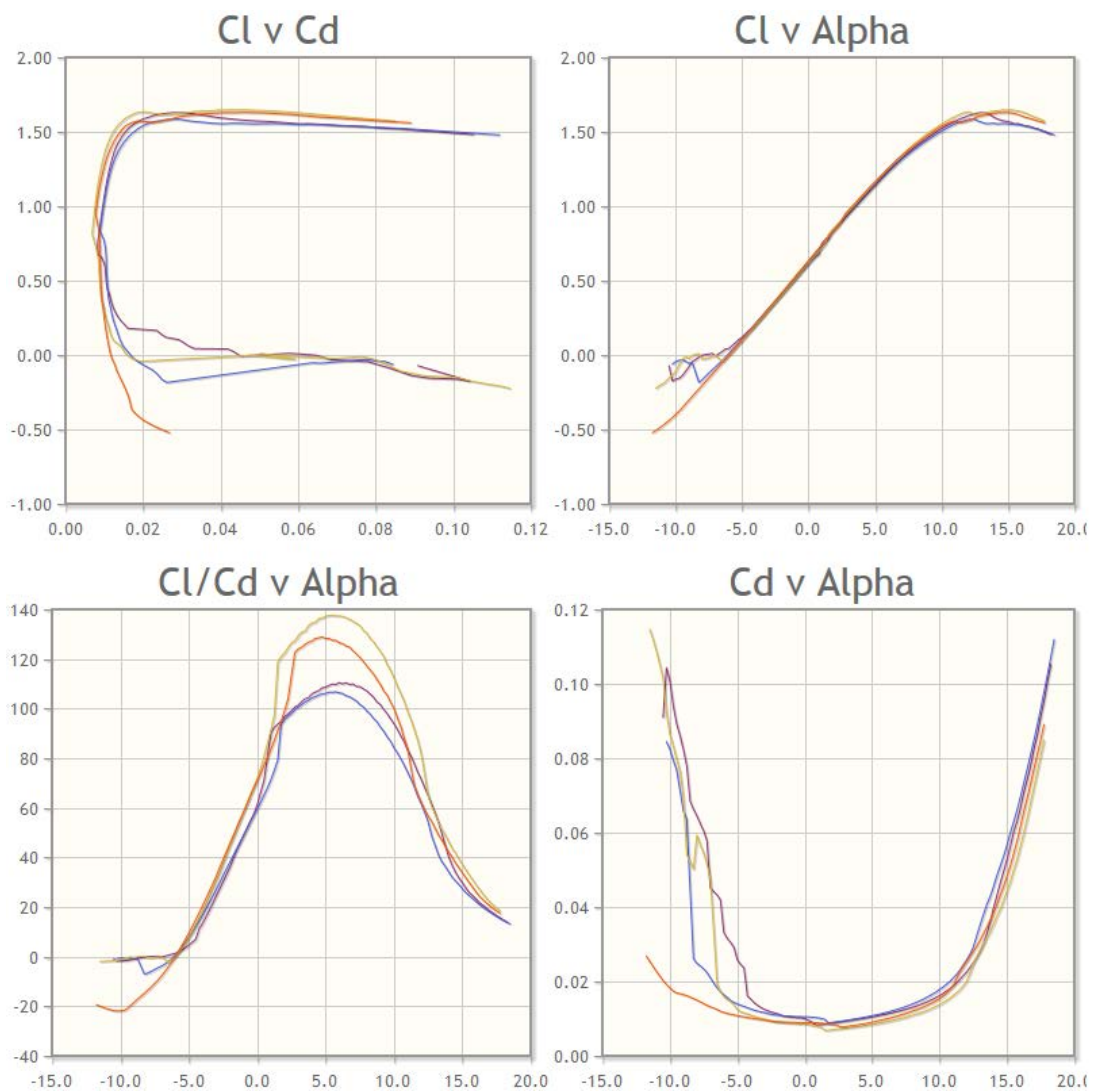


Figure 48. Gottingen GOE 528 airfoil polars

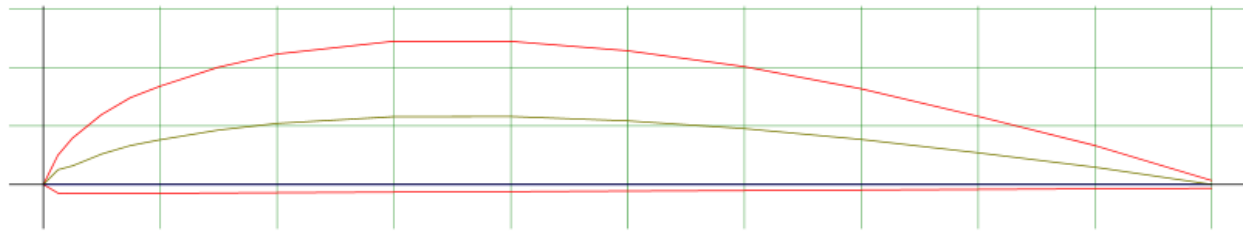


Figure 49. Drela DAE21 airfoil

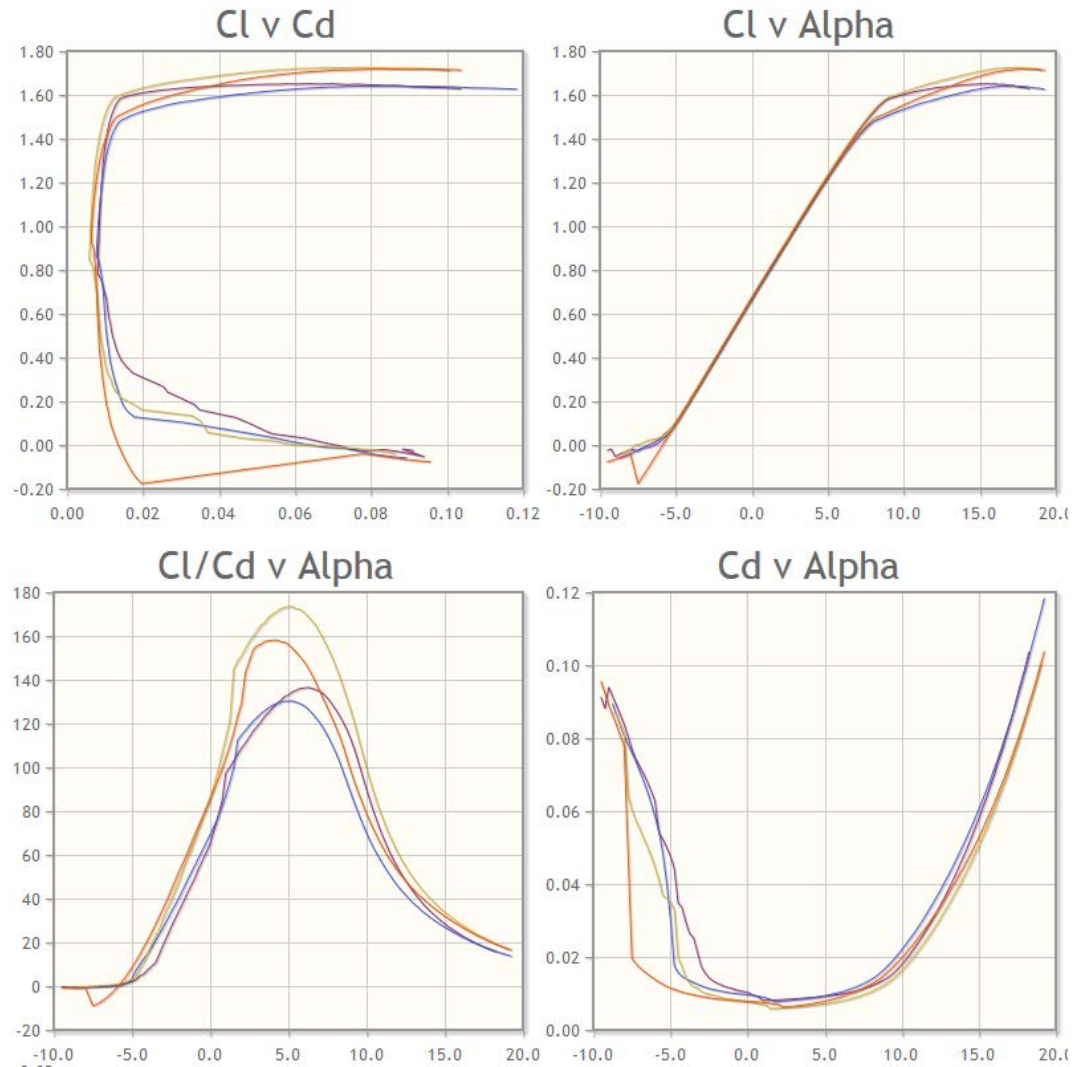


Figure 50. Drela DAE21 airfoil polars

The airfoil selection narrowed down three airfoils. Any of these airfoils should be able to fulfill the design requirements. When evaluated at specific performance points, the differences between them are very minute and will only work to create unique handling characteristics. For example, when evaluated at 5 degrees AOA, each airfoil will produce a Cl/Cd of roughly 110. When looking at the larger picture, the GOE 528 Cl/Cd polar shows that it has a higher Cl/Cd value at AOA of plus/minus 2 degrees from the evaluation point. Another example, the maximum Cl of

the airfoils are similar at ~1.6-1.7. The difference is the AOA at which it achieves this Cl. The GOE 332 and DAE21 airfoils have a higher Cl alpha which allows for the maximum Cl to be achieved earlier, reducing the risk of encountering flow separation and stall when driving the airfoil to the limits of performance. With this in mind, this eliminates the GOE 528 from consideration. The GOE 332 airfoil can also be eliminated from consideration as it is clear from the Cl vs. alpha polar that it experiences more abrupt stall characteristics than the DAE 21 airfoil as it quickly peaks and discontinues compared to the DAE 21 which gradually levels out.

Having selected an airfoil, the DAE 21, we must now determine the incidence angle of the wing. Wing incidence is primarily set to improve pilot visibility, reduce drag, and to keep the fuselage parallel to the ground. The first and third advantage is not very important as this is a UAV. The incidence can be set to a relatively modest 3 degrees to aid in lift generation at cruise while reducing the fuselage drag.

The wing will also feature twist, specifically washout, to reduce the chances of tip stall at high angles of attack. A moderate amount is chosen, 3 degrees, and should suffice in reducing tip stall without negatively affecting the performance.

### 2.6.3. Wing Design Evaluation

Input Parameters							
$C_{l_{max_{rw}}}$	1.450	$\Lambda_{c/4_w}$	0.0 deg	$C_{t_w}$	0.13 m	$C_{L_{max_{clean}}}$	1.100
$C_{l_{max_{tw}}}$	1.450	$C_{r_w}$	0.26 m	$f_{couple}$	1.00		
Output Parameters							
$\lambda_w$	0.50	$K_{\gamma_w}$	0.938	$C_{L_w_{max_{clean}}}$	1.361		

Figure 51. CL max evaluation (Attack)

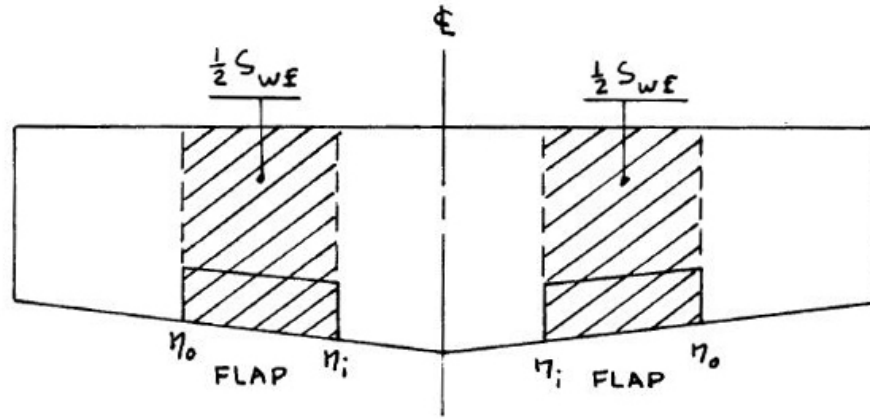
Input Parameters							
$C_{l_{max_{rw}}}$	1.600	$\Lambda_{c/4_w}$	0.0 deg	$C_{t_w}$	0.25 m	$C_{L_{max_{clean}}}$	1.100
$C_{l_{max_{tw}}}$	1.600	$C_{r_w}$	0.25 m	$f_{couple}$	1.00		
Output Parameters							
$\lambda_w$	1.00	$K_{\gamma_w}$	0.880	$C_{L_w_{max_{clean}}}$	1.408		

Figure 52. CL max evaluation (Surveillance/Resupply)

### 2.6.4. Design of the High-Lift Devices and Lateral Control Surfaces

#### 2.6.4.1. High Lift Devices

The high lift devices and lateral control surfaces were designed and sized utilizing methods outline in Roskam. For the high lift device, a single slot flap was chosen for its performance and relative simplicity. A single slot flap offered higher efficiency and performance over a plain flap as the slot allows for free stream air to pass through and energize the flow over the top of the wing, reducing the chance for flow separation when flaps are deployed.



**Figure 7.2 Definition of Flapped Wing Area**

Figure 53. Flap wing area

$$\Delta C_{l_{max}} = \Delta C_{L_{max}} \left( \frac{S}{S_{wf}} \right) K_{\Lambda}$$

$$\frac{S_{wf}}{S} = (\eta_o - \eta_i) \frac{2 - (1 - \lambda)(\eta_o - \eta_i)}{1 + \lambda}$$

In Roskam, it states we must determine the incremental maximum lift coefficients the high lift devices must produce. This value is known due to the performance sizing. Utilizing this value, we are able to work backwards and determine the inboard and outboard stations of the high lift devices which will produce the required increments.

The incremental maximum lift coefficient can then be related to the incremental sectional lift coefficient by:

$$\Delta C_l = \frac{1}{K} \Delta C_{l_{max}}$$

Where the factor K is determined by the flap-to-chord ratio in the following figure. The sectional lift coefficient can be utilized to calculate the required combination of flap deflection and sectional lift effectiveness to produce the required lift coefficient.

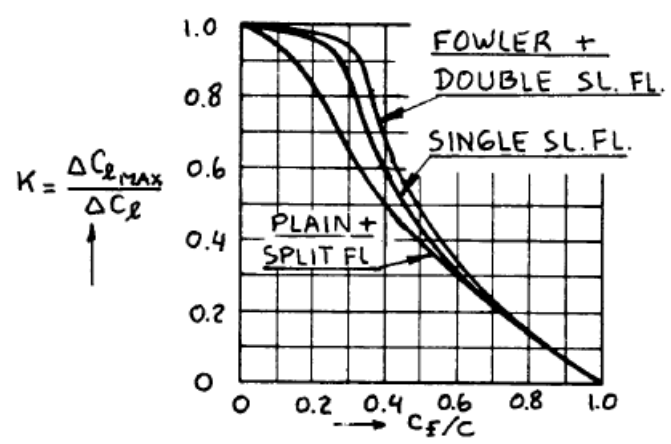


Figure 7.4 Effect of Flap Chord Ratio and Flap Type

Figure 54. Flap-to-chord ratio and flap type relation

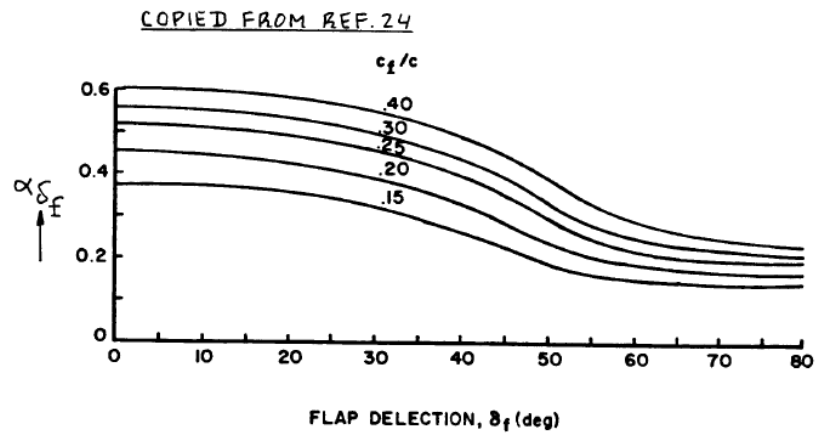
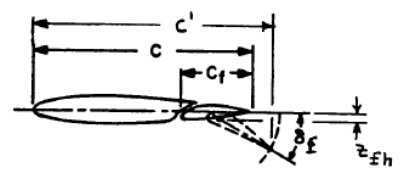


Figure 55. Sectional lift effectiveness parameter

$$\Delta C_l = C_{l_{a_f}} a_{\delta_f} \delta_f$$

$$C_{l_{a_f}} = C_{l_a} \frac{c'}{c}$$

$$\frac{c'}{c} = 1 + 2 \left( \frac{z_{fh}}{c} \right) \tan \left( \frac{\delta_f}{2} \right)$$

## 2.6.4.2. Lateral Control Surfaces

Initial sizing for the lateral control surfaces are much simpler than the high lift devices. Empirical data is gather from type types of aircraft that best fit the UAV in mission and configuration and used to determine the typical span and chord of the control surfaces. This is then averaged to determine a middle-of-the-road sizing of the control surfaces for the UAV. The jet transport and military bomb/transport plane references from Roskam are used.

Table 8.7b) Jet Transports: Vert. Tail Volume, Rudder, Aileron and Spoiler Data

Type	Wing Area S	Wing Span b	Vert. Tail Area S <sub>v</sub>	S <sub>r</sub> /S <sub>v</sub>	x <sub>v</sub>	$\bar{V}_v$	Rudder Chord root/tip	S <sub>a</sub> /S	Inb'd Ail. Span in/out	Inb'd Ail. Chord in/out
	ft <sup>2</sup>	ft	ft <sup>2</sup>		ft		fr.c <sub>v</sub>		fr.b/2	fr.c <sub>w</sub>
<b>BOEING</b>										
727-200	1,700	108	422	0.16	47.4	0.110	.29/.28	0.034	.38/.46	.17/.24
737-200	980	93.0	233	0.24	40.7	0.100	.25/.22	0.024	none	none
737-300	1,117	94.8	239	0.31	45.7	0.100	.26/.50	0.021	none	none
747-200B	5,500	196	830	0.30	102	0.079	0.30	0.040	.38/.44	.17/.25
747-SP	5,500	196	885	0.27	69.5	0.087	.31/.34	0.040	.38/.44	.17/.25
757-200	1,951	125	384	0.34	54.2	0.086	.35/.33	0.027	none	none
767-200	3,050	156	497	0.35	64.6	0.067	.33/.36	0.041	.31/.40	.23/.20
<b>MCDONNELL-DOUGLAS</b>										
DC-9 S80	1,270	108	168	0.39	50.5	0.062	.49/.46	0.030	none	none
DC-9-50	1,001	93.4	161	0.41	46.2	0.079	.45/.44	0.038	none	none
DC-10-30	3,958	163	605	0.18	64.6	0.060	0.35	0.047	.32/.39	.20/.25
<b>AIRBUS</b>										
A300-B4	2,799	147	487	0.30	79.5	0.094	.35/.36	0.049	.29/.39	.23/.27
A310	2,357	144	487	0.35	68.5	0.098	.33/.35	0.027	.32/.40	.23/.27
Lockheed L1011-500	3,541	164	550	0.23	58.2	0.055	.29/.26	0.051	.40/.49	.22/.23
Fokker F-28-4000	850	82.3	157	0.16	37.9	0.085	.29/.31	0.034	none	none
<b>Rombac/British Aerospace</b>										
1-11 495	1,031	93.5	117	0.28	31.6	0.038	.39/.37	0.030	none	none
<b>British Aerospace</b>										
146-200	852	86.4	224	0.44	38.9	0.12	0.29	0.046	none	none
Tu-154	2,169	123	341	0.27	43.3	0.055	0.37	0.036	none	none

Table 8.7c) Jet Transports: Vert. Tail Volume, Rudder, Aileron and Spoiler Data

Type	Outb'd Ail. Span in/out	Outb'd Ail. Chord in/out	Inb'd Spoiler Span Loc. in/out	Inb'd Spoiler Chord in/out	Inb'd Spoiler Hinge Loc. in/out	Outb'd Spoiler Span Loc. in/out	Outb'd Spoiler Chord in/out	Outb'd Spoiler Hinge Loc. in/out	
	fr.b/2	fr.c <sub>w</sub>	fr.b/2	fr.c <sub>w</sub>	fr.c <sub>w</sub>	fr.c <sub>w</sub>	fr.c <sub>w</sub>	fr.c <sub>w</sub>	
<b>BOEING</b>									
727-200	.76/.93	.23/.30	.14/.37	.09/.14	.79/.69	.48/.72	.16/.20	.65/.63	
737-200	.74/.94	.20/.28	.40/.66	.14/.18	.66/.67	none	none	none	
737-300	.72/.91	.23/.30	.38/.64	0.14	.64/.70	none	none	none	
747-200B	.70/.95	.11/.17	.46/.67	.12/.16	0.71	none	none	none	
747-SP	.70/.95	.11/.17	.46/.67	.12/.16	0.71	none	none	none	
757-200	.76/.97	.22/.36	.41/.74	.12/.13	.73/.69	none	none	none	
767-200	.76/.98	.16/.15	.16/.31	.09/.11	.85/.78	.44/.67	.12/.17	.74/.71	
<b>MCDONNELL-DOUGLAS</b>									
DC-9 S80	.64/.85	.31/.36	.35/.60	.10/.08	.69/.65	none	none	none	
DC-9-50	.78/.95	.30/.35	.35/.60	.10/.08	.69/.65	none	none	none	
DC-10-30	.75/.93	.29/.27	.17/.30	.05/.06	.78/.74	.43/.72	.11/.16	.75/.70	
<b>AIRBUS</b>									
A300-B4	.83/.99	.32/.30	.57/.79	.16/.22	.73/.72	none	none	none	
A310	none	none	.62/.83	.16/.22	.69/.66	none	none	none	
Lockheed L1011-500	.77/.98	.26/.22	.13/.39	.08/.12	.82/.73	.50/.74	.14/.14	.67/.67	
Fokker F-28-4000	.66/.91	.29/.28	no lateral control spoilers						
<b>Rombac/British Aerospace</b>									
1-11 495	.72/.92	0.26	.37/.68	.06/.11	.68/.63	none	none	none	
<b>British Aerospace</b>									
146-200	.78/1.0	.33/.31	.14/.70	.22/.27	.76/.68	none	none	none	
Tu-154	.76/.98	.34/.27	.43/.70	.14/.20	.62/.60	none	none	none	

Figure 56. Jet transport control surface data

Table 8.10b) Military Patrol, Bomb and Transport Airplanes: Vertical Tail Volume.

----- Rudder, Aileron and Spoiler Data -----										
Type	Wing Area	Wing Span	Vert. Tail Area	$S_r/S_v$	$x_v$	$\bar{v}_v$	Rudder Chord	$S_a/S$	Inb'd Ail. Span	Inb'd Ail. Chord
	S	b	$S_v$				root/tip		in/out	in/out
	ft <sup>2</sup>	ft	ft <sup>2</sup>		ft		fr.c <sub>v</sub>		fr.b/2	fr.c <sub>w</sub>
<b>Turbopropeller Driven</b>										
<b>LOCKHEED</b>										
C-130E	1,745	133	300	0.25	40.5	0.053	.26/.31	0.063	none	none
P3C	1,300	99.7	176	0.34	46.1	0.063	.32/.39	0.069	none	none
<b>ANTONOV</b>										
An-12BP	1,310	125	205	0.28	48.9	0.061	.42/.44	0.064	none	none
An-22	3,713	211	700	0.44	82.6	0.074	.34/.40	0.040	none	none
An-26	807	95.8	171	0.40	39.9	0.088	.41/.43	0.071	none	none
Grum.E2C	700	80.6	199	0.52	27.7	0.098	.44/.64	0.077	none	none
D/B Atl.2	1,295	123	179	0.56	44.3	0.050	.37/.42	0.044	none	none
Aer.G222	883	94.2	207	0.37	36.7	0.091	.39/.47	0.045	none	none
<b>Jet Driven</b>										
<b>LOCKHEED</b>										
S-3A Viking	598	68.7	129	0.29	20.0	0.063	.37/.35	0.022	none	none
C-141B	3,406	160	455	0.21	72.1	0.060	.24/.28	0.056	none	none
C-5A	6,200	223	961	0.24	113	0.079	.27/.31	0.041	none	none
BA Nimr.2	2,121	115	118	0.35	50.4	0.024	.45/.37	0.058	none	none
B. YC-14	1,762	129	650	0.26	55.7	0.160	0.40	0.048	none	none
MDD KC10A	3,958	165	605	0.18	62.9	0.058	.39/.40	0.047	.32/.39	.20/.25
Tu-16	1,772	108	276	0.24	48.5	0.070	.35/.29	0.057	none	none
Il-76T	3,229	166	596	0.26	60.7	0.068	.46/.38	0.040	none	none

Table 8.10c) Military Patrol, Bomb and Transport Airplanes: Vertical Tail Volume.

----- Rudder, Aileron and Spoiler Data -----									
Type	Outb'd Ail. Span	Outb'd Ail. Chord	Inb'd Spoiler Span	Inb'd Spoiler Chord	Inb'd Spoiler Hinge Loc.	Outb'd Spoiler Span	Outb'd Spoiler Chord	Outb'd Spoiler Hinge Loc.	Outb'd Spoiler Hinge Loc.
	in/out	in/out	in/out	in/out	in/out	in/out	in/out	in/out	in/out
	fr.b/2	fr.c <sub>w</sub>	fr.b/2	fr.c <sub>w</sub>	fr.c <sub>w</sub>	fr.c <sub>w</sub>	fr.c <sub>w</sub>	fr.c <sub>w</sub>	fr.c <sub>w</sub>
<b>Turbopropeller Driven</b>									
<b>LOCKHEED</b>									
C-130E	.70/.99	0.29	no lateral control spoilers						
P3C	.63/.96	.22/.25	no lateral control spoilers						
<b>ANTONOV</b>									
An-12BP	.68/.98	.31/.33	no lateral control spoilers						
An-22	.63/.98	.27/.32	no lateral control spoilers						
An-26	.66/.98	.32/.26	no lateral control spoilers						
Grum.E2C	.57/.98	.22/.33	no lateral control spoilers						
D/B Atl.2	.70/.95	.24/.25	.37/.65	.06/.08	.74/.68	none	none	none	none
Aer.G222	.72/1.0	.35/.45	.48/.70	.07/.08	.70/.66	none	none	none	none
<b>Jet Driven</b>									
<b>LOCKHEED</b>									
S-3A Vik.	.79/.96	.23/.25	.24/.79	.12/.15	.67/.56	none	none	none	none
C-141B	.67/1.0	.26/.23	.15/.41	.09/.12	.85/.80	.43/.66	.10/.13	.83/.83	
C-5A	.72/.93	.28/.30	.36/.70	.13/.12	0.80	none	none	none	
BA Nimr.2	.61/.96	.26/.27	no lateral control spoilers						
B. YC-14	.78/1.0	.37/.33	none	none	none	.53/.78	0.16	.74/.64	
MDD KC10A	.75/.93	.29/.27	.17/.30	.05/.06	.78/.74	.43/.72	.11/.16	.75/.70	
Tu-16	.66/.97	.25/.29	no lateral control spoilers						
Il-76T	.74/.98	.25/.26	.17/.71	.10/.13	.80/.69	none	none	none	

Figure 57. Military bomb/transport control surface data

From the two references, it can be seen that the outboard ailerons for the two types of aircraft with similar configuration range from 22% to 45% chord with a combined span of ~20-45% of the wing.

### 2.6.4.3. Layout of High Lift Devices and Lateral Control Surfaces

The results of the two previous sections are show below. The following drawings show the location of the high lift devices and lateral control surfaces.

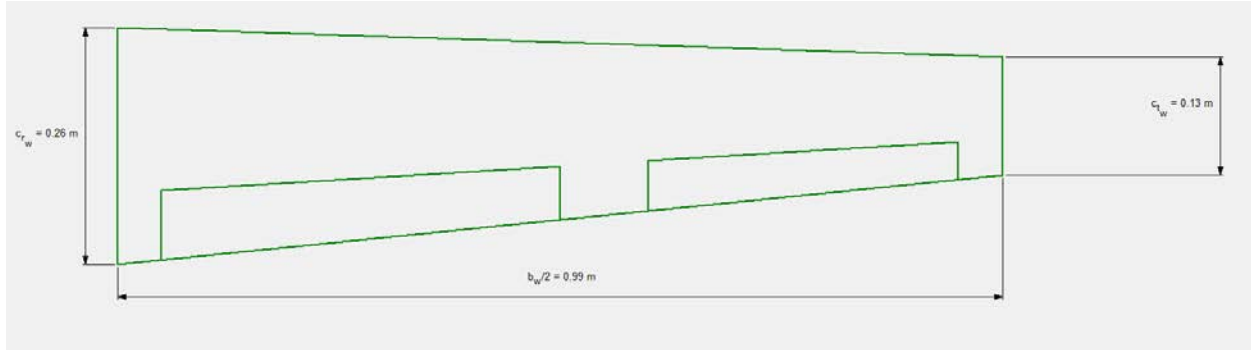


Figure 58. High lift device and lateral control surface layout (Attack)

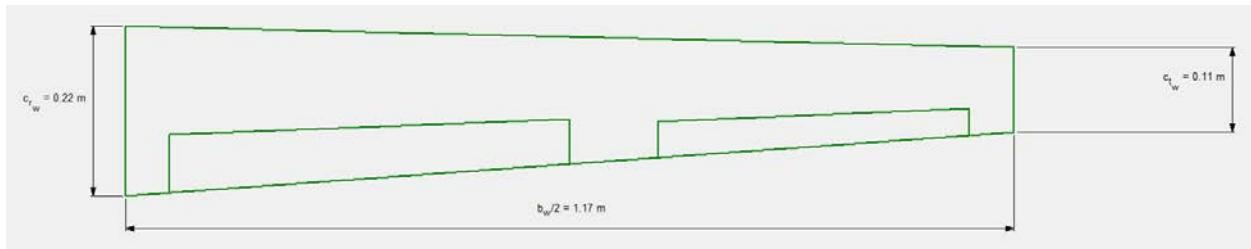


Figure 59. High lift device and lateral control surface layout (Surveillance/Resupply)

## 2.7. Design of the Empennage & the Longitudinal and Directional Controls

### 2.7.1. Overall Empennage Design

In order to correct size the empennage and the associated control surfaces, three variables must be determined: approximate empennage location, empennage volume, and stabilizer aspect ratio. The empennage location can be estimated based on the fuselage design and layout specified in Section 2.4. The empennage volume and stabilizer aspect ratio can be determined from empirical data from similar aircraft. As with the lateral control surface sizing, jet transport and military bomb transport planes will be considered. These two variables location can then be used to calculate the horizontal and vertical stabilizer surface area with the following equations:

$$\bar{V}_h = x_h \frac{S_h}{S\bar{c}}$$

$$\bar{V}_v = x_v \frac{S_v}{Sb}$$

Table 11. Approximate empennage location

Attack	$x_h = x_v = \sim 0.8 \text{ m (1.3)}$
Surveillance/Resupply	$x_h = x_v = \sim 0.5 \text{ m (1)}$

Table 12. Empirical data for stabilizer volume **THESE DATA ARE NOT RELEVANT TO A UAV, WHICH WEIGHS ONLY 20 KG. YOU SHOULD ONLY INCLUDE WHAT IS RELEVANT (SIMILAR) TO YOUR DESIGN.**

Jet Transport	$\bar{V}_h = 0.9 - 1.3$
	$\bar{V}_v = 0.067 - 0.1$
Military Bomb/Transport	$\bar{V}_h = 0.6 - 0.9$
	$\bar{V}_v = 0.06 - 0.08$

Table 13. Calculated stabilizer surface area

Attack	$S_h = 0.088 \text{ m}^2$
	$S_v = 0.078 \text{ m}^2$
Surveillance/Resupply	$S_h = 0.119 \text{ m}^2$
	$S_v = 0.146 \text{ m}^2$

Table 14. Empirical data for stabilizer aspect ratio

Jet Transport	$AR_h = 3.4 - 6$
	$AR_v = 0.7 - 2$
Military Bomb/Transport	$AR_h = 1.3 - 6.9$
	$AR_v = 0.9 - 1.9$

With these variables, the horizontal and vertical stabilizers can now be designed. AAA is utilized for ease of design.

### 2.7.2. Design of the Horizontal Stabilizer

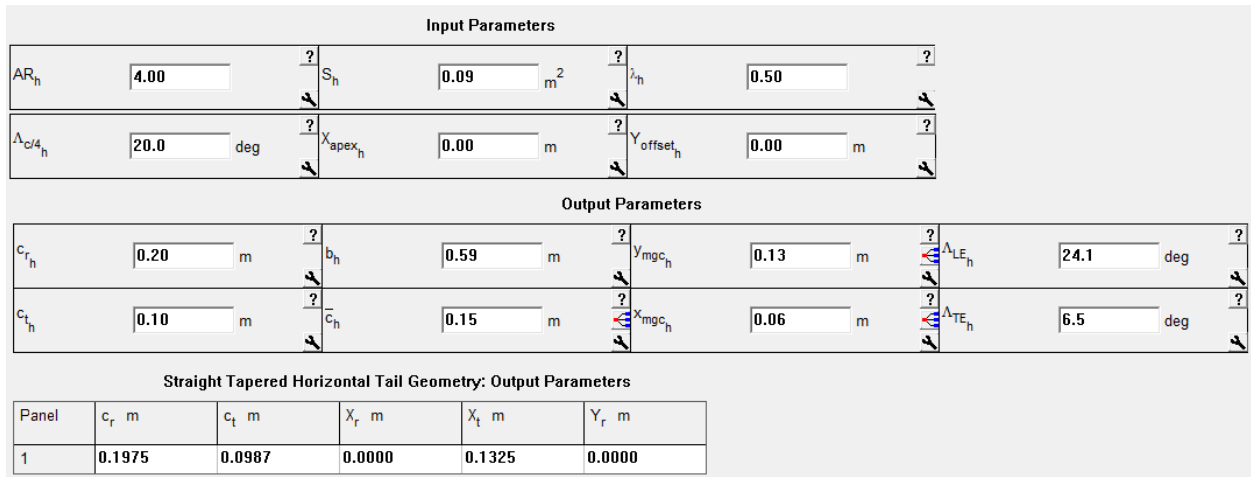


Figure 60. Horizontal stabilizer inputs (Attack)

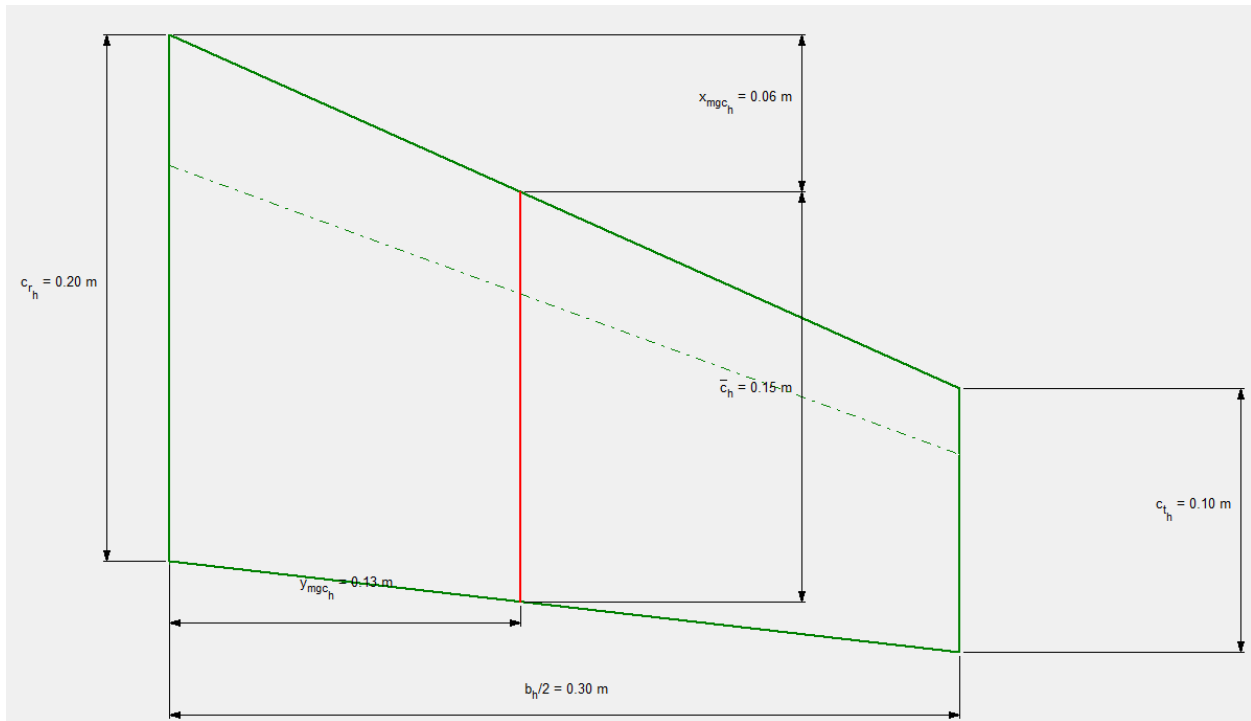


Figure 61. Horizontal stabilizer plot (Attack)

**Input Parameters**

$AR_h$	5.00	$S_h$	0.12 m <sup>2</sup>	$\lambda_h$	0.50
$\Lambda_{c/4_h}$	20.0 deg	$X_{apex_h}$	0.00 m	$Y_{offset_h}$	0.00 m

**Output Parameters**

$c_{r_h}$	0.21 m	$b_h$	0.77 m	$y_{mgc_h}$	0.17 m	$\Lambda_{LE_h}$	23.3 deg
$c_{t_h}$	0.10 m	$c_h$	0.16 m	$x_{mgc_h}$	0.07 m	$\Lambda_{TE_h}$	9.3 deg

**Straight Tapered Horizontal Tail Geometry: Output Parameters**

Panel	$c_r$ m	$c_t$ m	$X_r$ m	$X_t$ m	$Y_r$ m
1	0.2057	0.1028	0.0000	0.1661	0.0000

Figure 62. Horizontal stabilizer inputs (Surveillance/Resupply)

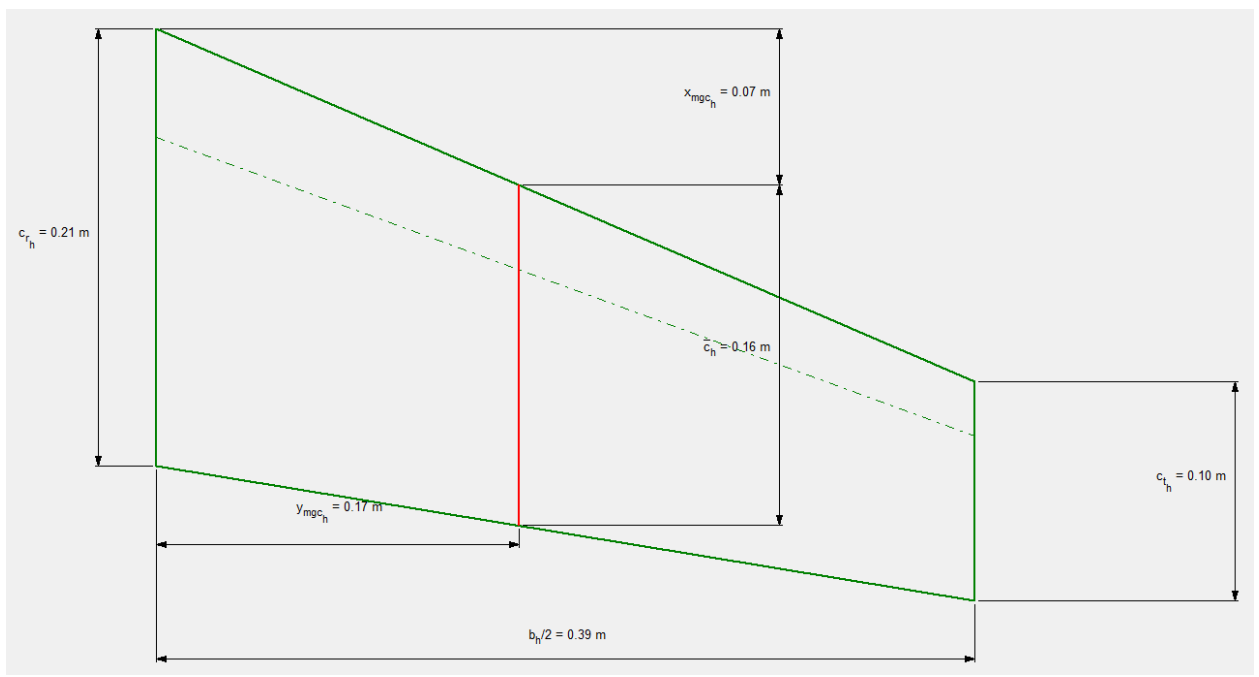


Figure 63. Horizontal stabilizer plot (Surveillance/Resupply)

### 2.7.3. Design of the Vertical Stabilizer

**Input Parameters**

$AR_V$	<input type="text" value="1.00"/>	$S_V$	<input type="text" value="0.08"/> m <sup>2</sup>	$\lambda_V$	<input type="text" value="0.50"/>
$\Lambda_{c/4_V}$	<input type="text" value="35.0"/> deg	$X_{apex_V}$	<input type="text" value="0.00"/> m	$Z_{apex_V}$	<input type="text" value="0.00"/> m

**Output Parameters**

$c_{r_V}$	<input type="text" value="0.38"/> m	$b_V$	<input type="text" value="0.28"/> m	$z_{mgc_V}$	<input type="text" value="0.13"/> m	$\Lambda_{LE_V}$	<input type="text" value="40.9"/> deg
$c_{t_V}$	<input type="text" value="0.19"/> m	$\bar{c}_V$	<input type="text" value="0.29"/> m	$x_{mgc_V}$	<input type="text" value="0.11"/> m	$\Lambda_{TE_V}$	<input type="text" value="11.3"/> deg

**Straight Tapered Vertical Tail Geometry: Output Parameters**

Panel	$c_r$ m	$c_t$ m	$X_r$ m	$X_t$ m	$Z_r$ m
1	0.3771	0.1886	0.0000	0.2452	0.0000

Figure 64. Vertical stabilizer inputs (Attack)

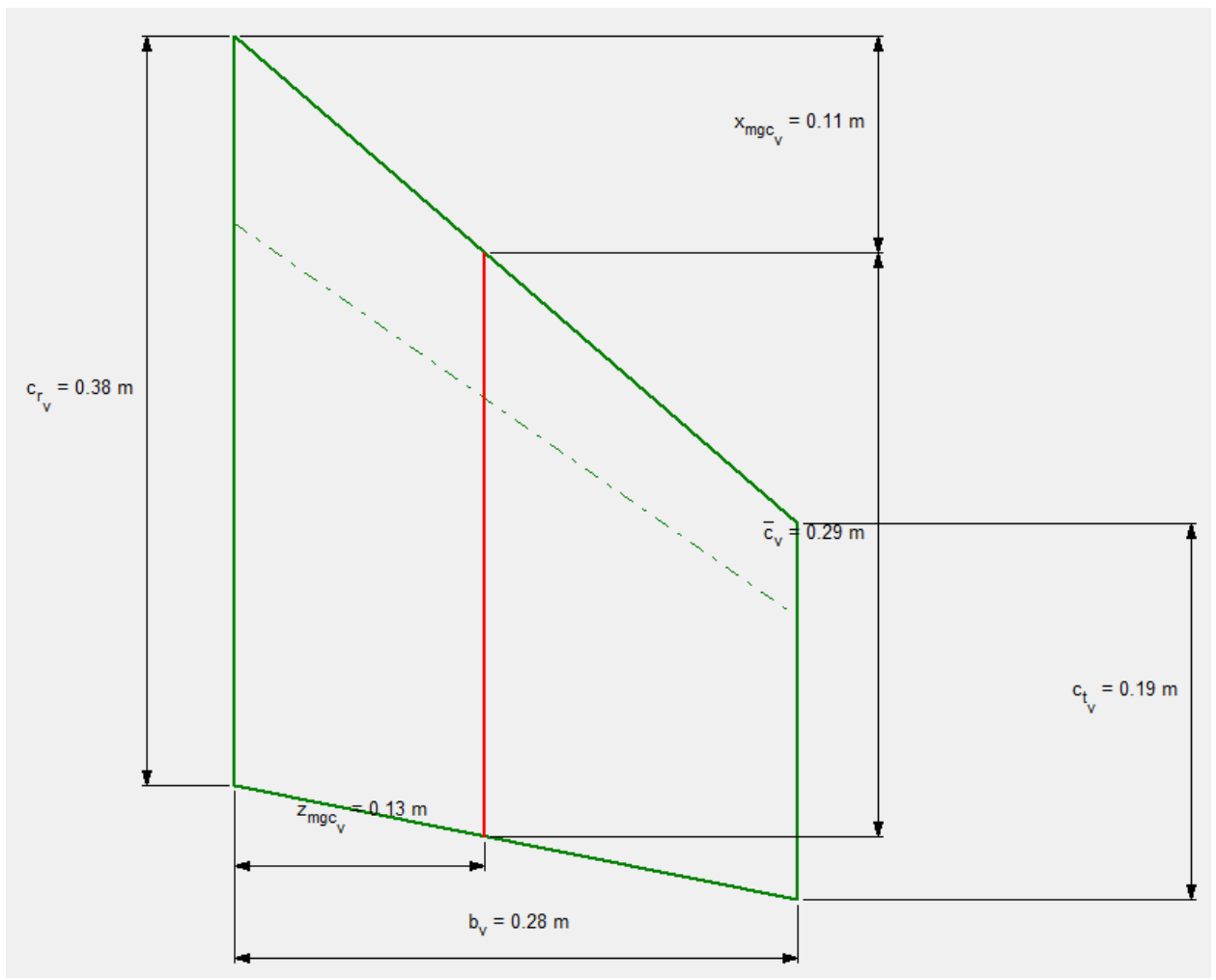


Figure 65. Vertical stabilizer plot (Attack)

**Input Parameters**

$AR_V$	<input type="text" value="1.50"/>	$S_V$	<input type="text" value="0.15"/> m <sup>2</sup>	$\lambda_V$	<input type="text" value="0.50"/>
$\Lambda_{c/4_V}$	<input type="text" value="25.0"/> deg	$X_{apex_V}$	<input type="text" value="0.00"/> m	$Z_{apex_V}$	<input type="text" value="0.00"/> m

**Output Parameters**

$c_{r_V}$	<input type="text" value="0.42"/> m	$b_V$	<input type="text" value="0.47"/> m	$Z_{mgc_V}$	<input type="text" value="0.21"/> m	$\Lambda_{LE_V}$	<input type="text" value="30.0"/> deg
$c_{t_V}$	<input type="text" value="0.21"/> m	$\bar{c}_V$	<input type="text" value="0.32"/> m	$X_{mgc_V}$	<input type="text" value="0.12"/> m	$\Lambda_{TE_V}$	<input type="text" value="7.6"/> deg

**Straight Tapered Vertical Tail Geometry: Output Parameters**

Panel	$c_r$ m	$c_t$ m	$X_r$ m	$X_t$ m	$Z_r$ m
1	0.4160	0.2080	0.0000	0.2702	0.0000

Figure 66. Vertical stabilizer inputs (Surveillance/Resupply)

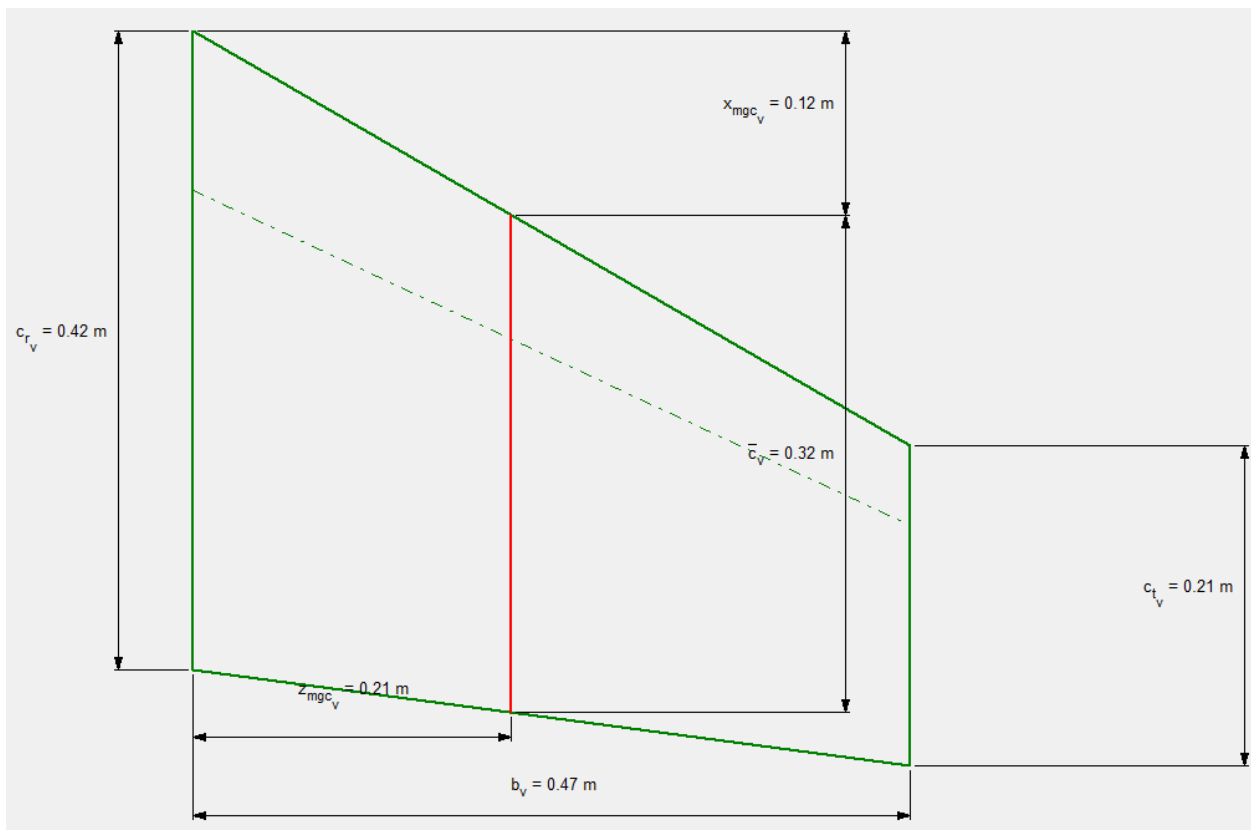


Figure 67. Vertical stabilizer plot (Surveillance/Resupply)

## 2.7.4. Design Of The Longitudinal And Directional Controls

### 2.7.4.1. Longitudinal Control

Input Parameters									
AR <sub>h</sub>	4.00	$\eta_h$	0.50	$(c_e/c_h)_i$	30.0 %	$(x_{h/c})_e$	10.00 %	$\eta_{1e}$	10.0 %
S <sub>h</sub>	0.09 m <sup>2</sup>	$\Lambda_{c/4_h}$	20.0 deg	$(c_e/c_h)_o$	30.0 %	$(x_{h/c})_{oe}$	10.00 %	$\eta_{1oe}$	90.0 %

Elevator Airfoils		
Panel	Root Airfoil	Tip Airfoil
1	naca0010.dat	naca0010.dat

Output Parameters									
c <sub>r<sub>e</sub></sub>	0.06 m	c <sub>b<sub>e</sub></sub>	0.01 m	c <sub>t<sub>e</sub></sub>	0.05 m	c <sub>e/c<sub>h</sub></sub>	27.0 %	C <sub>e</sub>	0.05 m
c <sub>t<sub>e</sub></sub>	0.03 m	c <sub>b<sub>oe</sub></sub>	0.00 m	c <sub>t<sub>oe</sub></sub>	0.03 m	S <sub>e</sub>	0.02 m <sup>2</sup>	Balance <sub>e</sub>	0.11

Figure 68. Elevator inputs (Attack)

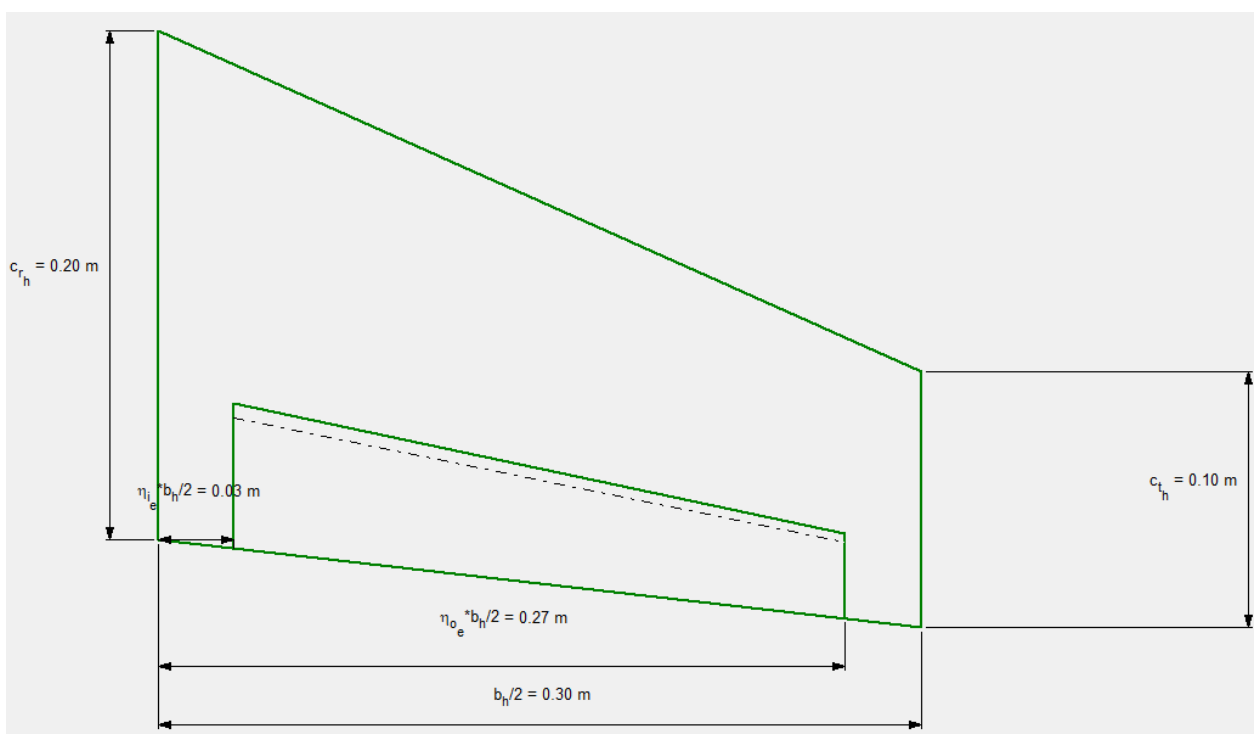


Figure 69. Elevator plot (Attack)

Input Parameters									
AR <sub>h</sub>	5.00	$\eta_h$	0.50	$(c_e/c_h)_i$	30.0 %	$(x_{h/c})_e$	10.00 %	$\eta_{1e}$	10.0 %
S <sub>h</sub>	0.12 m <sup>2</sup>	$\Lambda_{c/4_h}$	20.0 deg	$(c_e/c_h)_o$	30.0 %	$(x_{h/c})_{oe}$	10.00 %	$\eta_{1oe}$	90.0 %

Elevator Airfoils		
Panel	Root Airfoil	Tip Airfoil
1	naca0010.dat	naca0010.dat

Output Parameters									
c <sub>r<sub>e</sub></sub>	0.06 m	c <sub>b<sub>e</sub></sub>	0.01 m	c <sub>t<sub>e</sub></sub>	0.05 m	c <sub>e/c<sub>h</sub></sub>	27.0 %	C <sub>e</sub>	0.05 m
c <sub>t<sub>e</sub></sub>	0.03 m	c <sub>b<sub>oe</sub></sub>	0.00 m	c <sub>t<sub>oe</sub></sub>	0.03 m	S <sub>e</sub>	0.03 m <sup>2</sup>	Balance <sub>e</sub>	0.11

Figure 70. Elevator inputs (Surveillance/Resupply)

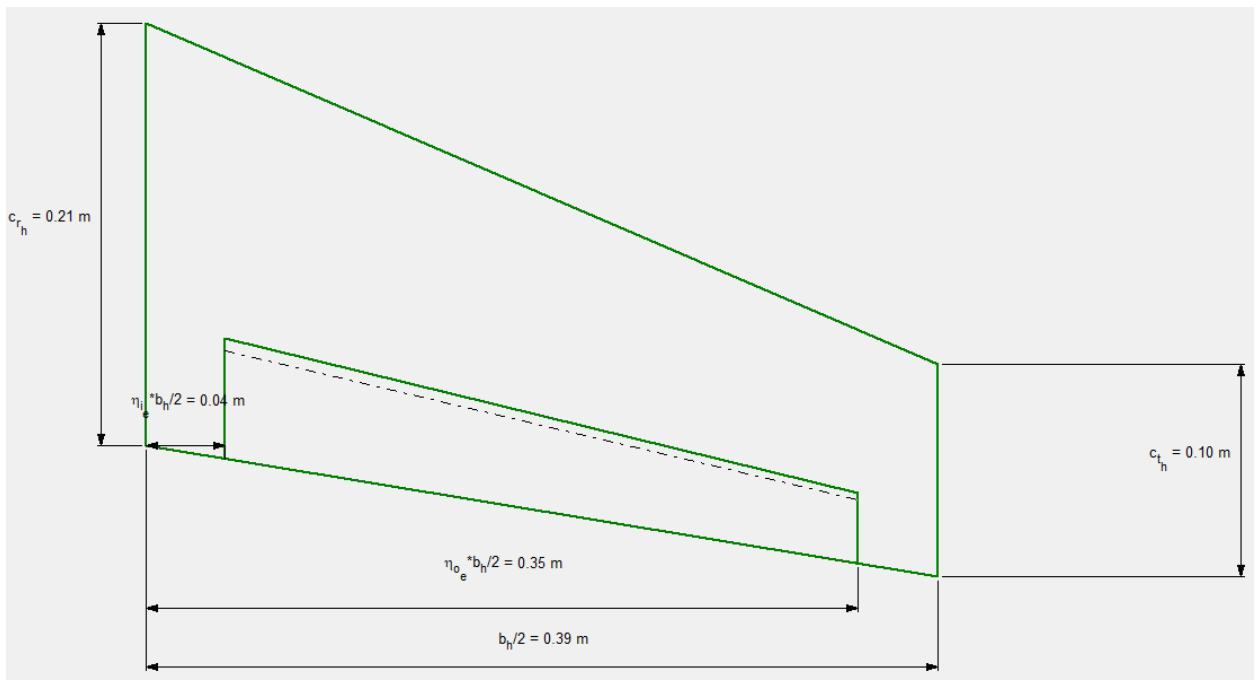


Figure 71. Elevator plot (Surveillance/Resupply)

2.7.4.2. Directional Control

Input Parameters															
AR <sub>v</sub>	1.00	?	$\gamma_v$	0.50	?	$(c_r/c_v)_i$	35.0	%	$(x_{tr}/c)_r$	10.00	%	$\eta_{tr}$	10.0	%	?
S <sub>v</sub>	0.08	m <sup>2</sup>	$\Lambda_{c4_v}$	35.0	deg	$(c_r/c_v)_o$	35.0	%	$(x_{tr}/c)_o_r$	10.00	%	$\eta_{or}$	90.0	%	?
Rudder Airfoils															
Panel	Root Airfoil	Tip Airfoil													
1	naca0010.dat	naca0010.dat													
Output Parameters															
$c_{r_r}$	0.13	m	$c_{b_r}$	0.01	m	$c_{t_r}$	0.11	m	$c_r/c_v$	31.5	%	$C_r$	0.10	m	?
$c_{t_r}$	0.07	m	$c_{b_{or}}$	0.01	m	$c_{r_{or}}$	0.07	m	S <sub>r</sub>	0.02	m <sup>2</sup>	Balance <sub>r</sub>	0.11		?

Figure 72. Rudder inputs (Attack)

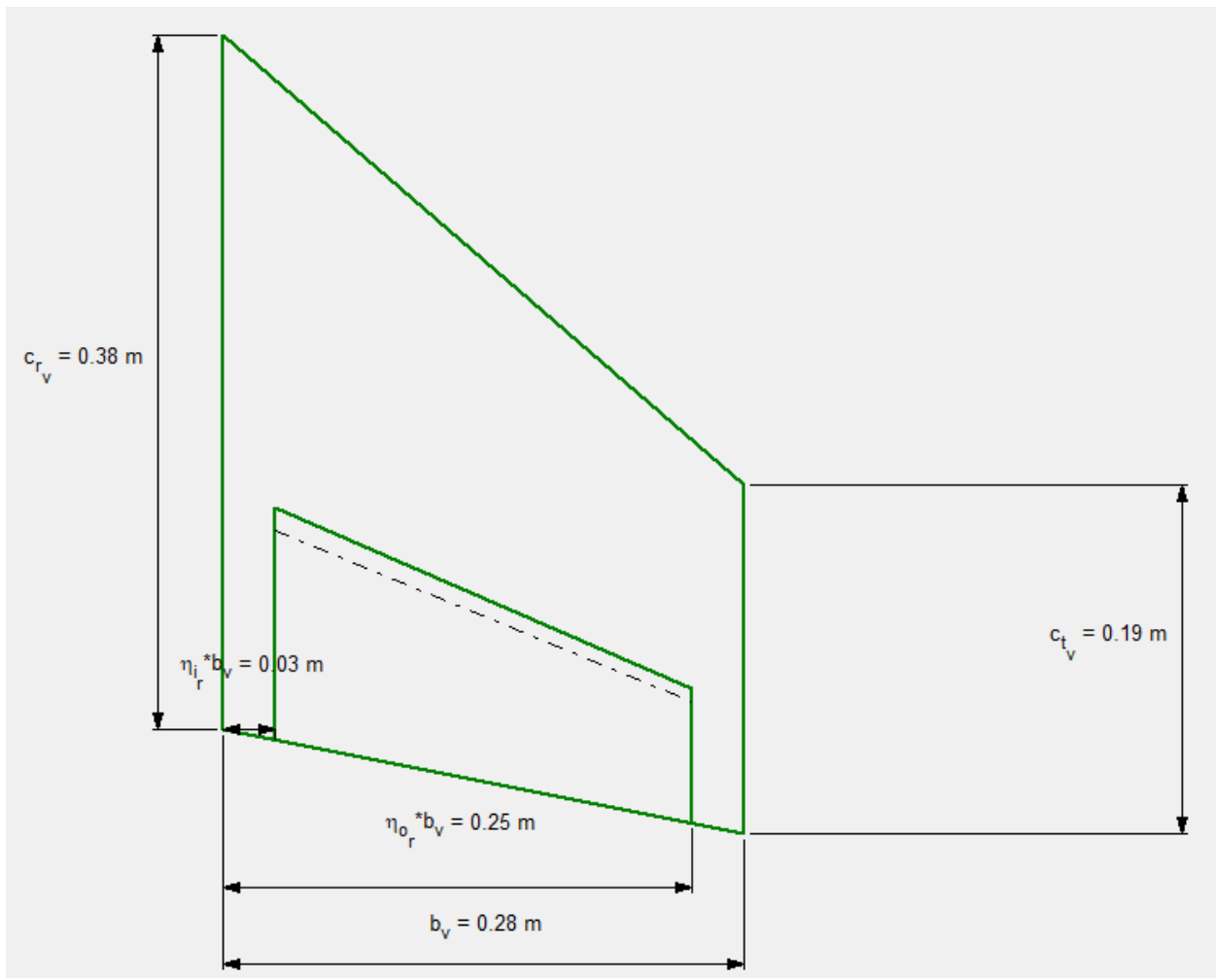


Figure 73. Rudder plot (Attack)

Input Parameters									
$AR_v$	1.50	$\lambda_v$	0.50	$(c_r/c_v)_i$	35.0 %	$(x_{hp}/c)_r$	10.00 %	$\eta_i$	10.0 %
$S_v$	0.15 m <sup>2</sup>	$\Lambda_{c/4_v}$	25.0 deg	$(c_r/c_v)_o$	35.0 %	$(x_{hp}/c)_o_r$	10.00 %	$\eta_o_r$	90.0 %
Rudder Airfoils									
Panel	Root Airfoil	Tip Airfoil							
1	naca0010.dat	naca0010.dat							
Output Parameters									
$c_{r_r}$	0.14 m	$c_{b_r}$	0.01 m	$c_{t_r}$	0.12 m	$c_r/c_v$	31.5 %	$C_r$	0.11 m
$c_{t_r}$	0.08 m	$c_{b_o_r}$	0.01 m	$c_{t_o_r}$	0.07 m	$S_r$	0.04 m <sup>2</sup>	Balance <sub>r</sub>	0.11

Figure 74. Rudder inputs (Surveillance/Resupply)

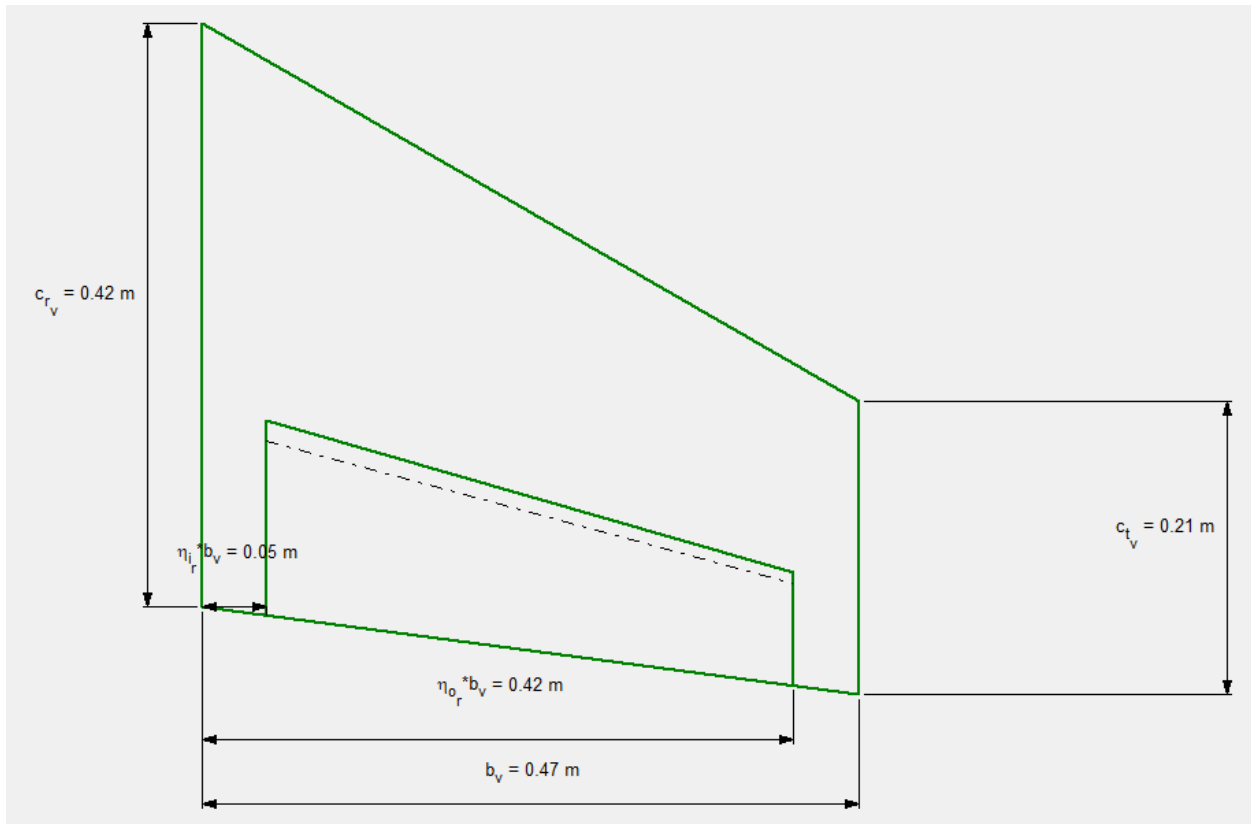


Figure 75. Rudder plot (Surveillance/Resupply)

## 2.8. Landing Gear Design and Weight & Balance Analysis

### 2.8.1. Estimation of the Center of Gravity Location for the Airplane

Table 15. Component CG location estimation

Component Group	Weight (Wi) (kg/N)	Xi (Attack/Surv.) (m)	WiXi	Zi (m)	WiZi
Fuselage	2.398/23.524	0.64	15.055	0.089	1.341
Wing	2.31/22.661	0.5/0.8	11.331/18.129	0.154	3.49
Empennage	0.55/5.396	0.95	5.126	0.25	1.349
Engine	1.754/17.207	0.4/0.7	6.883/12.045	0.089	1.531
Payload	10/98.1	0.49/0.8	48.069/78.48	0.098	9.614
Battery	6.472/63.49	0.9/0.39	57.141/24.761	0.089	5.651

Landing Gear (Front)	???	???	???	???	???
Landing Gear (Main)	???	???	???	???	???
Fixed Equipment	0.619/6.072	0.095	0.576	0.089	0.54
Total	236.45		144.182/154.172		23.516

The CG location without the landing gear factored in can be calculated with the following equations:

$$CG \text{ location (x vector)} = \frac{W_i X_i}{W_i} = 0.609/0.652 \text{ m}$$

$$CG \text{ location (z vector)} = \frac{W_i Z_i}{W_i} = 0.099 \text{ m}$$

This preliminary CG location will allow us to determine the optimal position of the landing gear to meet tipover and engine clearance requirements.

### 2.8.2. Landing Gear Design

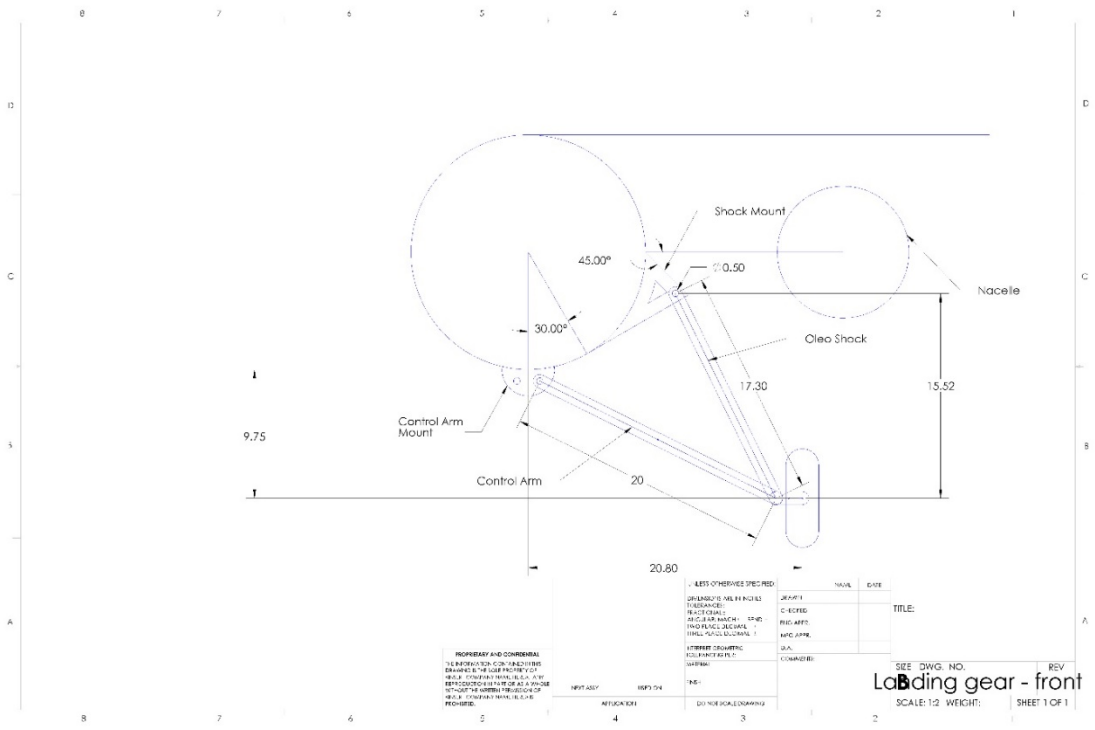


Figure 76. Landing gear design (front)

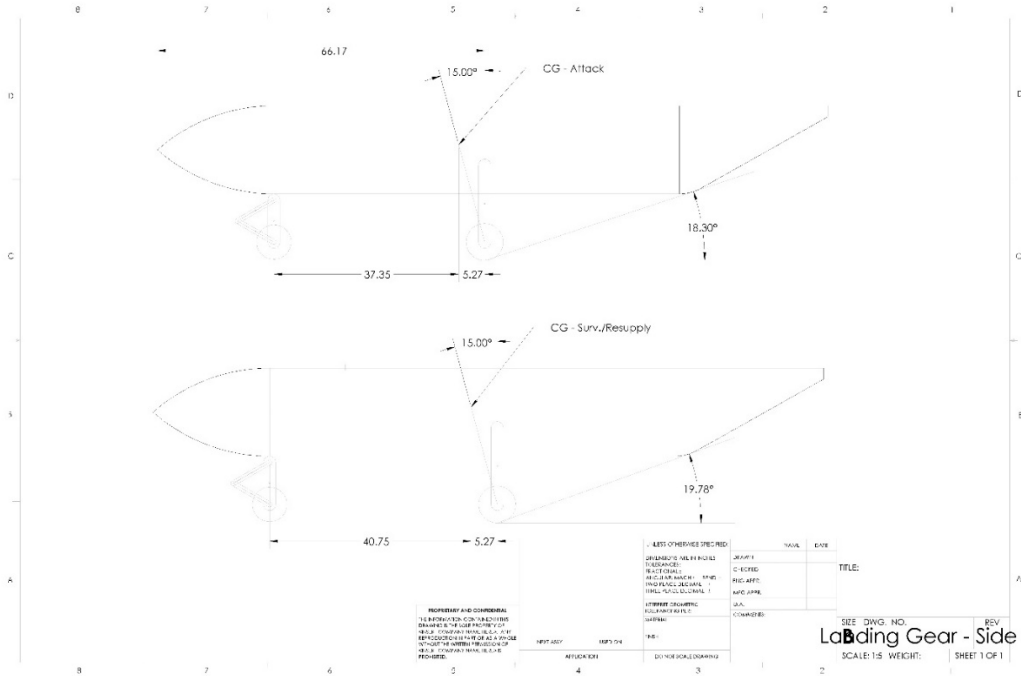


Figure 77. Landing gear design (side)

2.8.3. Weight And Balance

Table 16. Revised component CG location estimation

Component Group	Weight (Wi) (kg/N)	Xi (Attack/Surv.) (m)	WiXi	Zi (m)	WiZi
Fuselage	2.398/23.524	0.64	15.055	0.089	1.341
Wing	2.31/22.661	0.5/0.8	11.331/18.129	0.154	3.49
Empennage	0.7/6.867	1.17	6.524	0.25	1.716
Engine	1.754/17.207	0.4/0.7	6.883/12.045	0.089	1.531
Payload	10/98.1	0.49/0.8	48.069/78.48	0.098	9.614
Battery	6.472/63.49	0.9/0.39	57.141/24.761	0.089	5.651
Landing Gear (Front)	0.098/0.961	0.235	0.225835	-0.034	-0.033
Landing Gear (Main)	0.183/1.795	0.652/0.696	1.17/1.249	-0.076	-0.136

Fixed Equipment	0.619/6.072	0.095	0.576	0.089	0.54
Total	240.679		148.485/158.5538		23.347

$$CG \text{ location (x vector)} = \frac{W_i X_i}{W_i} = 0.608/0.65 \text{ m}$$

$$CG \text{ location (z vector)} = \frac{W_i Z_i}{W_i} = 0.097 \text{ m}$$

With the landing gear factored into the CG calculation, the resultant CG location changed very little. The landing gear design does not need a revision to accommodate the change in CG.

Table 17. CG location and aircraft weight for different loading scenarios

	Configuration	CG Location (Attack) (cm)	CG Location (Surv.) (cm)	Weight (N)
1	Empty	55.298	70.711	71.55
2	Empty+Fixed	51.714	67.209	77.623
3	Empty+Fixed+Batt.	68.934	54.514	141.123
4	Empty+Fixed+Batt.+Payload	60.734	64.942	239.323

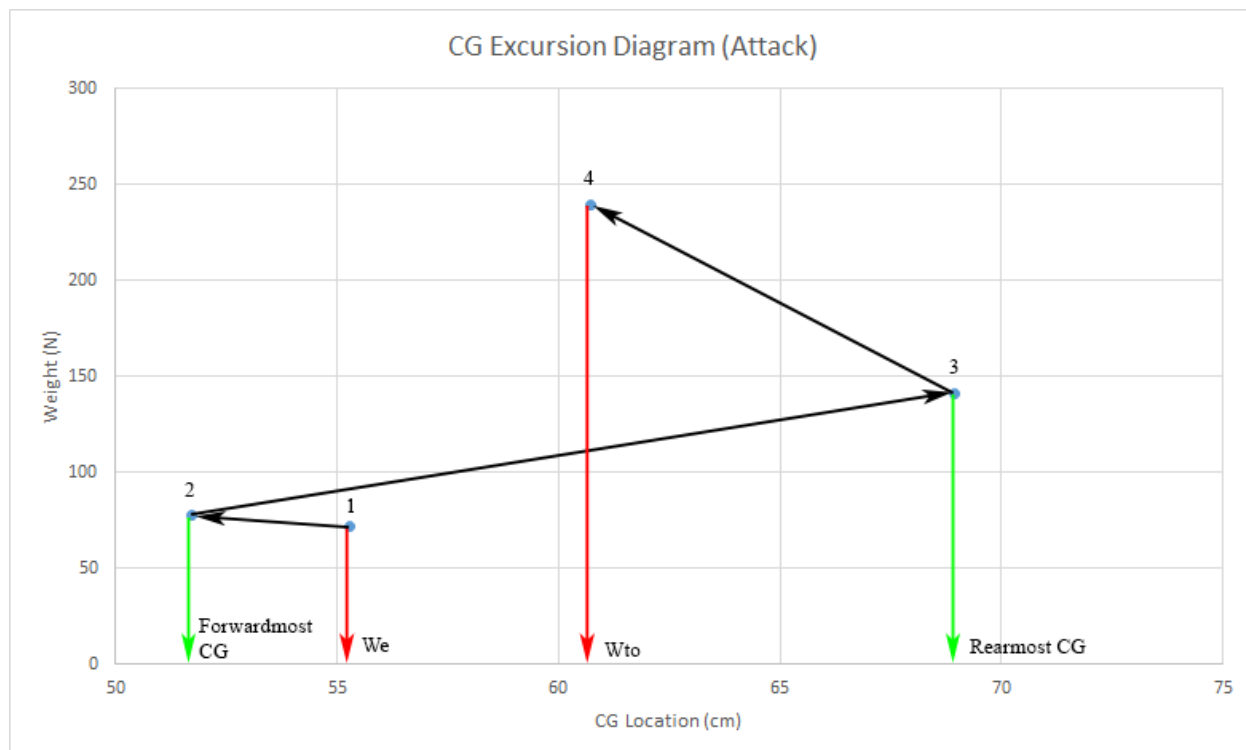


Figure 78. CG excursion diagram for the attack configuration

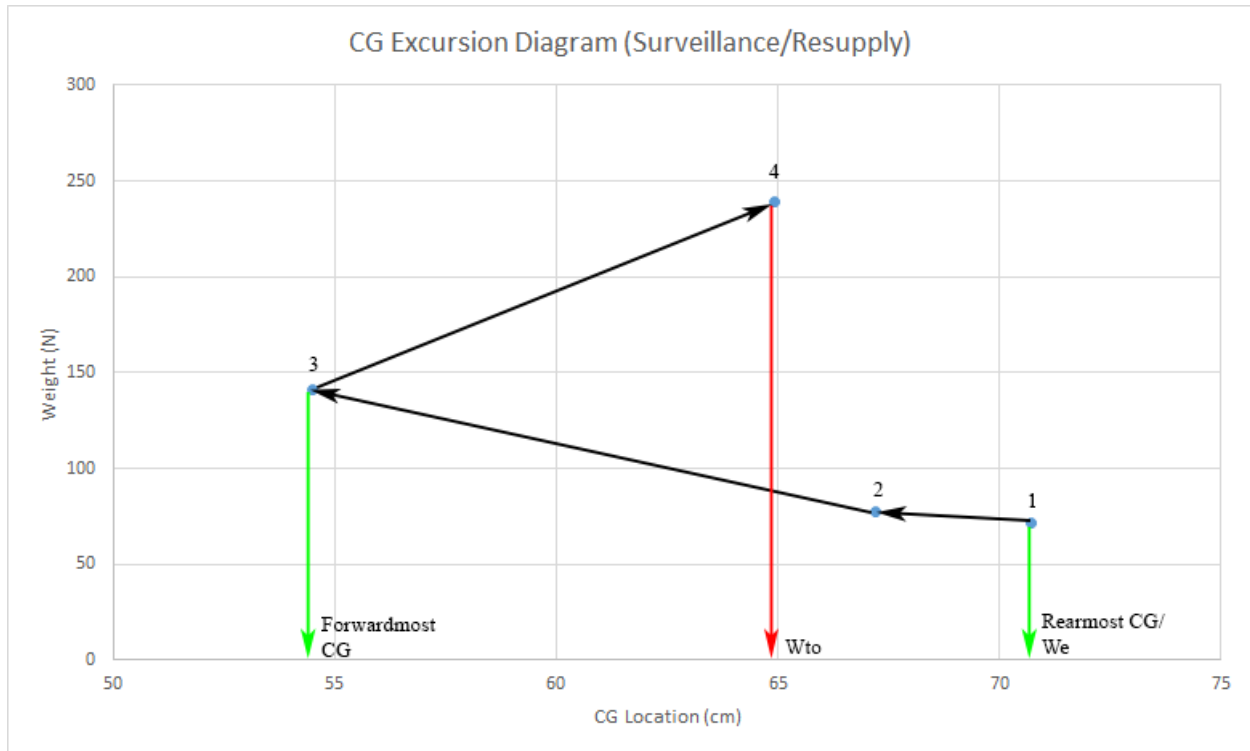


Figure 79. CG excursion diagram for the surveillance/resupply configuration

## 2.9. Stability and Control Analysis

### 2.9.1. Static Longitudinal Stability

$$\bar{x}_{acA} = \frac{\bar{x}_{acwb} + C_{l\alpha_h} \left( 1 - \frac{d\varepsilon_g}{d\alpha} \right) \left( \frac{S_h}{S} \right) \bar{x}_{acn}}{F}$$

$$F = 1 + C_{l\alpha_h} \left( 1 - \frac{d\varepsilon_g}{d\alpha} \right) \left( \frac{S_h}{S} \right)$$

$$\frac{\partial \varepsilon}{\partial \alpha} = \frac{21^\circ C_{L\alpha}}{AR^{0.725}} \left( \frac{c_{avg}}{l_h} \right) \left( \frac{10-3\lambda}{7} \right) \left( 1 - \frac{z_h}{b} \right)$$

$$\frac{d\varepsilon_g}{d\alpha} = 0.144 \text{ (attack)}$$

$$\frac{d_{\epsilon_g}}{d_{\alpha}} == 0.134 \text{ (surv./resupply)}$$

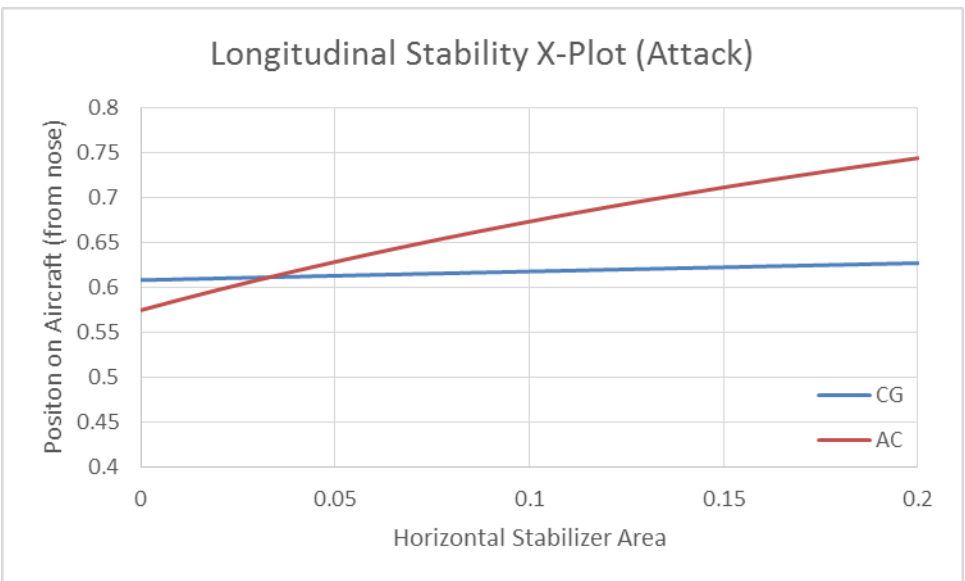


Figure 80. Longitudinal stability X-plot for the attack configuration

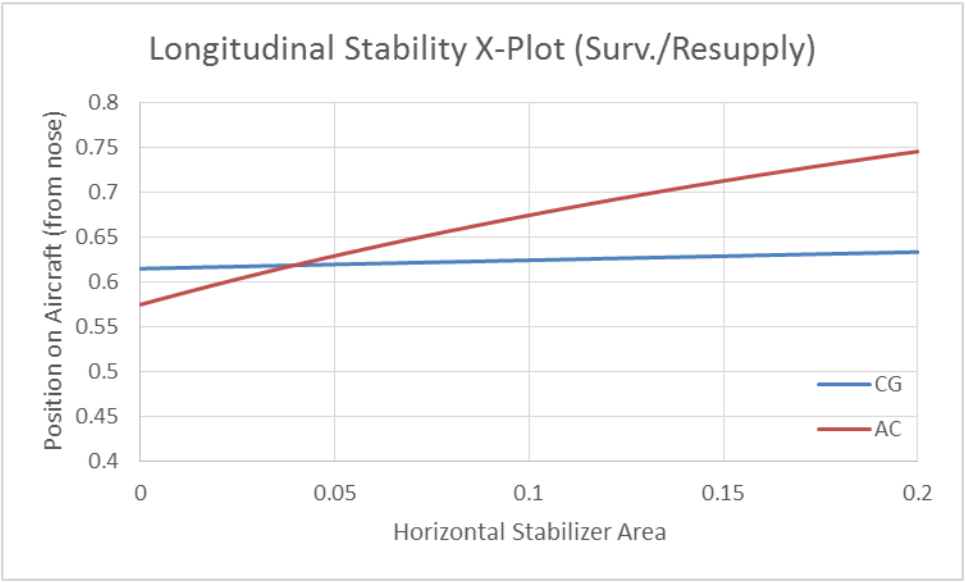


Figure 81. Longitudinal stability X-plot for the surveillance/resupply configuration

From the figures above, the aircraft will achieve a 10% static margin with a minimum horizontal stabilizer area of 0.063 and 0.069 meters squared for the attack configuration and surveillance configuration, respectively.

## 2.9.2. Static Directional Stability

The directional X-plot illustrates the change in directional stability for various vertical tail areas. The desired de facto level of directional instability is  $C_n\beta = 0.0010$ . From the following figure, the vertical stabilizer achieves a  $C_n\beta = 0.0010$  at a surface of around 0.119 meters squared.

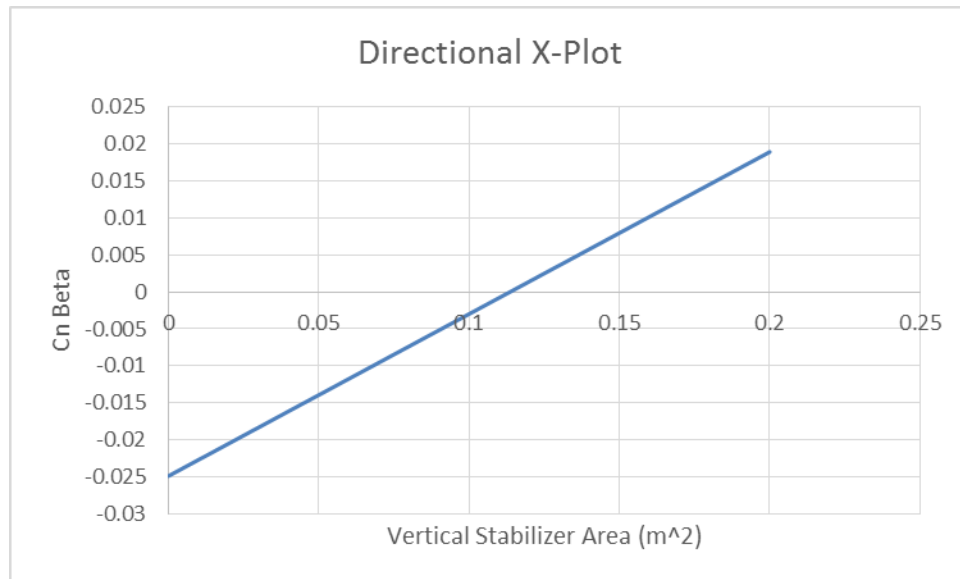


Figure 81. Directional stability X-plot

## 2.10. Drag Polar Estimation

### 2.10.1. Airplane Zero Lift Drag

There are three main contributions to the zero lift drag of the airplane: the fuselage, the wing, and the engine nacelles. As the aircraft is mostly designed, it is possible to accurately determine the zero lift drag through the calculation of the surface area of each contribution. The equivalent parasitic drag can be calculated and, in turn, the clean zero lift drag coefficient.

$$S_{wet_{fus}} = \pi * D_f * l_f \left(1 - \frac{2}{\lambda_f}\right)^{\frac{2}{3}} \left(1 + \frac{1}{\lambda_f^2}\right)$$

$$S_{wet_{fus}} = 6558.17 \text{ cm}^3 = 0.655817 \text{ m}^3$$

$$S_{wet_{wing}} = 2S_{exp} \left(1 + \frac{0.25 \left(\frac{t}{c}\right)_r (1 + \tau\lambda)}{1 + \lambda}\right)$$

$$\tau = \frac{\left(\frac{t}{c}\right)_r}{\left(\frac{t}{c}\right)_t} = \frac{0.12}{0.12} = 1$$

$$\lambda = \frac{c_t}{c_r} = 0.5$$

$$S_{wet_{wing}} = 2(0.39) \left( 1 + \frac{0.25(0.12)(1 + (1 * 0.5))}{1 + 0.5} \right) = 0.8034 \text{ m}^2$$

$$S_{wet_{fan}} = l_n D_n \left\{ 2 + \frac{0.35 l_1}{l_n} + \frac{0.8 l_1 D_{hl}}{l_n D_n} + \frac{1.15(1 - l_1 l_n) D_{ef}}{D_n} \right\}$$

$$S_{wet_{fan}} = 0.16 * 0.152 \left\{ 2 + \frac{0.35 * 0.02}{0.16} + \frac{0.8 * 0.02 * 0.12}{0.16 * 0.152} + \frac{1.15(1 - 0.02 * 0.16)0.12}{0.152} \right\}$$

$$S_{wet_{fan}} = 0.7363 \text{ m}^2$$

$$S_{wet_{gen}} = \pi l_g D_g \left[ 1 - \left(\frac{1}{3}\right) \left(1 - \frac{D_{eg}}{D_g}\right) \left\{ 1 - 0.18 \left(\frac{D_g}{l_g}\right)^{\frac{5}{3}} \right\} \right]$$

$$S_{wet_{gen}} = 0$$

$$S_{wet_{plug}} = 0.7 \pi l_p D_p$$

$$S_{wet_{plug}} = 0$$

$$S_{wet_{total}} = 0.6558 + 0.8034 + 0.7363 = 2.1955 \text{ m}^2$$

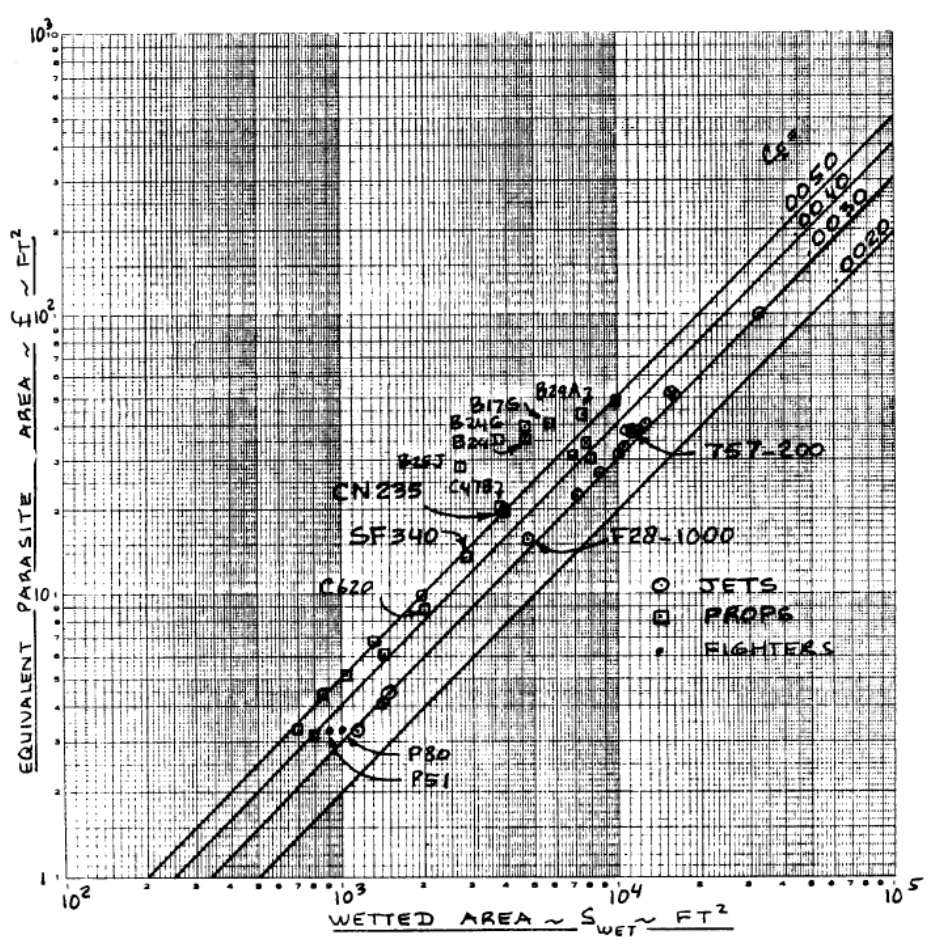


Figure 82. Wetted surface area vs. parasitic area

Table 3.4 Correlation Coefficients for Parasite Area  
 Versus Wetted Area (Eqn. (3.21))

Equivalent Skin Friction Coefficient, $c_f$	a	b
0.0090	-2.0458	1.0000
0.0080	-2.0969	1.0000
0.0070	-2.1549	1.0000
0.0060	-2.2218	1.0000
0.0050	-2.3010	1.0000
0.0040	-2.3979	1.0000
0.0030	-2.5229	1.0000
0.0020	-2.6990	1.0000

Figure 83. Correlation coefficients for parasitic area and wetted area

$$\log f = a + b \log S_{wet}$$

$$a = -2.5229$$

$$b = 1$$

$$f = 0.006586$$

$$C_{d_0} = \frac{f}{S}$$

$$C_{d_0} = 0.03$$

The zero lift drag coefficient is estimate to be about 0.03. This is a relatively high value but is not unexpected.

### 2.10.2. Low Speed Drag Increments

With the zero lift drag coefficient calculate, the low speed drag increments can be estimated and the drag polars formed. Roskam has a table for estimating the drag increment of various stages of flight.

$$C_d = C_{d_0} + \frac{C_l^2}{\pi e AR}$$

**Table 3.6 First Estimates for  $\Delta C_{D_0}$  and 'e'**

With Flaps and Gear Down		
Configuration	$\Delta C_{D_0}$	e
Clean	0	0.80 - 0.85
Take-off flaps	0.010 - 0.020	0.75 - 0.80
Landing Flaps	0.055 - 0.075	0.70 - 0.75
Landing Gear	0.015 - 0.025	no effect

Figure 84. Low speed drag increments

### 2.10.3. Airplane Drag Polars

Table 18. Drag polars for different flight configurations

Configuration	Attack Polar	Surveillance/Resupply Polar
Clean (no landing gear)	$C_d = 0.03 + 0.0358C_l^2$	$C_d = 0.03 + 0.0255C_l^2$

Clean (fixed landing gear)	$C_d = 0.055 + 0.0358C_l^2$	$C_d = 0.055 + 0.0255C_l^2$
Takeoff (fixed landing gear)	$C_d = 0.075 + 0.0424C_l^2$	$C_d = 0.075 + 0.0303C_l^2$
Landing (fixed landing gear)	$C_d = 0.13 + 0.0455C_l^2$	$C_d = 0.13 + 0.0325C_l^2$

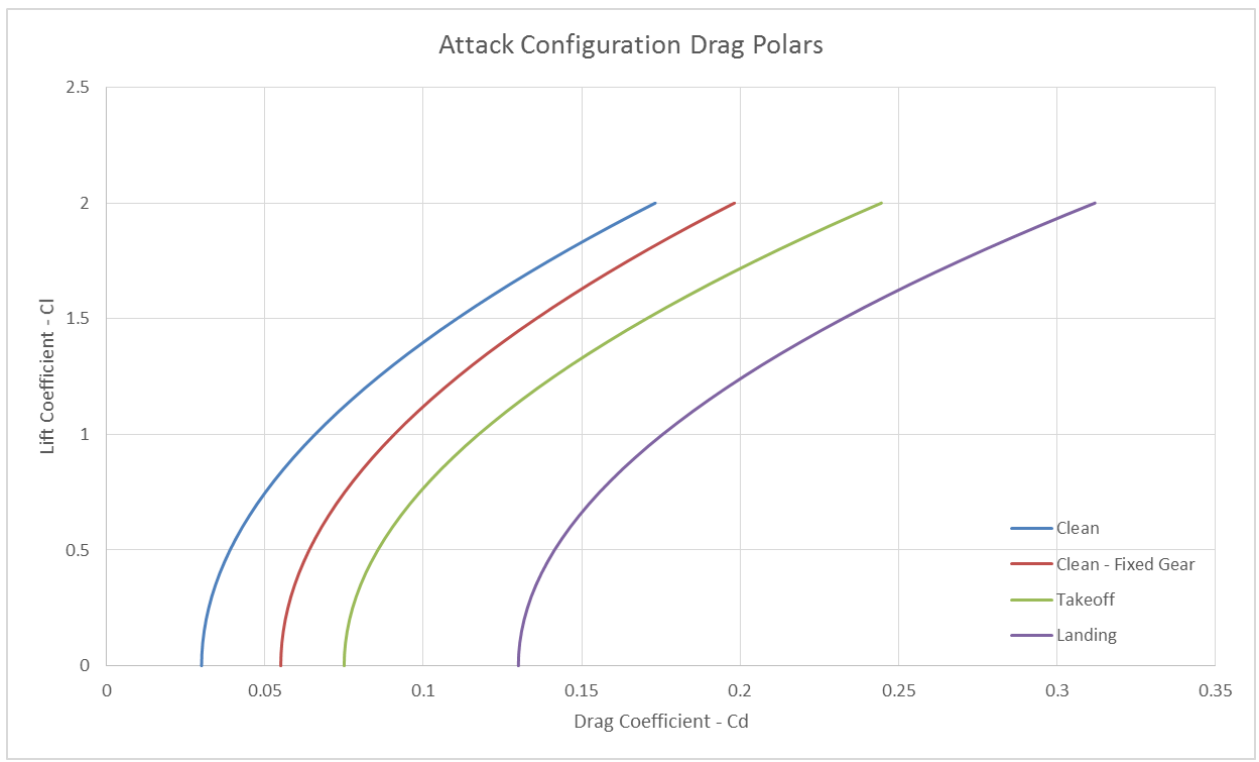


Figure 85. Drag polars for the attack configuration

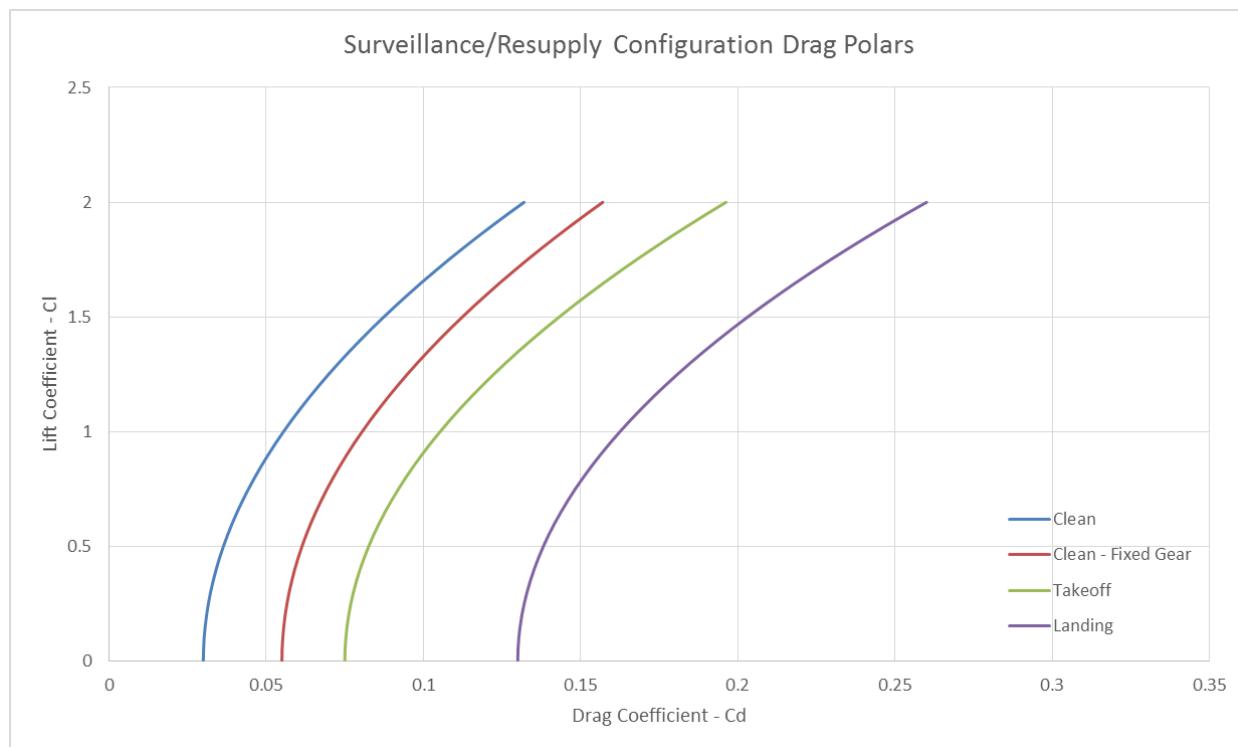


Figure 86. Drag polars for the surveillance/resupply configurations

### 3. Manufacturing and Build Process

#### 3.1. Methodology

As proposed in Section 1, the desire for this project is to utilize additive manufacturing in the construction of the various components and structures that makeup the aircraft. It allows for rapid construction and modifications to the design of the aircraft without large investments in manufacturing time and resources. This is due to material costs that are relatively low when compared to traditional construction methods as additive manufacturing utilizes a base material while traditional methods utilize various types of raw materials and specially manufactured products.

There are important considerations when utilizing additive manufacturing when constructing components. Structural integrity is one of the main limitations when to consider. Due to the nature of the process, the finished component does not have the strength of a homogenous component. This is primarily associated with FDM manufacturing as the bonding of the layers introduces a weak point in the structure. SLS manufacturing has more advantages in terms of the structural integrity of the finished component but at a higher cost. As such, the manufacturing method must be taken into strong consideration when creating CAD/CAM models of the components and certain structural elements must be designed in to meet strength requirements.

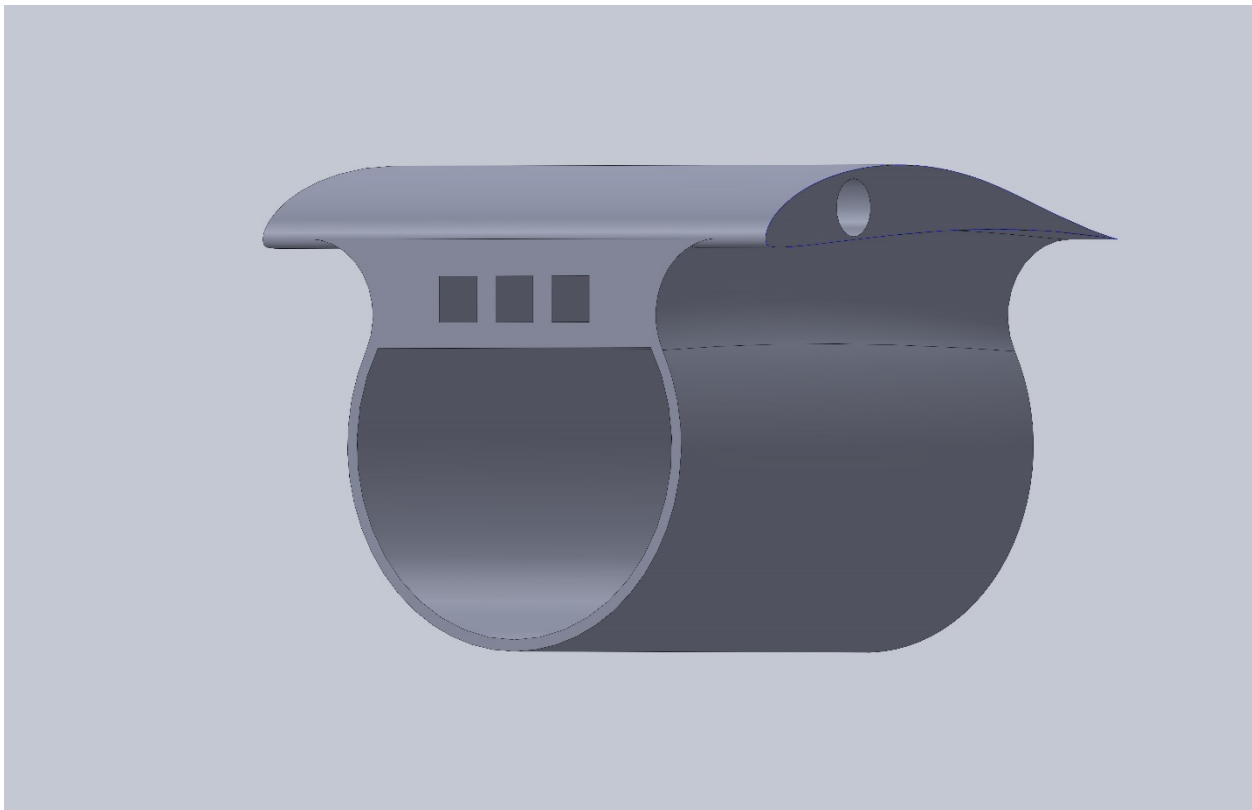


Figure 87. CAD/CAM model of the wingbox.

The figure above shows the preliminary model of the center section of the fuselage. This features an incorporated wingbox over the fuselage. This section is one of the most structurally critical

sections of the aircraft. The weight of the aircraft and payload is transferred to the wing through this section. Certain design elements are incorporated in order to ensure this component will be able to handle the stresses that may be experienced. The aircraft utilizes pre-manufactured spars running along the length of the fuselage and wing. These spars will cross in this fuselage section. These pre-manufactured spars are some of the off the shelf materials needed in order to support and strengthen the 3D printed component.

Due to build volume limitations of commercial 3D printers, many large components are required to be split up and constructed in sections, reducing the overall strength of the component as connection methods are required. The idea of incorporating modularity into the design of the aircraft was to offset such a disadvantage and use the construction requirement as a means to improve performance and increase the capabilities of the aircraft.

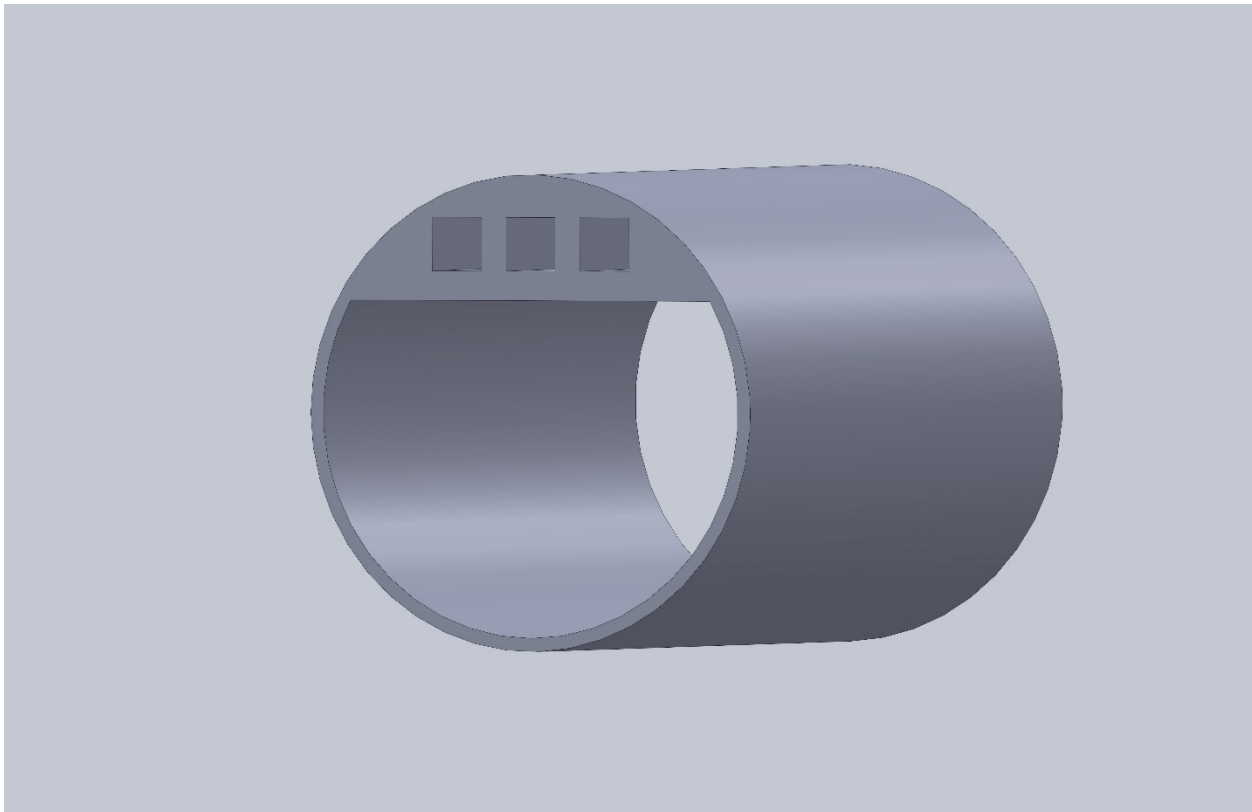


Figure 88. CAD/CAM model of the fuselage section.

The figure above shows a model of the fuselage section that attaches to the wingbox. Various section combinations can be fitted together in order to lengthen or shorten the fuselage for the desired capacity or even stability/aerodynamic requirements. This concept will be primarily applied to the wing design in order to achieve the necessary aerodynamic performance to fulfill the different mission specifications.

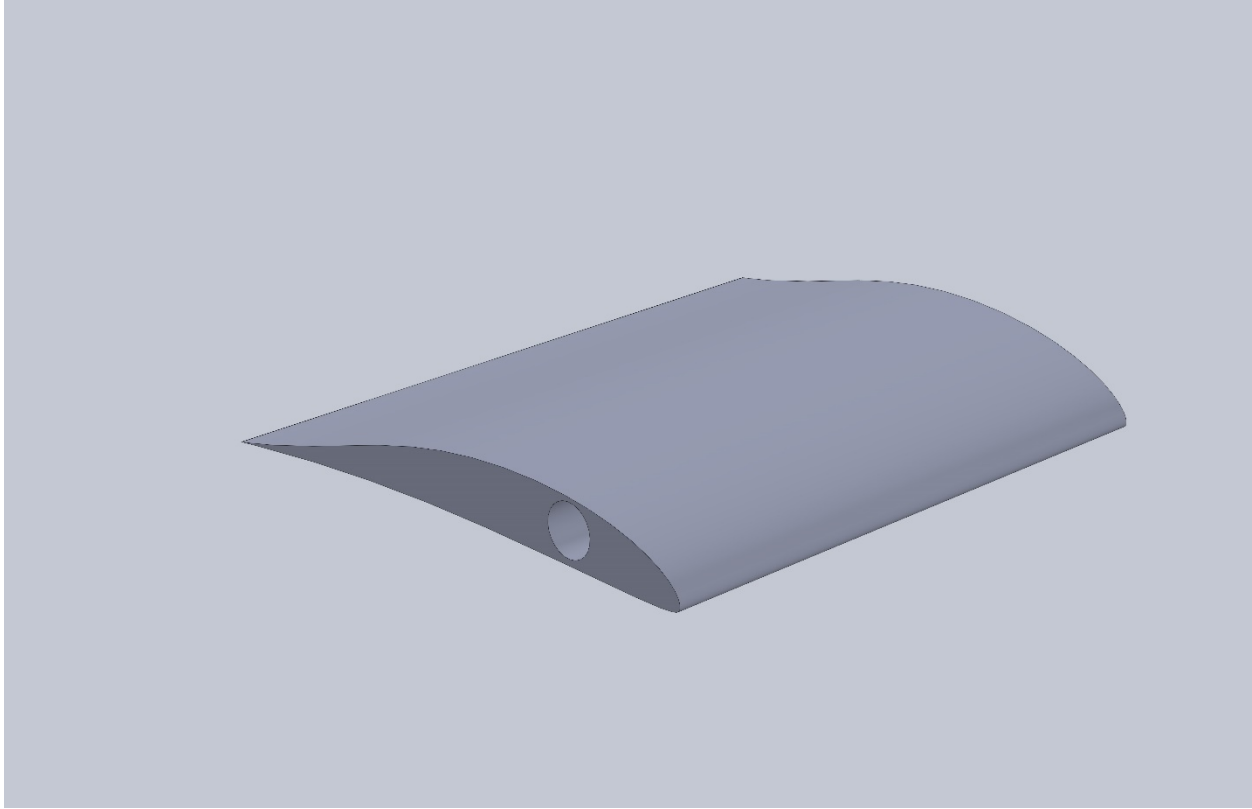


Figure 89. CAD/CAM model of the wing section.

The main difficulty in incorporating modularity into such a design is to develop a connection/joining method that is secure and strong enough to withstand operational loads and stresses while allowing for the ease of disassembly/reassembly. The main advantage of modularity is the potential cost savings from reusing components for multiple missions. As this project is primarily focused on the design of the aircraft itself, modularity may or may not be explored at this time and manufactured components may be permanently fixed together to reduced development time.

### 3.2. Manufacturing

Although composite structural members will be incorporated to take the majority of the loads and stresses of the aircraft, the choice of construction material for the sections will play an important part in the overall durability of the aircraft. For FDM manufacturing, there are a variety of materials available, each with their own different advantages and disadvantages. These are covered briefly in Section 1.

The selected raw material, polycarbonate, is one of the strongest 3D printer filaments available to the public. It is extremely durable and resistant to both physical impact and heat. It is an ideal 3D printer filament for parts that need to retain their strength, toughness, and shape in high-temperature environments, such as electrical, mechanical, or automotive components. Use of the carbon fiber reinforced variant yields a structural component with high heat, high modulus, excellent surface quality, dimensional stability. The downside of using such a material is the high cost, relative to other filament materials, and the demanding printer capabilities for successful

printing. Modifications are required to my existing printer before it is able to handle printing finished components.

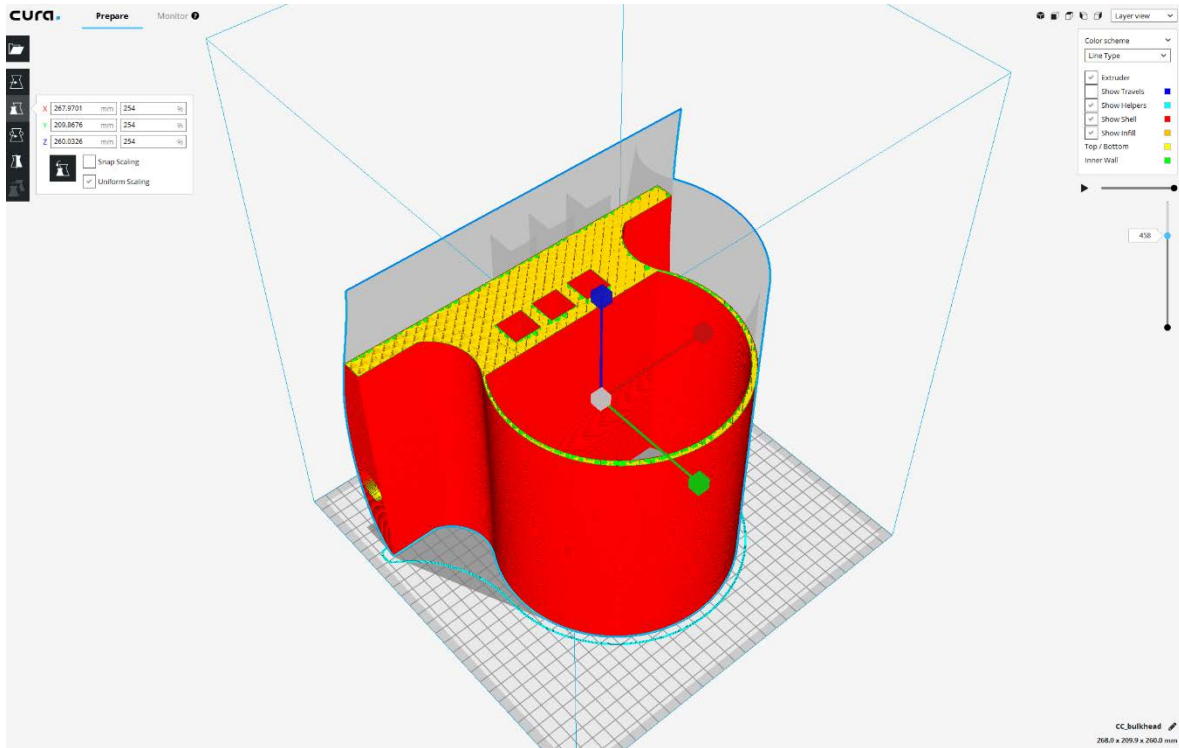


Figure 90. 3D printer pathway model of the wingbox.

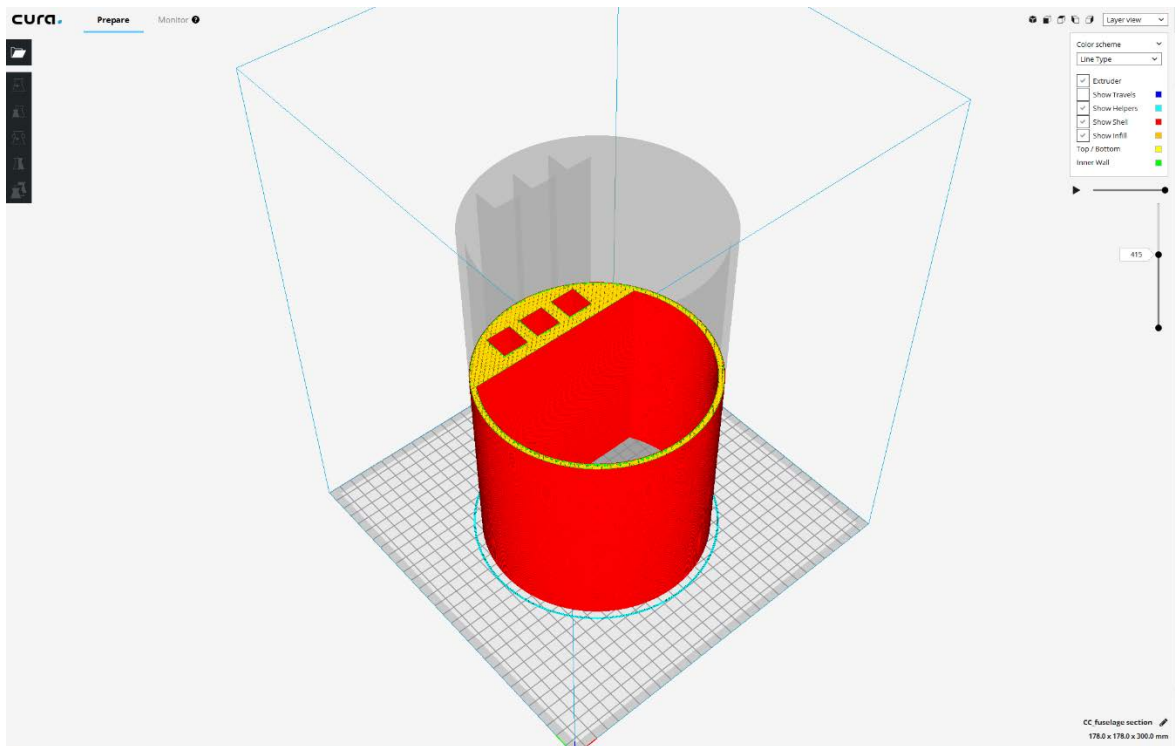


Figure 91. 3D printer pathway model of the fuselage.

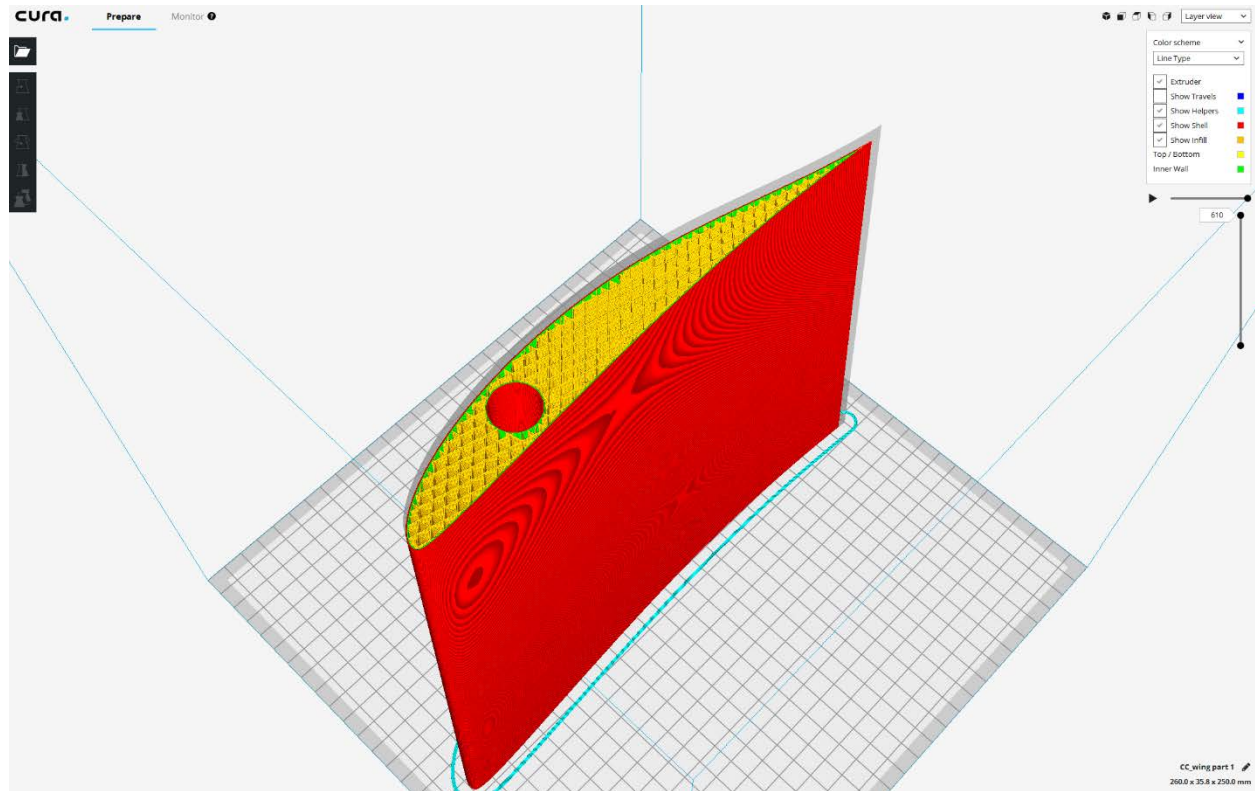


Figure 92. 3D printer pathway model of the wing.

The figures above are the various structural sections converted and rendered by the 3D printer slicing software. The slicing software calculates the printing path based on various inputs regarding layer height/quality, shell thickness/quality, infill pattern and density, and print speed. All these variables affect the speed, quality, strength, and weight of the finished product. Selecting the correct settings are vital to producing a finished section with the right balance of strength, weight, and manufacturing time.

In order to save costs, cheaper and easier printing PLA is utilized to create prototype components to test and validate the printer inputs. These prototype components will also be used to test fitment and alignment of the parts. Revisions and changes will be made as necessary. The figure below shows the wingbox section being printed. Very low infill percentages and a coarse layer height are utilized to reduced printing time. This results in a product with various surface imperfections and very low rigidity and strength. This component will only be used to test fitment with other components.

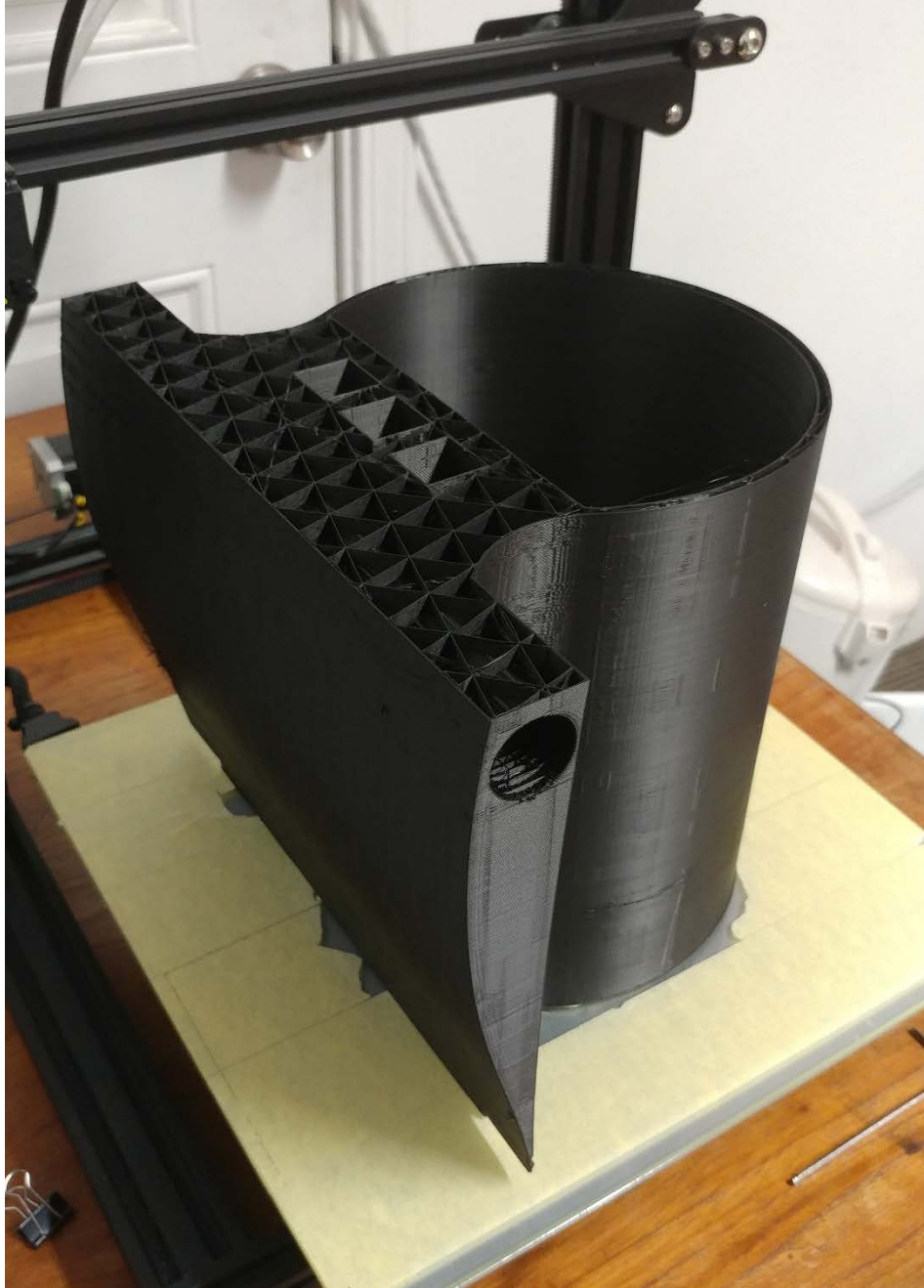


Figure 93. Wingbox section being constructed.

At this point in the project, modifications to the printer are required to create components that can be used in the flight testing and further development of the aircraft.

## 4. Flight Testing

### 4.1. Objectives

The objective of conducting flight testing is multifold. One is to verify the design of the aircraft itself and the interactions of the components and subsystems that make up the aircraft. One must remember that an aircraft is a culmination of various engineering disciplines working together as a unified object. Another objective is to determine the assess man-machine interface and determine the limitations of such connection. This can highlight certain weaknesses and areas of improvement in order to maximize performance through enhanced ergonomics and/or workload reduction by streamlining various processes.

### 4.2. Methodology

There are numerous reasons flight testing is performed. One reason has been the desire to push the limits of what is thought possible and to enhance the depth of knowledge. This comes in the form of research flight testing programs such as NASA's X-Plane program. Another is to further product development. This often occurs with prototype aircraft in order to determine the characteristics of a design and to iron out any potential problems with the product. A third reason is to validate if the aircraft is able to complete its intended mission. This usually occurs with near-production examples as a means of verifying the design and not to further development. Lastly, flight testing is done in order to comply with established requirements and regulations, often in regards to safety.

In all these cases, there is an established sequence in which flight testing is conducted. The sequence is progressive in nature as to limit the dangers the test pilots and engineers may face. Ironically, flight testing begins on the ground. Static ground testing is used to test functionality of various components and systems before the aircraft is flown. This insures that the aircraft can fly at a minimum. After ground testing, performance flight testing is performed. This phase of testing is used to determine basic performance characteristics of the aircraft such as range, endurance, climb performance, drag polars and increments, and power characteristics. After baseline performance characteristics are established, testing can progress into more dynamic categories. Usually, stability and control testing is conducted in order to determine if the aircraft can complete its intended mission in a safe and controllable manner. Testing often goes through various types of stability, particularly static and dynamic stability in the longitudinal and lateral-directional axes. The last phase of flight testing involves determining and pushing the limits of the aircraft. In this phase, the pilots and engineers seek to reach the limits of stall, spin, and vibration conditions in order to understand how far the aircraft can safely operate. As such with testing at the limits, this phase is the most dangerous and is usually reserved until the stability and control characteristics of the aircraft are documented and well known.

In any phase, it is best to set specific test objectives in order to be able to effectively plan out the testing program. The testing program will determine the type of information needed to be extracted from the flight tests in order to meet or fulfill the specified objectives. Different tests can be used to achieve objects while some objectives require multiple tests of differing conditions in order to gather the required information. Flight data cards should be utilized in order to keep track of testing conditions. In addition to general test data like test date/time, test purpose, aircraft weight, test technique, configuration, ect., the data cards should also include test specific data such as trim conditions (airspeed, altitude, temperature, ect.), test limitations (airspeed, altitude, control

force/range, power, ect.), and comments on the testing itself, ie conditions such as turbulence or specific data points.

### 4.3. Uncertainties in Testing Data

As with all methods of data collection and testing, there exists uncertainties and errors which can skew data points and affect end results. In flight testing, there are several sources ranging from instrument accuracy to human induced errors. It is important to identify areas of in which uncertainties and errors may occur in order to reduce and minimize their effect on the data and results.

One source of uncertainty is with instrumentation errors. Instrumentation error occurs as two main types: hysteresis error and bias error. Hysteresis error is the difference in readings between increasing and decreasing values. Nearly all instruments have hysteresis; but it can be minimized through testing and calibration in controlled settings such a laboratory. Bias error can be described as the difference between the correct value and the average of the hysteresis error. The figure below shows the method in plotting the error for a mechanical instrument. The graph can be used to calibrate the instrument over the range of operational values.

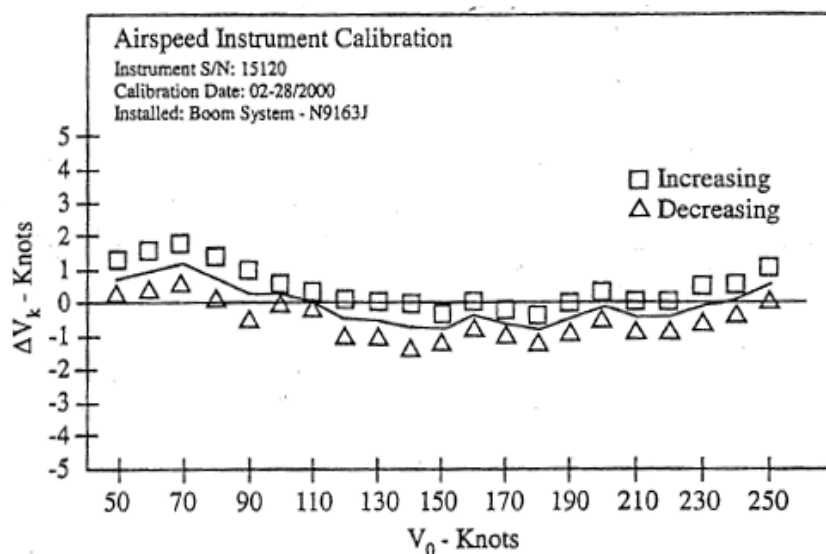


Figure 94. Airspeed instrumentation calibration [7]

Another source of error can be the result of the placement of sensors, specifically the static pressure sensor. This is significant as an accurate airspeed and altitude reading is essential to all flight, addressing and reducing error from this source is important. Since the error from this source can only be determined in flight, which in itself introduces errors, the best method in obtaining confidence in the readings and results is through repeated sampling of varying conditions. Increasing the sample size of the data can help weed out outliers and increase confidence in the correct data.

Although not as significant through the proliferation of digital readouts, reading errors by humans can be a source of uncertainty. This is more profound in testing with mechanical instruments.

A significant source of error in collected data and results can be due to the changing conditions of the flight test. Pressure and temperature changes across the atmosphere can skew results and data. It normally occurs as data is collected at varying altitudes. Climb and descent data are particularly affected due to this. Often times, atmospheric errors can be large and uncorrectable. Therefore, it is best to avoid atmospheric conditions, such as turbulence, that introduce these errors. One method of reducing atmospheric error can be to send a secondary aircraft to survey the test area and record the conditions. The test aircraft can then utilize this information to avoid the areas in which error may be introduced.

One example of atmospheric error is humidity or water vapor in the air. Most water vapor is concentrated in the first 3000-4000 ft. above sea level. Testing in this regime and at higher altitudes can result in disagreements in the flight data. As such, it is best to avoid these conditions but it is not always possible. One method of correcting for humidity can be to take temperature measurements at each test condition. This will allow for the partial pressure and eventually the density ratio to be calculated and used to correct the flight data.

Other uncertainty factors include pilot technique and thrust determination error. Errors induced by pilot technique may stem from simple human error, improper aircraft setup or configuration, or gross violation of testing principles. Thrust/power determination error often occurs if the engine cannot be calibrated prior to the flight test. In this case, tolerances must be set in order to factor in the uncertainty into the results.

#### 4.4. Testing Phases

##### 4.4.1. Static/Ground Testing

###### 4.4.1.1. Weight and Center of Gravity

The aircraft weight and center of gravity are important parameters to measure as their values are utilized in a wide range of calculations to determine various test parameters such as drag, stability, control and thrust available. The aircraft should be weighed and the center of gravity determined, either by mechanical means or digital means. Digital scales offer the ability to weight an aircraft while also calculating the center of gravity of the object. The aircraft should be weighed in various operating configurations and the center of gravity calculated for each configuration. The center of gravity should then be plotted in a CG excursion diagram.

Knowledge of the center of gravity for each aircraft configuration is important in order to understand how the stability and control of the aircraft will shift. If the center of gravity shift is determined to be too much, use of ballast can be an option of correct the issue.

FAA regulations require that the aircraft be tested at the most forward center of gravity at the maximum takeoff gross weight. This is to ensure the aircraft can operate in the most extreme of circumstances.

###### 4.4.1.2. Thrust

The thrust of an aircraft is an important parameter as it is a variable in many flight tests and used to calculate many variables such as drag, lift, speed, and climb performance. Aircraft engine performance should be tested and calibrated on the ground for the conditions and environments the aircraft will be operating in. The engine thrust can be best determined using an engine test

stand. The engine should be installed with the proposed inlet and nozzle as to simulate its operating configuration. The use of a different nozzle and inlet can skew thrust figures by as much as 15%.

## 4.4.2. Performance Testing

### 4.4.2.1. Stall Speed

The aircraft stall speed is one of the most important parameters determined in flight testing, since most other criteria are based on multiples of the stall speed. One difficulty in determining stall speed is defining the point at which stall occurs. From an aerodynamic standpoint, the stall speed is the speed at which the maximum lift coefficient occurs. From a regulatory standpoint, the civilian and military sector both have differing viewpoints for when stall occurs.

The FAA 14 CFR 23.49 defines stalling speed as the minimum steady flight speeds at which the airplane is still controllable. This is set at 110% of the true stall speed of the aircraft.

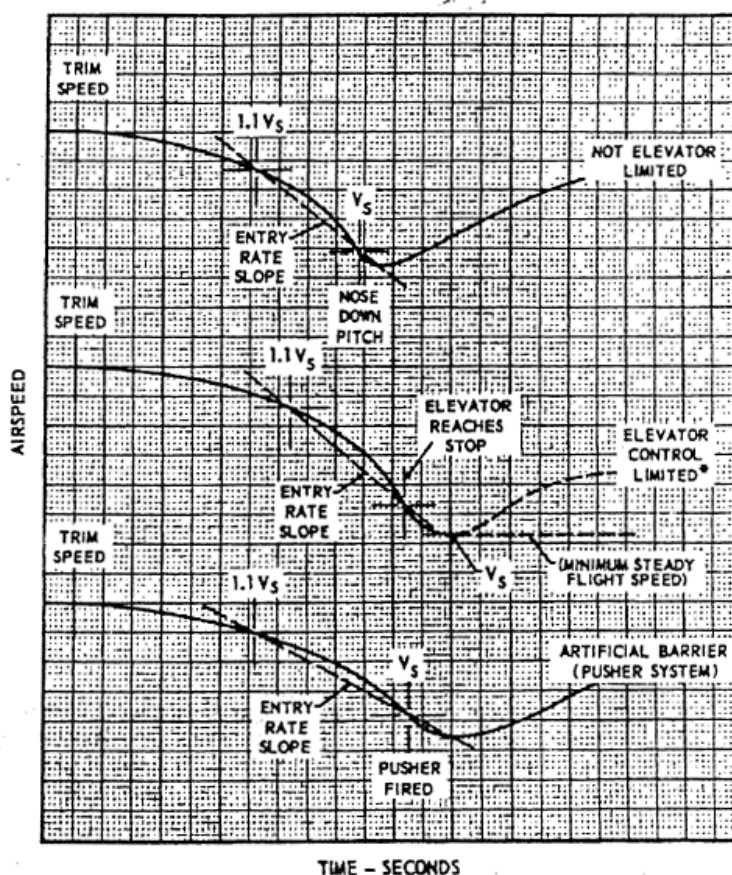


Figure 95. FAA stall speed definitions [7]

Stall occurs over a wing when an adverse pressure gradient develops over the upper surface as the angle of attack is increased. This causes the airflow to separate from the upper surface. The point at which the flow separation occurs is affected by various 2D and 3D parameters of the wing. These parameters include:

- Wing camber

- Wing thickness
- Leading edge radius
- Surface roughness
- Leading and trailing edge devices
- Wing planform
- Wing sweep
- Wing aspect ratio

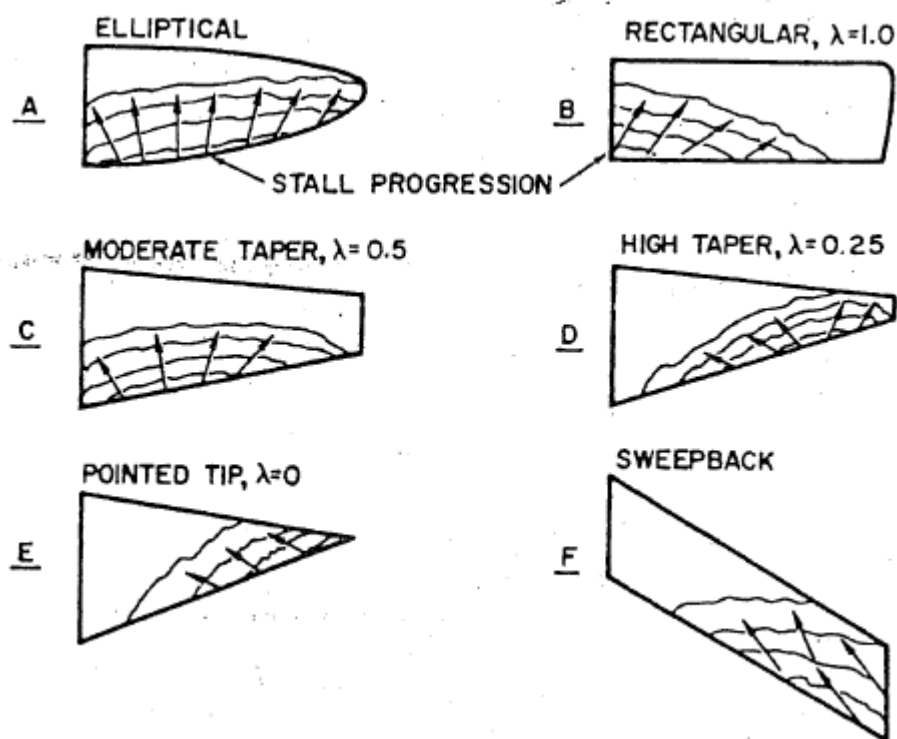


Figure 96. Effects of wing planform on stall [7]

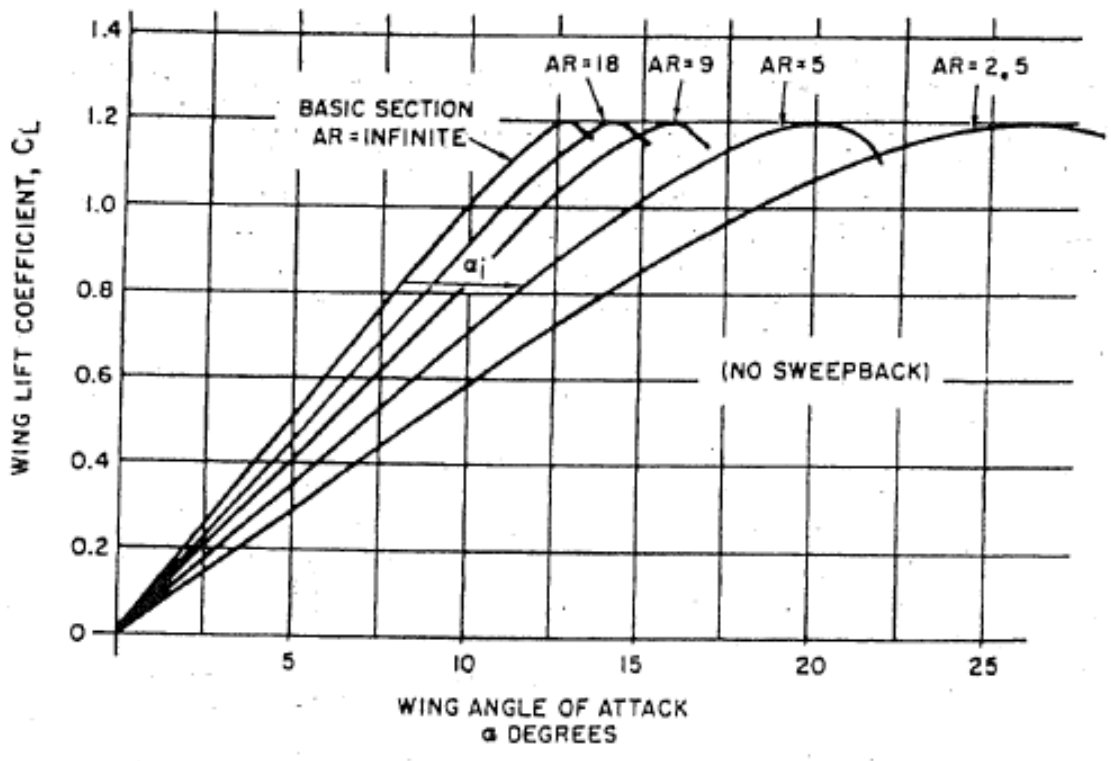


Figure 97. Effect of aspect ratio on lift coefficient [7]

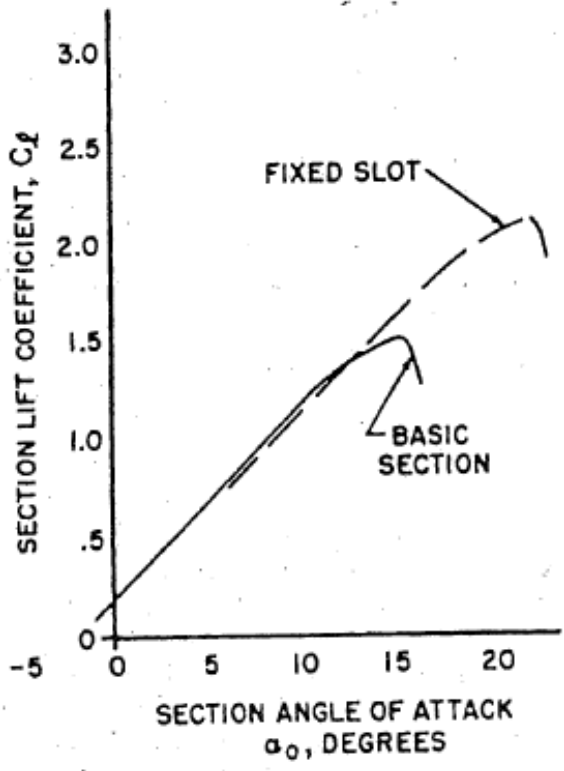


Figure 98. Effect of slots/slats on lift coefficient [7]

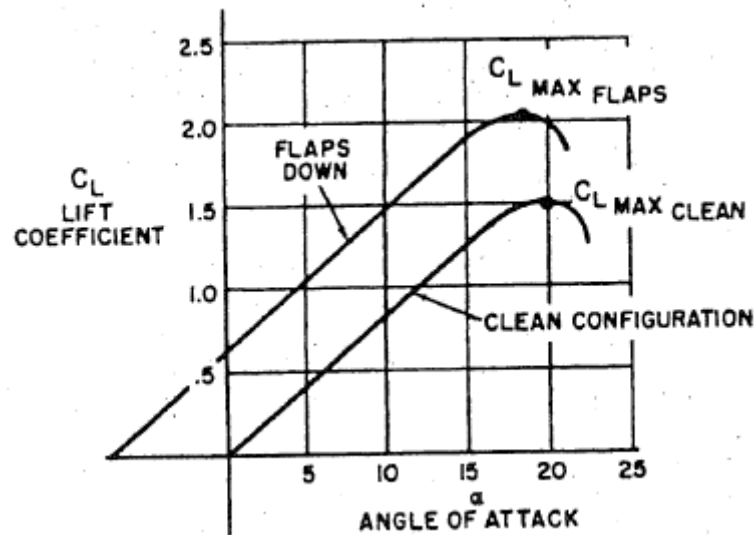


Figure 99. Effect of flaps on lift coefficient [7]

As we can see from the previous figures, different configurations can drastically affect the lift coefficient of the aircraft, effectively shifting the stall speed. FAR Part 23 provides conditions on how stalling speed is measured. These conditions can serve as the basis for the flight test method. FAR Part 23 states:

1. Stall speed is measured at forward gross loading
2. Aircraft is trimmed at 150% of true stall speed
3. Power idle or thrust zero
4. Deceleration rate to stall at 1 knot per second

#### 4.4.2.2. Thrust Available

It is important to test for the available thrust in an aircraft in order to determine airplane drag, which leads to a host of other important performance parameters. In many cases, it is not actually necessary to measure the actual thrust. Instead, flight data can be referenced to a variable that can indicate the thrust output, such as a “referred rpm” or fuel flow. This presents the problem if the engine is not producing the rated thrust for a given rpm or fuel flow rate. There are several ways in which thrust can be measured in flight. Each method has its weaknesses.

##### 4.4.2.2.1. Jet Flow Measurement

The jet flow measurement method is one of the most common methods in measuring engine thrust as it works well with a wide variety of jet engines. Gross thrust is determined by measuring the engine pressure ratio and solving for the gross thrust with the following equations for choked flow and unchoked flow, respectively.

$$\frac{F_G}{\delta A_e} = C_f \left( \frac{2\gamma}{\gamma - 1} \right) P_{SL} \left[ \left( \frac{P_{Tt}}{P_A} \right)^{\frac{\gamma-1}{\gamma}} - 1 \right]$$

$$\frac{F_G}{\delta A_e} = C_f P_{SL} \left[ 1.26 \left( \frac{P_{Tt}}{P_A} \right) - 1 \right]$$

For these equations, the thrust coefficient is determined by measuring the thrust during a static ground calibration as a function of EPR (Engine Pressure Ratio) and plotting  $C_f$  as a function of EPR. Since the static ground calibration cannot realistically simulate a high enough EPR as in flight, the relation must be extrapolated. This is where the source of error occurs with this method.

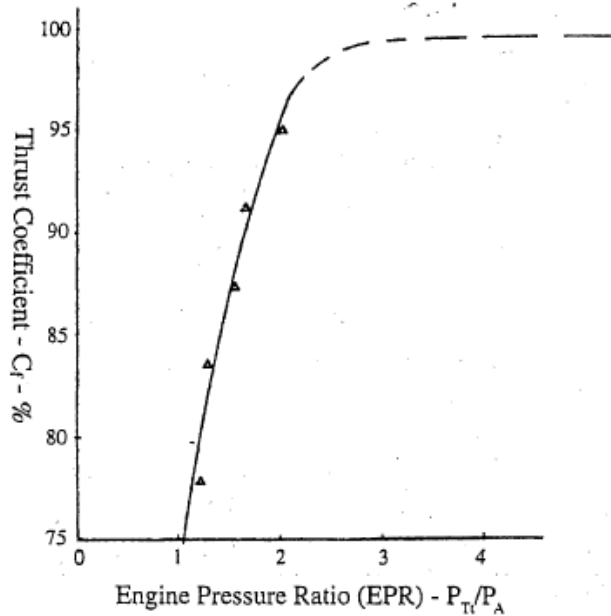


Figure 100. Thrust coefficient vs. EPR [7]

#### 4.4.2.2.2. Manufacturer Data

Another method of determining in-flight thrust is to simply use the engine manufacturer's thrust curves and calibration data. Due to the simplicity of this method, it is also one of the least accurate as it fails to account for many variables that may affect the net thrust. The main differences occur from installed thrust losses and engine calibration that may not be well suited for the proposed operating conditions.

#### 4.4.2.2.3. Wind Tunnel Calibration

An improvement over the previous method would be to calibrate the engine in a wind tunnel utilizing the proposed inlet and nozzle at the proposed operating conditions. This would allow for more accurate data regarding the engine performance in flight.

#### 4.4.2.3. Drag Polar

The accurate determination of drag is one of the most difficult tasks in flight testing. It is an important item in that the drag polar, in conjunction with the thrust output, will allow for the calculation of all the performance characteristics. There are several methods in which drag can be determined in-flight. Each of these methods has several strengths and weakness that will dictate the situation they should be used.

The speed power method is a fairly simple and straightforward method in which the assumption that at steady and level flight, the thrust generated by the aircraft is equal to the drag. Thus, if we know or can calculate the thrust, we can determine the drag, and ultimately the drag coefficient, of the aircraft at the given speed. With the additional assumption that lift is equal to weight in steady flight, the lift coefficient can also be calculated at that airspeed and a drag polar created.

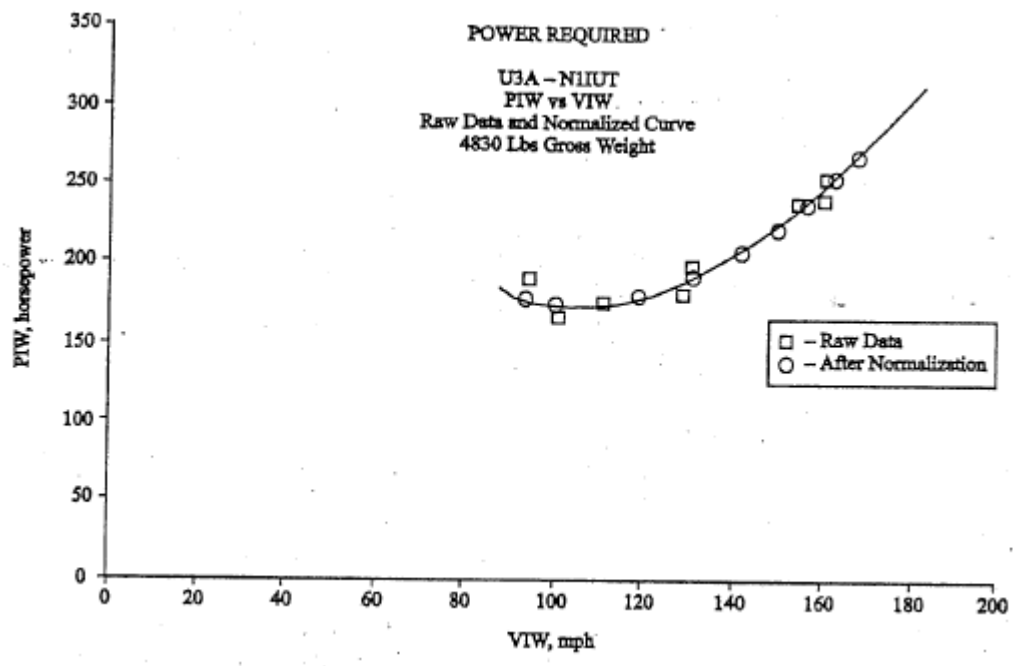


Figure 101. Power required vs. velocity [7]

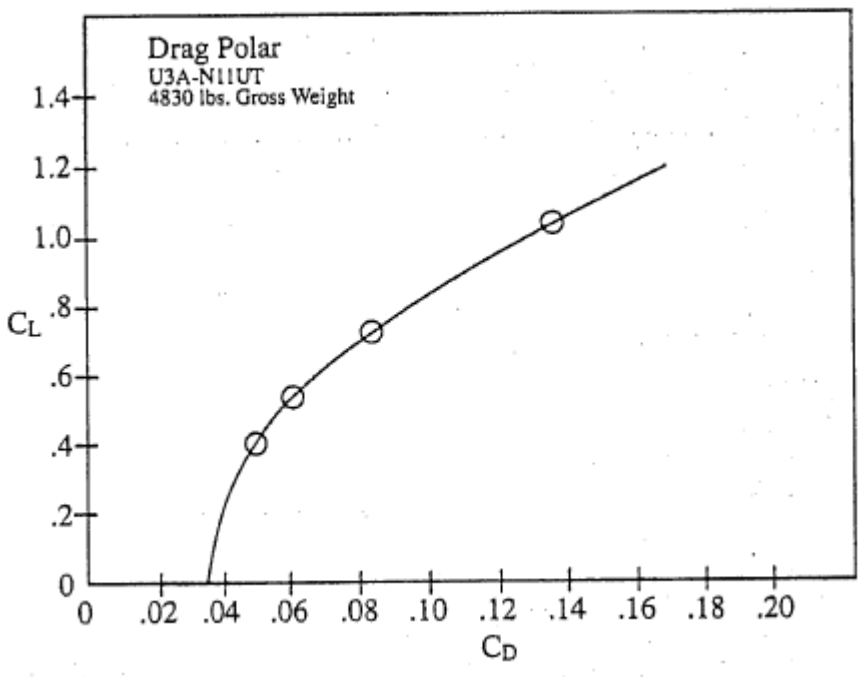


Figure 102. Drag polar [7]

The strength of this method is that the test is relatively simple and straightforward with the data being very easy to reduce to accurate figures. The disadvantages of the method come from the determination of the installed thrust or power. The method completely relies on the accurate determine of this figure.

A second method of determining drag is through the use of glide polars. The theory is that in a steady-state glide, the only forces acting on the aircraft are lift and drag, no thrust. As such, the drag will slow the aircraft down at a specific rate, reducing the lift generated.

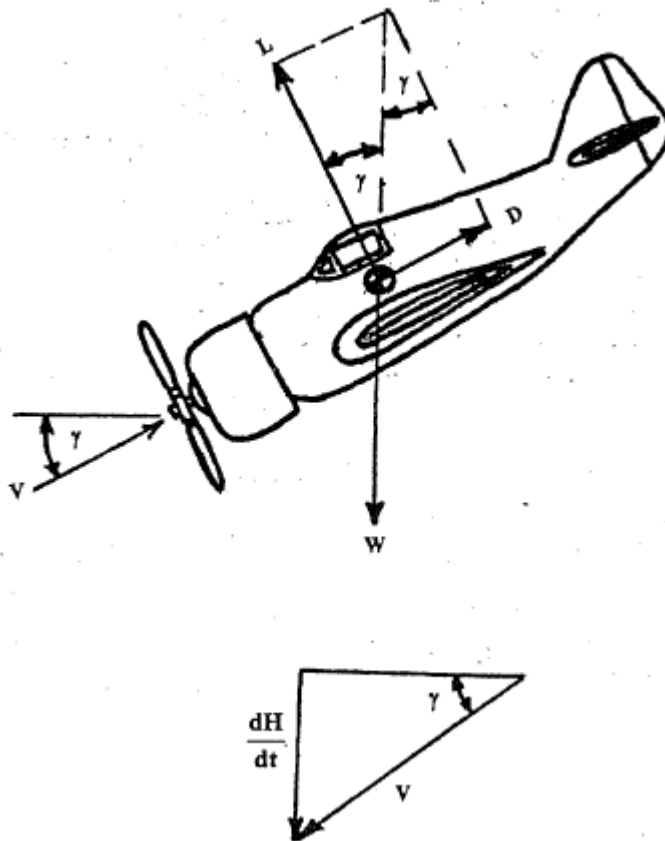


Figure 103. Forces on aircraft [7]

$$L = W_T \cos \gamma$$

$$D = -W_T \sin \gamma$$

From the above figure and equations, we only need to know the glide path and the weight of the aircraft. The glide path can be determined by the rate of descent and the airspeed.

The strengths of this method are its simplicity as it does not require any calculation or assumption about the power/thrust or the propeller efficiency. The disadvantages of the method are mainly related to propeller aircraft regarding the propeller configuration/feathering. In addition, this method should not be conducted on high wing or high wing loading aircraft as they tend to lost altitude very rapidly.

#### 4.4.2.4. Range and Endurance

Two important characteristics of an aircraft are its ability to cover large distances and to stay aloft for a minimal amount of fuel. These parameters are range and endurance, respectively.

Testing these parameters are relatively straightforward but the variables encountered in the testing can highly alter the results. As such, when performing range and endurance tests, it is important to take notes of the testing conditions in order to evaluate the performance in the correct context. Difference in air temperature, air density, aircraft loading, altitude, wind speed, ect. can drastically alter results.

The range and endurance of the aircraft ultimately rely on the efficiency of the aircraft. It is beneficial to refer to the specific range and specific endurance of the aircraft when talking about these performance parameters. The specific range is the distance traveled divided by an amount of fuel, either nautical miles per pound or kilometers per kilogram. The specific endurance is similar, hours flown divided by fuel amount, hours per pound or hours per kilogram.

With so many variables affecting the results, it is best to divide the variables in relation to the aircraft and the powerplant. For jet aircraft, the fuel used is dependent on the thrust produced. This leads to the evaluation of the aircraft using the thrust-required curve. The best range point is located where a straight line from the origin is tangent to the curve. This point occurs when the ratio of the root of the lift coefficient and drag coefficient are at a maximum.

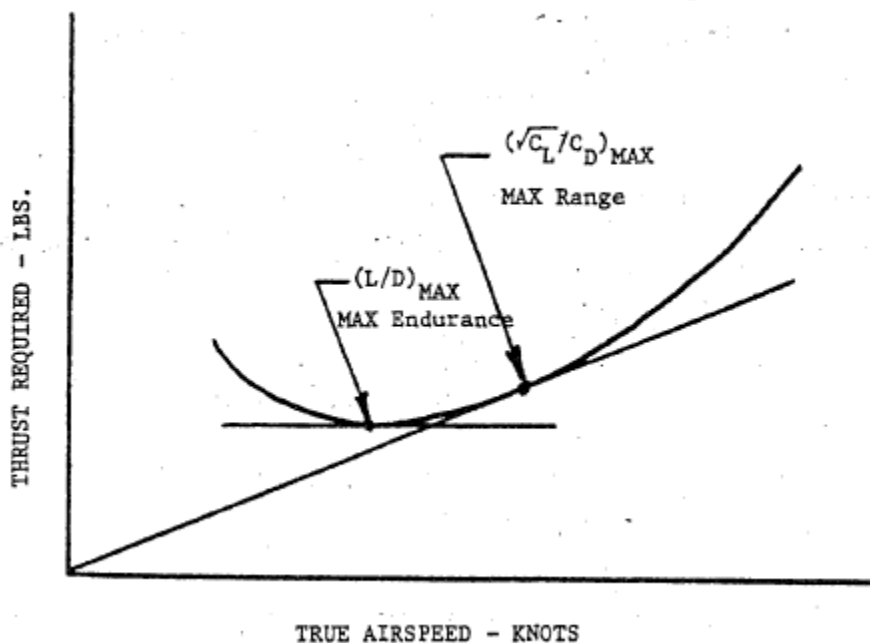


Figure 104. Thrust required curve [7]

With regards to the powerplant efficiency, it is known that increasing altitude can improve the efficiency of jet engines in two ways. First is that at higher altitudes, the inlet air temperature is reduced, reducing thrust specific fuel consumption. At higher altitude, density is also reduced, allowing for the engine to spin at a higher rpm to produce the same amount of thrust. Jet engines

operated at higher efficiency at higher rpm's. Thus, an aircraft will have an optimal airspeed and altitude to maximize range.

For endurance, we look again to the thrust-required curve, as fuel flow is a function of thrust. Therefore, the lowest fuel flow occurs at the lowest thrust required to keep the aircraft airborne. This point occurs at the maximum lift to drag ratio. In addition, we know that thrust and lift to drag ratio does not vary with altitude.

#### 4.4.2.5. Climb

Climb performance is a basic requirement in performance testing. Both the FAA regulations and military specifications have requirements for climb performance. Its importance is also highlighted by other parameters such as takeoff which rely on climb performance to meet design criteria.

There are two techniques to measure climb performance: steady climb and level acceleration. Steady climb is generally used on low speed aircraft and for all FAA climb performance requirements. Thus, we will be focusing on the steady climb flight test method.

The regulations in FAR Part 23 are divided into aircraft under 6000 lbs gross weight and aircraft over 6000 lbs gross weight. For multi-engine aircraft like the Modular UAV, climb must be tested in the clean configuration, in an engine out configuration, and a rejected landing configuration. The specific performance requirements of FAR Part 23 are not very relevant to this aircraft and thus only the method is derived.

The steady climb method, also call the sawtooth climb method, is conducted by performing a series of climbs at various airspeeds and altitudes. The climbs are several minutes in duration at each airspeed. Climbs are also conducted at each airspeed and altitude to eliminate wind gradient effects. Plots of pressure altitude and time are made for each airspeed and altitude and an average curve is drawn between the data of opposing climbs.

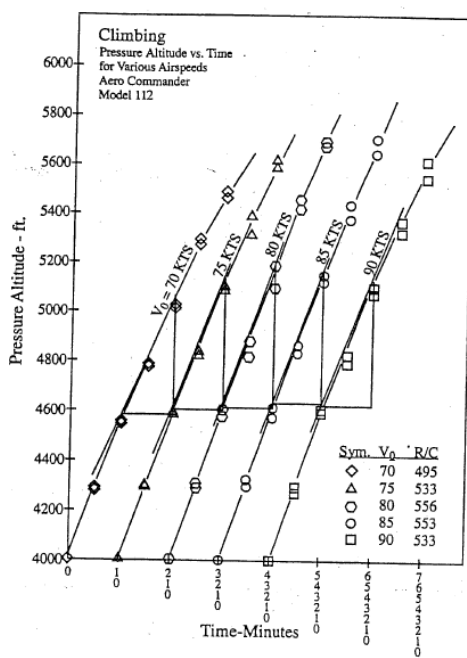


Figure 105. Altitude vs. time [7]

The resulting climb rates for each airspeed are plotted.

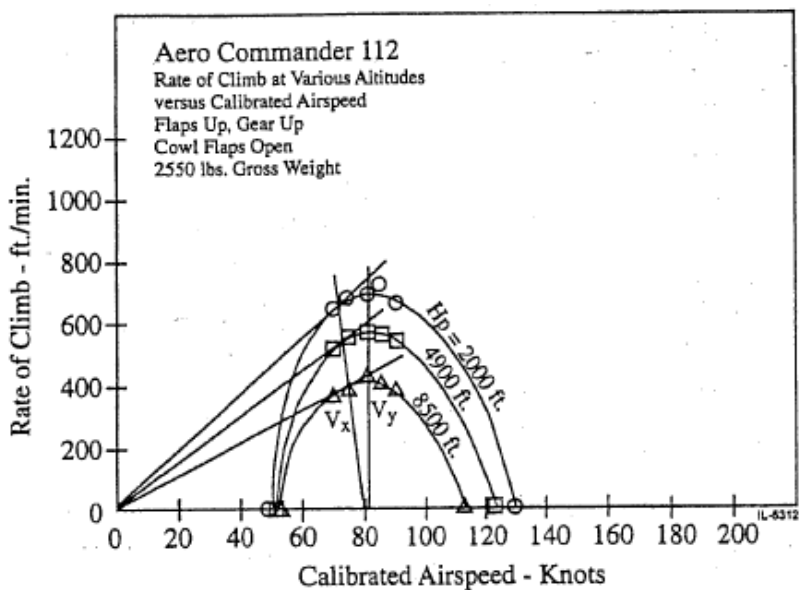


Figure 106. Climb rate vs. Airspeed [7]

The best climb rates at each altitude can then be determined. A line drawn from the origin tangent to the curve plots the best angle of climb speed.

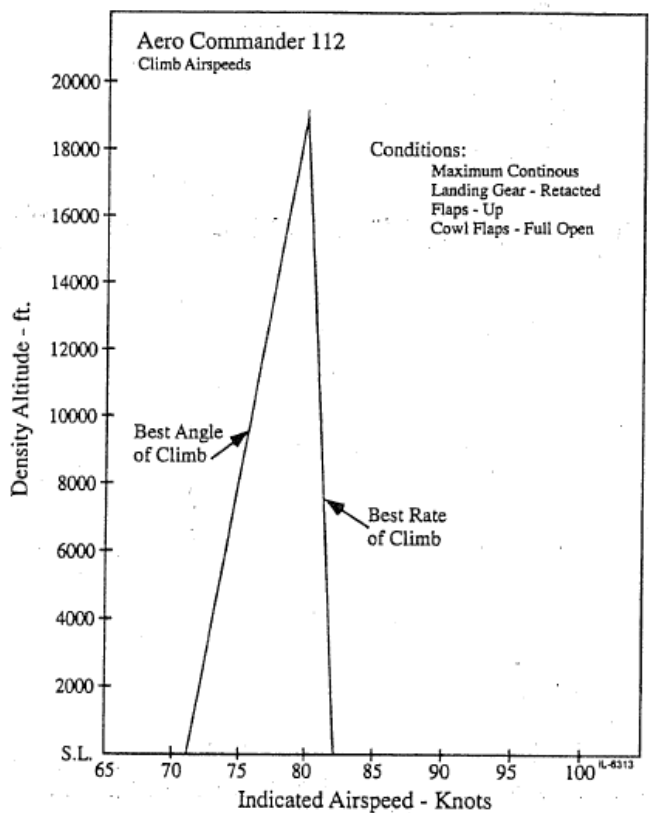


Figure 107. Altitude vs. Airspeed [7]

Once this speed is determined, climb tests at this airspeed can be conducted at various altitudes. These are called “check climbs”. They are used to validate the previous performance tests.

#### 4.4.2.6. Takeoff and Landing

Takeoff and landing performances are one of the most difficult flight data to obtain. This is due to the large amount of variables that may affect each test and skew or alter the data of that test run, mainly pilot technique. As such, takeoff and landing data may often be taken as approximations due to the large part pilot technique has over the results. As a result, the FAA did not have a regulatory requirement for light aircraft under 6000 lbs. The FAA has set requirements for light aircraft greater than 6000 lb but under 12500 lbs and transport aircraft greater than 12500 lbs. They are specifically covered by FAR 23 and FAR 25 regulations, respectively. There are several differences in the regulations but the main point is in the obstacle height that must be cleared by the aircraft.

For the FAR regulations, they state that the obstacle for the light aircraft (FAR 23) is 50 ft while the transport aircraft requirement is set at 35 ft for takeoff and 50 ft for landing. It is interesting that the light aircraft requirement is stricter. This requirement makes sense as the varying quality and types of airports that light aircraft have to operate out of necessitates a stricter requirement. As such, we shall focus on the FAR 23 regulation.

The FAR 23 regulation defines the variable, rotation speed, as the speed at pilot makes control input with the intention of lifting the aircraft out of contact with the runway. For single engine aircraft, the rotation speed must be greater than the true stall speed. For multi-engine aircraft, it must be greater than 110% of the true stall speed. For the determination of takeoff distance and climb to 50ft, it must be determined for each weight, altitude, and temperature within the operating limits of the aircraft in order to have a complete understanding of the takeoff performance. The tests must be conducted with takeoff power on each engine, flaps in takeoff position, and landing gear extended.

FAR 23 regulation defines the landing distance to be determined from the point at which the aircraft is 50 ft above the landing surface to the point it comes to a complete stop. This must be accomplished using a steady approach speed greater than the defined reference speed, which is 130% true stall speed, and an approach gradient less than 5.2% or 3 degrees.

There are several methods in which takeoff and landing performance can be tested and measured. They range from simple and inexpensive to complex and expensive. As previously stated, the data collected from these test can vary greatly due to a number of variables. In particular, the ground roll portion of takeoff can be affected by wind, runway slope, aircraft weight, air density, air temperature, pilot technique, and runway surface condition. The shortest runway roll may not result in the shortest total takeoff distance as the airborne portion must also be considered. The airborne portion can be affected by wind, wind shear, aircraft weight, air density, air temperature, pilot technique, and ground effect.

##### 4.4.2.6.1. Sighting Bar Method

The sighting bar method is one of the simplest and least expensive testing methods. The method consists of one or two sighting bars located at known distances from the runway. In conjunction with runway observers and a stopwatch, takeoff and landing data can be recorded. Although

relatively crude, the simplicity of the method allows for repeated tests that will provide for a greater sample of data, allowing for greater accuracy.

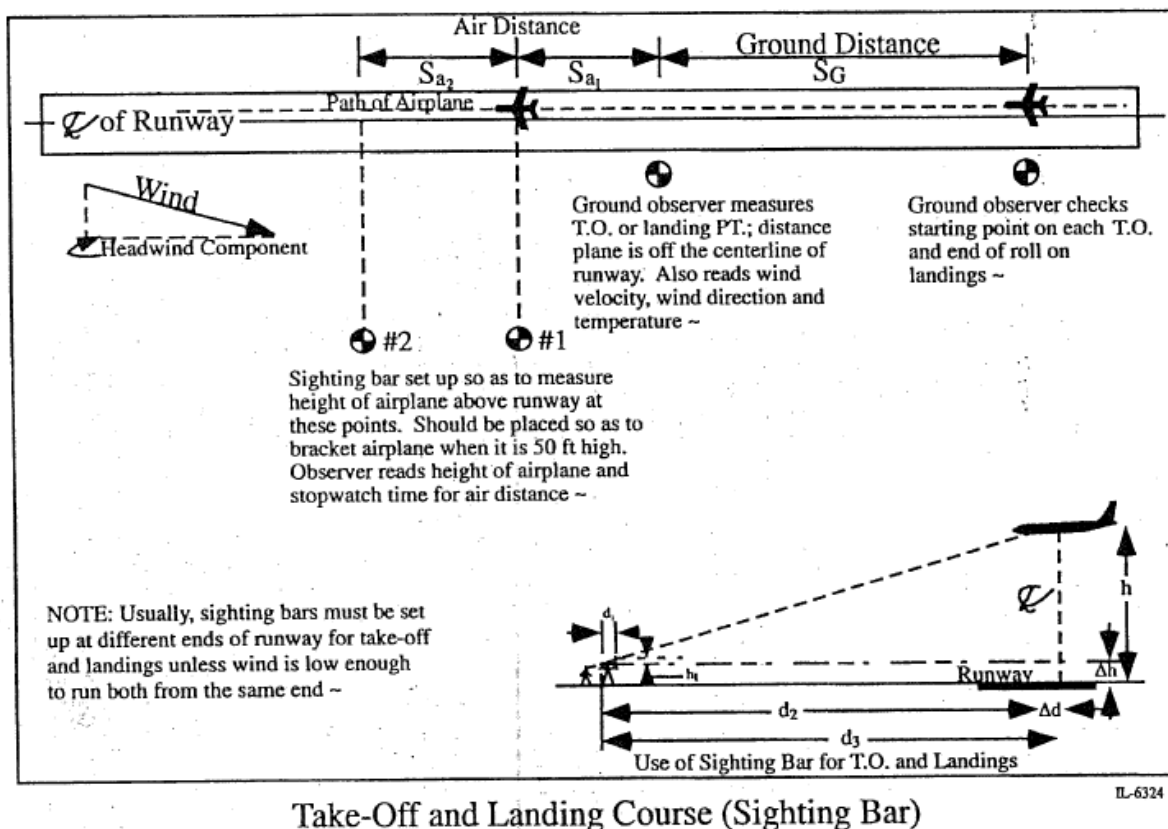


Figure 108. Sighting bar method [7]

Although there are other more complex methods involving cameras and film analysis, the sighting bar method is deemed to be the most practical for this project.

#### 4.4.2.6.2. Testing Method

With such a large number of variables affecting the takeoff and landing data, every effort must be taken to reduce these inconsistencies. Atmospheric variables such as wind, outside air temperature, and pressure altitude should be recorded at the time of test for each test run. The wind velocity and direction should also be recorded at both the 50ft object and 6ft above the runway. Tests should not be conducted at wind speeds greater than 10 knots as wind corrections are unreliable above those speeds.

The takeoff procedure should also be standardized to minimize data scatter. The aircraft should be:

1. Stopped at the starting point
2. Power increased to takeoff power and allowed to stabilize
3. Brakes released

The pilot technique for ground roll, rotation, and climb should be consistent across all test runs.

The procedure for landing tests are similar to the takeoff procedures, only in reverse. The power setting is not nearly as important in this scenario but special consideration should be taken to ensure residual power does not remain and skew the landing data. Braking should be applied at the maximum force without skidding the tires. The brakes should also be given ample time to cool so as to not fade during the following tests. As with the takeoff procedure, the landing procedure should be performed as consistently as possible across all test runs.

#### 4.4.3. Stability and Control

All aircraft must have adequate stability and control to perform its intended mission. The quantity of each of these traits are determined by the mission itself and the purpose of the aircraft. For example, a transport aircraft will place a high priority for stability in order to increase safety and give the passengers a smooth and comfortable ride. A fighter aircraft would place a high priority on control and agility for combat maneuvering and performance. As such, regulations differ depending on the aircraft purpose.

In terms of stability, there are two types: static and dynamic. Static stability is defined as the tendency to return to equilibrium is a system is disturbed. Figure 102 shows the different types of static stability. These types can be further divided into stick-fixed or stick-free conditions as the aircraft can exhibit different levels of stability depending on the control conditions.

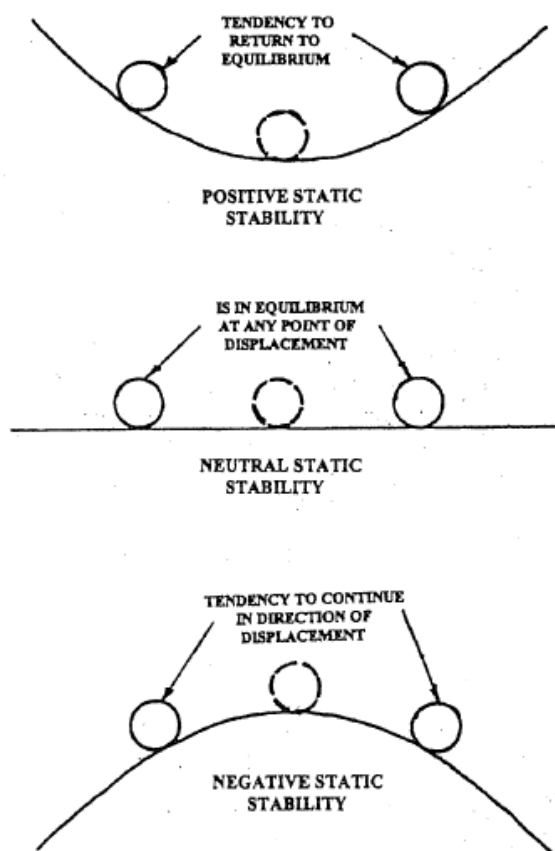


Figure 109. Static Stability [7]

Dynamic stability can be defined as the resultant motion of the aircraft with respect to time. An aircraft is deemed to display positive dynamic stability if the amplitude of the resulting motion decreases with respect to time. Dynamic stability can be divided into two modes, each describing a type of motion. Figure 103 shows a representation of different static and dynamic stability combinations and their resulting motion.

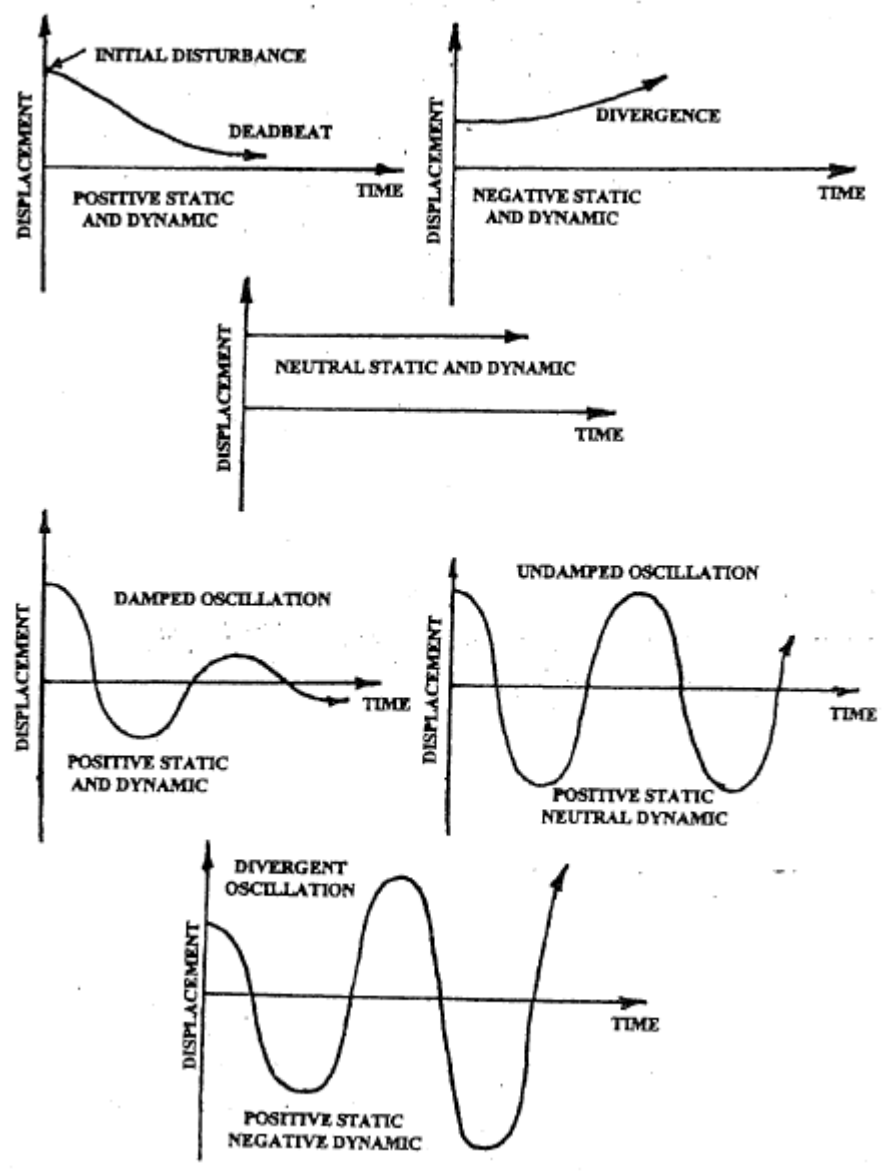


Figure 110. Dynamic stability [7]

In order to quantify different stability direction and attributes, aircraft have a body axis system to illustrate their motion.

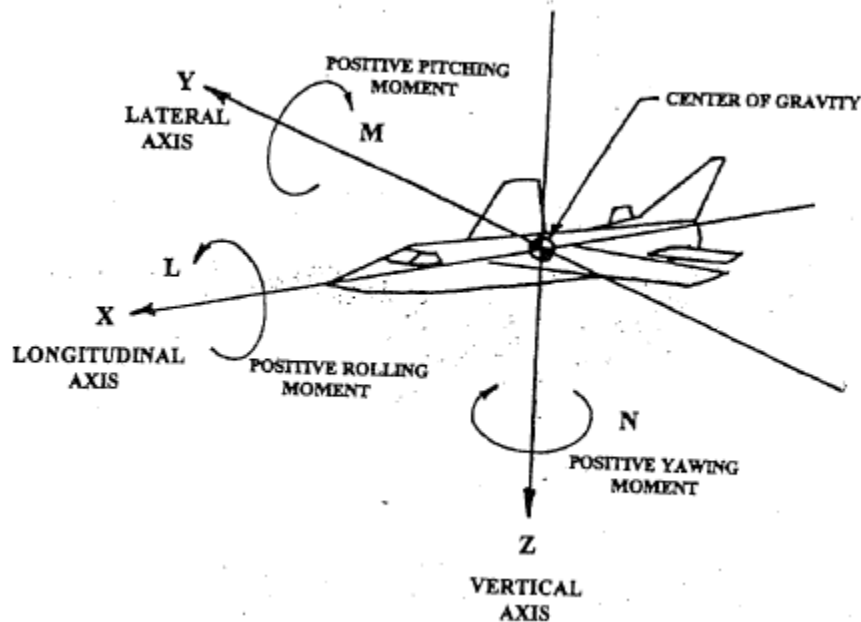


Figure 111. Aircraft body axis system [7]

#### 4.4.3.1. Static Longitudinal Stability

When speaking of longitudinal motion, we are talking about motion in the plane of symmetry of the aircraft. For small disturbances, longitudinal motion is not coupled with other axes and can be analyzed as 2D motion. This greatly simplifies the analysis.

In discussing longitudinal stability and control, the discussion can be separated into maneuvering and nonmaneuvering motions. Nonmaneuvering motions include:

- Takeoff
- Climb
- Cruise
- Holding
- Gliding
- Descent
- Approach

In each of these motions, several characteristics define the stability during these motions. These characteristics include gust stability, speed stability, and flight path stability. Gust and speed stability are related to the traditional definitions of static longitudinal stability and are based on stability margins while flight path stability is related to the pilots opinion of the aircraft.

The FAA has defined requirements for static longitudinal stability since its inception. However, the requirements are only for the stick-free case in which the aircraft is displaced from equilibrium, or trim. There is no requirement for stick-fixed longitudinal static stability or flight path stability. In the simplest terms, positive static longitudinal stability can be described as requiring a pull force to obtain and maintain speeds below trim and a push force to obtain and maintain speeds above trim. FAR Part 23 only defines a return of speed within plus or minus 15% of the original trim

speed when the stick force is slowly released. There is no requirement for measuring pull/push force.

The flight test method for determining the neutral points involve setting the airspeed of the aircraft and recording the following data points:

- Observed trim speed
- Elevator position (non-zero)
- Longitudinal control force (zero)
- Fuel consumed (test weight calculation)
- Power setting
- Altitude
- Ambient air temperature

The airspeed is then increased or decreased through the use of the longitudinal control and held by exerting a constant force on the control. The above data points are then recorded for this control condition. The test is then alternated, increase airspeed of previous test was a decrease in airspeed. The change in airspeed between tests should be 5-10 knots apart and continued until the stable range is covered. Then the longitudinal control is slowly released toward trim. This airspeed is recorded as the “free return airspeed.” This airspeed should be within the regulation requirements.

#### 4.4.3.2. Dynamic Longitudinal Stability

As previously mentioned, dynamic longitudinal stability involves evaluating the resultant motion over time due to a disturbance. As such, the flight test method must differ from the static stability method. In addition, more sophisticated data collection methods must be considered as aircraft responses may be oscillatory or short period. As such, dynamic stability must be separated to evaluate the phugoid (long period) or short period motion.

FAR Part 23 regulation requirements mirror CAR 3 regulations stating that any short period oscillations that occurs between stalling speed and the maximum permissible speed must be heavily damped with fixed-stick and free-stick controls. FAR Part 23 goes further in dealing with short period motion and phugoid motion, stating the airplane should not exhibit a dangerous characteristic when controls are released from a displacement of greater than plus-minus 15% of trim speed. In addition, the phugoid motion should not be so unstable as to increase the pilot workload or endanger the aircraft.

The method to evaluate phugoid motion is relatively simple. It involves setting the aircraft up to the test configuration (power, gear, flaps) and trimming to a test trim speed. Airspeed is then displaced by 10-15 knots with the elevator controls. The elevator is then returned to the trimmed condition with controlled movement at the aircraft’s long period frequency and the oscillation recorded. The test can then be conducted for the opposing condition.

For short period motion, methods differ depending on if the test is evaluating the aircraft short period or the elevator short period. To evaluate the aircraft short period, there are three motions that can be utilized to excite the short period motion: the double input, the pulse input, and the 2-g pull-up.

The double input is a good method for evaluating short period motion as it will excite the short period while the second input suppresses the phugoid. The input is performed by quickly moving the down, then up, and back to trim condition.

The pulse input is best described as half of a double input. It is performed by either moving the control forward or aft of trim. Since this input is lacking the second motion, the resulting motion will contain phugoid motion. As such, this is not as effective of a test input as the double input. This input is useful for airplanes that have a very high short period frequency.

The 2-g pull-up input is a good method for evaluating short period motion as it also suppresses the phugoid. It is also a good method for aircraft that have a low short period frequency. It is performed by trimming the aircraft and the pilot pulling up on the controls, gaining altitude and decreasing airspeed. The pilot then pushes the control down and enters a fairly steep nose down dive. The aircraft is slowly rotated to return to trim speed and altitude.

To evaluate the elevator short period, the pulse input is utilized while stick-free. The motion is expected to be heavily damped.

#### 4.4.3.3. Longitudinal Control and Trim

In the previous sections, it is discussed how longitudinal stability is affected by the center of gravity of the aircraft. Generally, an aircraft becomes more stable as the center of gravity travels farther forward toward the nose. The aircraft's stability is critical at its rearmost center of gravity location. In the same sense, the change in center of gravity location also affects the longitudinal control and trim of the aircraft. This is due to the reduction in the moment arm the elevator is able to act on as the center of gravity is moved rearward. Elevator control power does not increase as rapidly as longitudinal stability as the center of gravity moves forward, thus the forward center of gravity location is limited by control power. In addition, the ability of the trimming device to trim out longitudinal control forces throughout the speed range is also a subject of center of gravity location.

The FAA has requirements on longitudinal control and trim. For control, the FAA has three requirements that must be met. First, the aircraft should be able to maintain a power-off glide with a minimal amount of stick force (10 lbs specified) for any weight or center of gravity location. Second, the airplane should be able to be brought to a landing altitude by normal use of all normal controls except the primary longitudinal control. Third, the aircraft should be able to achieve a load factor of 1.5G.

For trim, the FAA has specified the aircraft must be able to be trimmed for hands-off flight for three flight conditions.

1. Climb at max continuous power at climb speed
2. Powered approach for 3 degree descent at approach speed
3. Climb with OEI, clean configuration and engine at max power up to 140% stall speed

These three cases represent the most extreme and common cases in which the trim is used.

#### 4.4.3.4. Static Lateral-Directional Stability

Lateral-directional stability is the reaction of the airplane when its flight path deviates from the plane of symmetry. It is referred to lateral-directional as these motions are often coupled to one

another. The angle that the plane of symmetry makes with the relative headwind is called the sideslip angle. The angle that the plane of symmetry makes with some fixed reference is called the yaw angle. The goal of direction stability is to have the aircraft maintain zero sideslip. This is called the weathervane or weathercock effect. Lateral stability refers to the tendency to return to level flight due to sideslip creating differential lift across the wings, causing the aircraft to roll and turn.

The FAA requirement on lateral and directional stability state that the aircraft should exhibit static directional stability for all landing gear, flap, and symmetrical power settings for speeds of 120% stall to the maximum airspeed. In addition, rudder deflections and forces should be proportional to the sideslip angle. It also states that the aircraft should exhibit positive lateral stability by demonstrating the ability to raise the lower wing back from a bank of 10 degrees or greater.

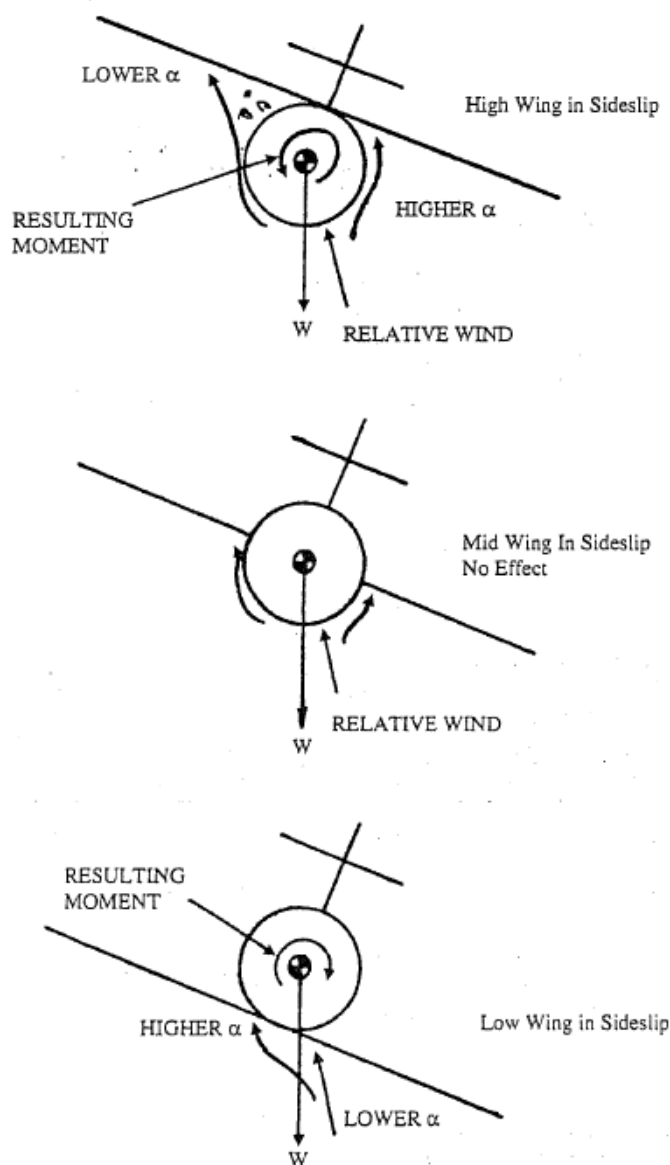


Figure 112. Effect of wing configuration on lateral stability [7]

The flight testing method for this parameter yields qualitative results. However, this is sufficient to satisfy FAA regulations. The test method is fairly simple: for the lateral stability test the aircraft is held to a bank angle of at least 10 degrees while maintaining a steady heading. Compliance with the regulation is demonstrated when the aircraft returns to level flight when the aileron controls are released. The directional stability test is conducted in a similar method. The rudder is utilized to generate a yaw angle. The aircraft satisfies the directional stability requirement if the aircraft returns to straight flight. Improvements can be attempted depending on the satisfactory nature of the aircraft characteristics during these tests.

#### 4.4.3.5. Dynamic Lateral-Directional Stability

In the static lateral-directional stability flight testing, the coupled nature of the responses were not considered as they did not manifest itself. In free flight, it is often not the case and the couple nature must be considered during dynamic stability testing. As with dynamic longitudinal stability, dynamic lateral-direction stability refers to oscillations in the responses to inputs.

In lateral-directional motion, there exists three modes: the spiral mode, the roll mode, and the Dutch roll mode. The spiral mode is the motion in which an initial sideslip disturbance induces a small roll, causing a yaw angle to form. If unstable in the spiral mode, the aircraft will continue to steadily increase roll angle and thus yaw, resulting in a spiral flight path. The roll mode refers to the motion of the aircraft due to disturbance rolling moment due to asymmetric lift. If the aircraft is unstable in this mode, the aircraft will keep rolling in the direction of the disturbance. The Dutch roll mode is a motion in which a rolling moment causes the aircraft to roll, changing the lift and drag between the wings. This change causes a yawing moment to develop which further changes the lift and drag, resulting in another rolling moment. The Dutch roll refers to this couple, oscillatory motion.

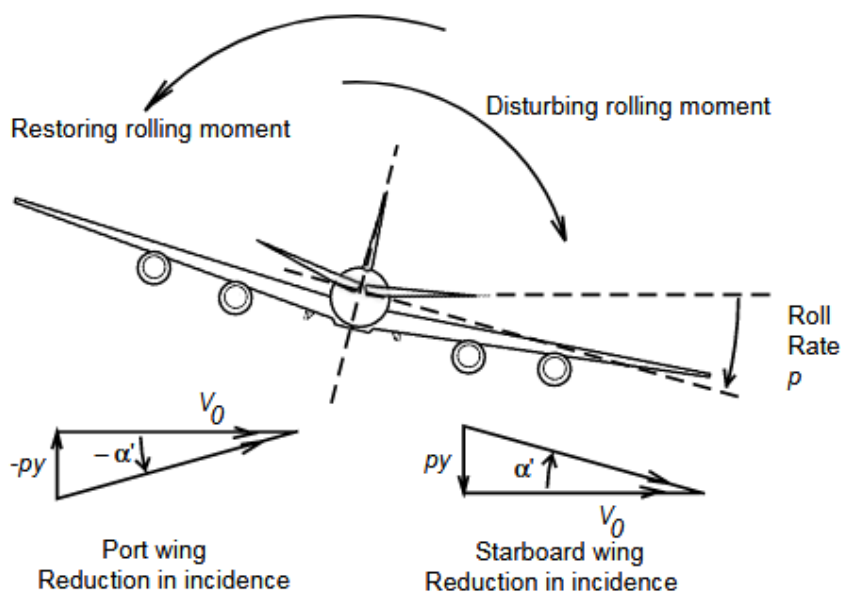


Figure 113. Roll mode [7]

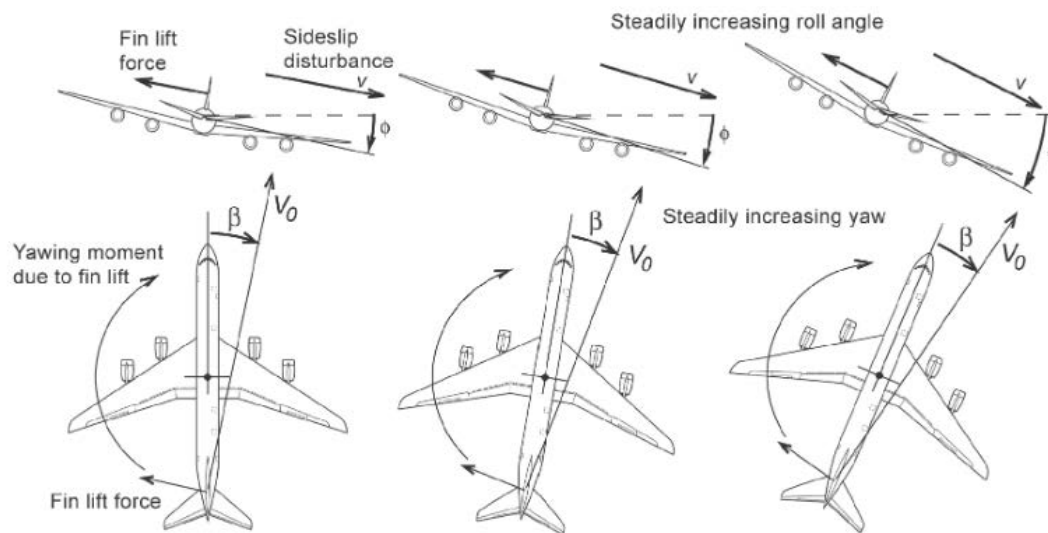


Figure 114. Spiral mode

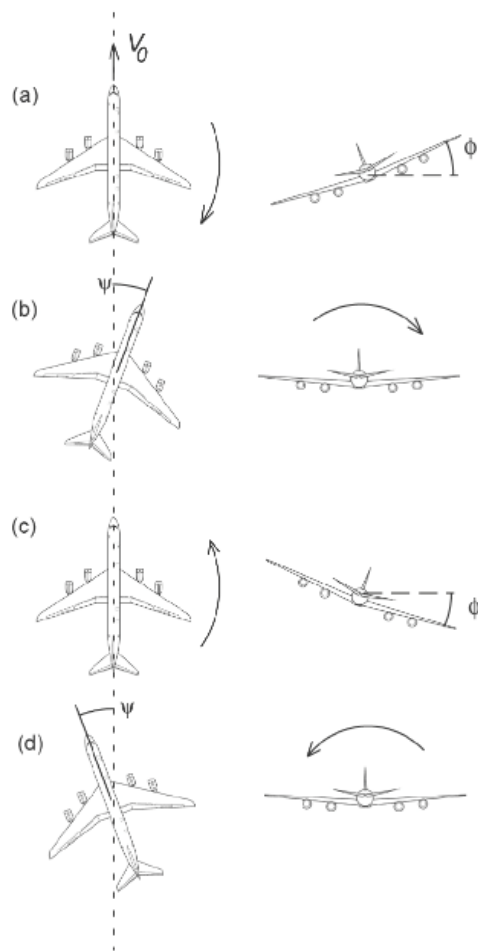


Figure 115. Dutch roll mode

The FAA has set fairly vague regulations regarding short period and long period oscillations for aircraft. For the short period oscillations, it reads similarly to the longitudinal stability section in that and short period oscillations must be heavily damped in both the fixed-stick and free-stick situations. FAR Part 23 also includes a regulation on long period, Dutch roll motion. It states that Dutch roll oscillation that occurs between stall speed and maximum allowable speed be damped to one-tenth amplitude within 7 cycles with primary controls in the fixed and free case.

The FAA does not have any regulations regarding spiral mode stability as it is fairly easy to correct through trim or pilot input. This is also the case for the roll mode and will be evaluated further in the lateral-directional control testing.

As stated above, the FAA does have regulations regarding damping requirements of the Dutch roll mode. There are two common methods to incite the Dutch roll mode for damping ratio calculation: rudder kicks and doublet inputs. In the rudder kicks, the rudder is depressed and released rapidly. The problem with this method is that this also excites the spiral mode, causing a wing to drop. A better method is the doublet input. In this case, the rudder is moved left and right in phase with the airplane. The airplane is then returned to normal or trimmed in roll before the rudder is released. This will cause a pure yaw moment, exciting the Dutch roll mode without exciting the spiral mode.

#### 4.4.3.6. Lateral-Directional Control

Lateral and directional control is the ability to roll and yaw. Lateral control power is important as banking is the most efficient way to make a heading change. In addition to large heading changes, lateral control is important in making small lateral corrections and movements. In this case, the pilot is only worried about the initial response as the airplane never reaches steady state. For large heading changes, the pilot is considering the initial response, roll acceleration, as well as the steady state response of the input. Thus, it is important to ask if the lateral control is sufficient in providing adequate roll acceleration for minute inputs as well as enough control authority to provide a steady state rate for large motions.

The FAA specifies a rate of roll requirement for aircraft that fall under FAR Part 23. The requirement exists as a takeoff condition and as an approach condition. For the takeoff requirement, it states that it must be possible to roll the aircraft from a 30 degree bank in the opposite direction (60 degree change) in less than 5 seconds for aircraft under 6000 lbs and 10 seconds for aircraft over 6000 lbs. For the approach requirement, the aircraft must be able to roll through 60 degrees in less than 4 and 7 seconds respectively for aircraft under and over 6000 lbs.

Directional control is entirely determined by the rudder of the aircraft. The directional control requirement for aircraft is set depending on the configuration of the aircraft. In the multi-engine case, it is always set by the engine-out parameter. Thus, the size and location of the engines often dictate the size of the rudder. The FAA has set two regulations governing the control authority required and the minimum control speed required for operation. For the control authority requirement, it states that the rudder should have sufficient authority to conduct heading changes of 15 degrees with one engine out and the others operating at maximum continuous power. For the control speed requirement, it states that the minimum speed be set at a speed in which it is possible to recover the aircraft from one engine suddenly made inoperative. It should be possible to maintain level flight with zero yaw or a bank into the good engine to not exceed 5 degrees.

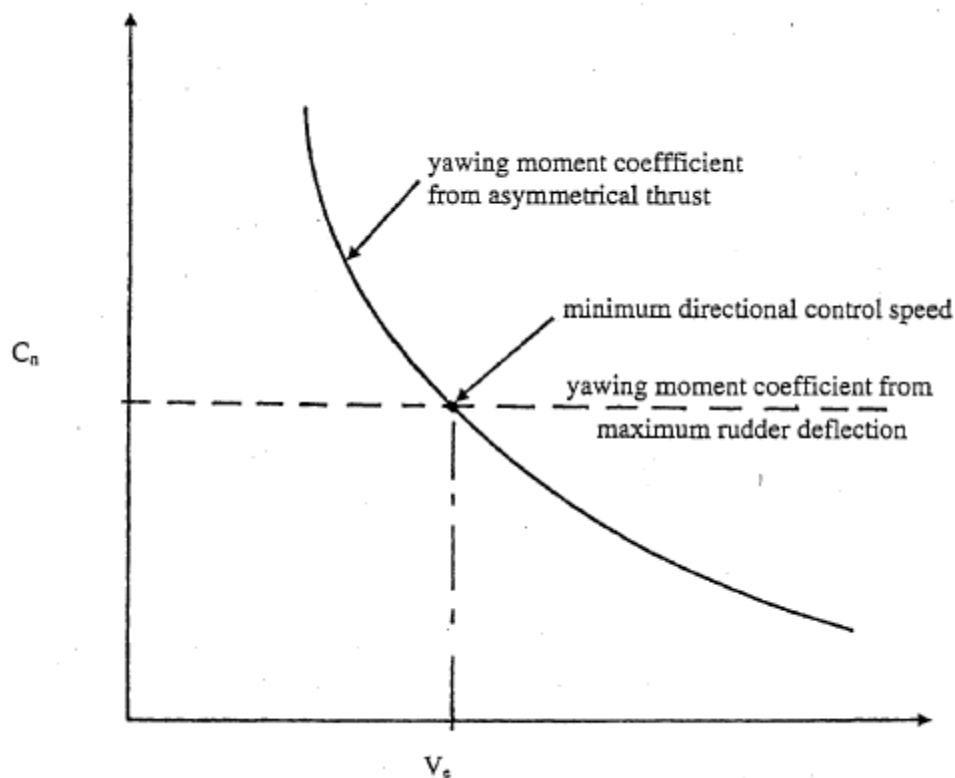


Figure 116. Minimum control speed estimation [7]

#### 4.4.4. Aircraft Limitations

##### 4.4.4.1. Stall Characteristics

In addition to stall speed, it is important to determine the stall characteristics in the case the aircraft is forced to operate in this regime. Ideally, an aircraft should be well behaved during stall and now have any unstable tendencies.

As we are mainly utilizing the FAR Part 23 regulations as a guideline on conducting flight tests, we will be following their guidelines for conduction stall characteristic testing. The FAR Part 23 regulations dictate several scenarios in which stall characteristics are tested: wing level stalls, turning flight and accelerated stalls, one-engine inoperative stalls, and stall warning.

For wings level stall, the aircraft is flown at an airspeed specified 150% above the stall speed at maximum engine thrust in which it does not accelerate the aircraft above the set speed. The elevator control is then pulled back until the downward pitching motion occurs. The regulation states that the airplane should exhibit stall characteristics in which it must be possible to prevent more than 15 degrees of roll or yaw by the normal use of controls.

For turning flight and accelerated stalls, the aircraft is entered into a 30 degree banked turn. The speed of the aircraft is reduced and the turn tightened continuously through the use of the elevator. The recovery criteria states the aircraft should be recoverable without excessive pitching up or the bank angle exceeding 60 degrees in the direction of the turn or 30 degrees in the opposite direction.

For one-engine inoperative, the aircraft should not show any unwanted spinning tendencies when stall and should be recoverable without applying power to the inoperative engine.

The Modular UAV does not have a stall warning thus this part of the regulation is not considered.

In all scenarios, the regulations call for the aircraft to be trimmed at 150% of the stall speed. In addition, stall characteristics should be tested with the aircraft loaded at the maximum gross weight with the most forward center of gravity. Through stability testing, the center of gravity should be moved back and stall characteristics should be evaluated to reach a complete set of characteristics of the aircraft.

Two main potential problems exist and must be considered when testing stall characteristics: wing drop or roll off and deep stall lock-in or pitch up. For wing drop/roll off, there exists two possibilities for the cause of this problem. One is sideslip at stall and the other is differences between the left and right wings. Sideslip may be caused by pilot technique due to insufficient rudder to counter P-factor during power on stalls. Wing contour differences due to minute inconsistencies and tolerances during manufacturing may produce wings with small differences in shape, resulting in differing stall points and characteristics.

Deep stall or pitch up problems are usually associated with swept wings and T-tail configurations. These problems occur when the wing completely shadows the empennage during stall so the rudder or elevator may not be used in the recovery of the aircraft due to the lack of airflow. In addition, swept wings cause spanwise flow in which the wing tips stall first. This causes the tip vortex to move inward and increase the downwash on the tail, producing a pitch up moment.

There are several methods in which stall problems can be addressed. They fall into two categories: aerodynamic and electromechanical fixes. Aerodynamic fixes can include stall strips, wing fences, drooped leading edges, and tail-lets. Electromechanical fixes are used more as backup devices in case the aerodynamic fixes fail to prevent a stall. Electromechanical fixes can include stick shakers, stick pushers, and stall barrier devices. While aerodynamic fixes work to increase the operable envelope of the aircraft or improve the characteristics, electromechanical fixes work to prevent the operation of reaching dangerous points.

Stall strips are powerful tools that can alter the stall characteristics of an aircraft. They work by stalling the wing at certain points. It is desirable to stall the wing at certain locations first, usually near the root, in order to allow the pilot to react while they still have use of the ailerons.

Wing fences are also common tools to improve the airflow over the wing by limiting spanwise flow. This reduces the chance of flow separation as well as the effect of the tip vortices. By limiting spanwise flow, they prevent the proliferation of the stall to the ailerons, allowing the pilot to maintain control.

A drooped leading edge can also be used to improve stall characteristics of an aircraft. This works by reducing the overall camber of the wing. This reduces the chance of airflow separation at higher angles of attack. It is generally used more prominently towards the wing tip as it's more desirable to have the flow stay attached at the location of the control surfaces.

#### 4.4.4.2. Flutter, Vibration, Buffeting

Determining if an aircraft is free from flutter, vibration, and buffeting is the most hazardous testing in aircraft certification. The range of speeds that tests are conducted are from stall speed to its top operational speed. This also includes a test at design dive speed. As such, this usually occurs at the end of aircraft testing after all other performance and flight characteristics have been documented.

The FAA separates flutter from vibration and buffeting testing. The regulation for vibration and buffeting states that there should be no vibration or buffeting severe enough to cause structural damage to the aircraft, interfere with the control of the aircraft, or cause excessive fatigue to the crew. Regarding flutter, FAR Part 23 requires that aircraft should be free of flutter for airspeeds up to the designed dive speed though in flight testing and up to 120% of designed flight speed by another method, such as wind tunnel testing.

Flutter is the main danger when conducting this type of test as it can quickly cause catastrophic failure of the structure. Aerodynamic flutter is defined as the resonance of an aircraft structure caused by the atmosphere or control inputs. It is a function of the structural stiffness, inertia properties, and aerodynamic forces. The resonance or natural frequency of the structure will dictate the regime in which flutter occurs. Most frequencies associated with the atmosphere and aviation occur at 50 Hz or lower so it is desirable to have the natural frequency of the structure higher than that. Generally, an increase in structure stiffness will increase the natural frequency.

It is important to also understand the flutter modes than can occur for a structure. The flutter mode refers to the degrees of freedom the structure has to move. Examples include: wing bending, wing torsion, aileron rotation, elevator rotation, horizontal tail bending, horizontal tail torsion, fuselage bending, ect. The coupling of the resonant frequencies of these modes will create flutter, with the torsional modes creating the most destruction.

For the flight test method, there are a few points in which the aircraft should be setup in order to effectively determine the proper characteristics. Regarding the control surfaces, they should be set to the most underbalanced (tail heavy) configuration and trim tabs set to the maximum free play. If the aircraft has any control system damping, they should be set to a minimum. Aircraft mass can also affect flutter modes. Configurations with maximum and minimum load should be tested with the center of gravity at the aft most location to reduce the load on the horizontal tail to a minimum in the event flutter does occur. As a final point, the tests should use a build-up technique to minimize risk and danger. Altitude specific tests should be done at higher altitudes first while airspeed specific tests should begin at the initial flutter clearance airspeed and work its way up to the designated speed.

## References

1. Agarwala, S., Liang, G., Dikshit, V., Sing, S., Yeong, W., & Goh, G. (2017). Additive manufacturing in unmanned aerial vehicles (UAVs): Challenges and potential. *Aerospace Science and Technology*, 140-151. Retrieved February 24, 2018.
2. Amatte, I., Dutra, T., Bürger, D., & Ferreira, R. T. (2017). 3D printed PLA and PLA reinforced with short carbon fibers: an experimental characterization. *Proceedings of the 24th ABCM International Congress of Mechanical Engineering*, 1-24. doi:10.26678/abcm.cobem2017.cob17-0135
3. Chin, W., & Sern, V. (n.d.). *Unmanned Aerial Vehicle Development Trends & Technology Forecast* (Singapore, Defence Science and Technology Agency). Retrieved February 24, 2018, from <https://www.google.com/url?sa=t&rct=j&q=&esrc=s&source=web&cd=1&cad=rja&uact=8&ved=0ahUKEwiXxPuRtMDZAhUG42MKHaI4C00QFgguMAA&url=https%3A%2F%2Fwww.dsta.gov.sg%2Fdocs%2Fdefault-source%2Fdsta-about%2Fdh01200502-unmanned-aerial-vehicle-development-trends-technology-forecast.pdf%3Fsfvrsn%3D2&usg=AOvVaw3cAZ5yNhMUa9qf9wCRKtrH>
4. Dahlgren, R., Alonso, J., & Fladeland, M. (2016, September 13). Progress on Modular Unmanned Aircraft Technology. In *ASPRS UAS Mapping*. Retrieved February 24, 2018.
5. Harshman, W. R. (1990). *Army Unmanned Aerial Vehicle (UAV) Requirements and the Joint UAV Program* (Unpublished master's thesis). U.S. Army Command and General Staff Colicge. Retrieved February 24, 2018.
6. Joshi, S. C., & Sheikh, A. A. (2015). 3D printing in aerospace and its long-term sustainability. *Virtual and Physical Prototyping*, 10(4), 175-185. Retrieved February 24, 2018.
7. Kimberlin, R. D. (2003). *Flight testing of Fixed-Wing Aircraft*. Reston: American Institute of Aeronautics and Astronautics.
8. K. Reynolds, R. Dahlgren, et al., "Repurposing surplus unmanned aircraft systems into UAS platforms for science missions," presented at the AUVSI 2015 Annual Meeting, Atlanta, Georgia, May 2015.
9. Moon, S. K., Tan, Y. E., Hwang, J., & Yoon, Y. (2014). Application of 3D printing technology for designing light-weight unmanned aerial vehicle wing structures. *International Journal of Precision Engineering and Manufacturing-Green Technology*, 1(3), 223-228. doi:10.1007/s40684-014-0028-x
10. Neubauer M, Gunther G, Fullhas K. Structural design aspects and criteria for military UAV. RTO-MP-AVT 145 UAV Design Processes and Criteria 2007.
11. S. Engelbrecht, L. Folgar, D. W. Rosen, G. Schulberger, J. Williams, Cellular structures for optimal performance, Proc. SFF Symp. Austin (2009) 831-842.
12. Saff, C.R. (2007) Airframe Certification Methods for Unmanned Aircraft. In *UAV Design Processes / Design Criteria for Structures* (pp. 1.1-1 – 1.1-16). Meeting Proceedings RTO-MP-AVT-145, Paper 1.1. Neuilly-sur-Seine, France: RTO. Available from:.
13. Siddiqi, A., & Weck, O. L. (2008). Modeling Methods and Conceptual Design Principles for Reconfigurable Systems. *Journal of Mechanical Design*, 130(10), 101102. doi:10.1115/1.2965598

14. Sullivan, M. J. (2009, July). *Opportunities Exist to Achieve Greater Commonality and Efficiencies among Unmanned Aircraft Systems* (USA, Government Accountability Office). Retrieved February 24, 2018, from <https://www.gao.gov/products/GAO-09-520>
15. U.S. Air Force, "The U.S. Air Force Remotely Piloted Aircraft and Unmanned Aerial Vehicle Strategic Vision" (2005). *U.S. Air Force Research*. 1. <http://digitalcommons.unl.edu/usafresearch/1>
16. United Nations, Office for Disarmament Affairs. (2015). *Study on Armed Unmanned Aerial Vehicles* (pp. 1-62). New York City, NY: United Nations.
17. USA, Defense Advanced Research Projects Agency, Tactical Technology Office. (2010). *Transformer (TX) Vertical Takeoff and Landing Roadable Air Vehicle* (pp. 1-58). Arlington, VA: DARPA. Retrieved February 24, 2018.
18. USA, U.S. Army, U. S. Army UAS Center of Excellence. (2010). *U.S. Army Unmanned Aircraft Systems Roadmap 2010-2035: Eyes of the Army* (pp. 1-140). Fort Rucker, Ala.: U.S. Army Unmanned Aircraft Systems Center of Excellence.
19. Vergouw, B., Nagel, H., Bondt, G., & Custers, B. (2016). Drone Technology: Types, Payloads, Applications, Frequency Spectrum Issues and Future Developments. *Information Technology and Law Series The Future of Drone Use*, 21-45. doi:10.1007/978-94-6265-132-6\_2
20. Weller, C., Kleer, R., & Piller, F. T. (2015). Economic implications of 3D printing: Market structure models in light of additive manufacturing revisited. *International Journal of Production Economics*, 164, 43-56. doi:10.1016/j.ijpe.2015.02.020
21. Zhu, J., Zhang, W., & Xia, L. (2015). Topology Optimization in Aircraft and Aerospace Structures Design. *Archives of Computational Methods in Engineering*, 23(4), 595-622. doi:10.1007/s11831-015-9151-2